THE IMPACT OF STDP AND CORRELATED ACTIVITY ON NETWORK STRUCTURE

A Dissertation

Presented to

the Faculty of the Department of Mathematics

University of Houston

In Partial Fulfillment

of the Requirements for the Degree

Doctor of Philosophy

By

Changan Liu

May 2017

THE IMPACT OF STDP AND CORRELATED ACTIVITY ON NETWORK STRUCTURE

Changan Liu

APPROVED:

Dr. Krešimir Josić,
Chairman
Department of Mathematics, University of Houston

Dr. Zachary P. Kilpatrick,
Department of Mathematics, University of Houston

Dr. Demetrio Labate,
Department of Mathematics, University of Houston

Dr. Harel Z. Shouval,
Department of Neurobiology and Anatomy,
University of Texas Health Science Center
at Houston

Dean, College of Natural Sciences and Mathematics

Acknowledgements

Firstly, I hope to express my sincerest gratitude to my Ph.D. advisor, Dr. Krešimir Josić, for his consistent guidance, inspiration, patience and encouragement. It is an honor to have him as my Ph.D. advisor. This work could never have been done without his help. What's more, I want to thank him for his financial support during my research period.

I am also grateful to my committee members Dr. Krešimir Josić, Dr. Zachary P. Kilpatrick, Dr. Demetrio Labate, and Dr. Harel Z. Shouval for spending their times to read my thesis carefully, and for their valuable comments and suggestions.

I would like to thank my advisor's former Ph.D. Students James Trousdale, José Manuel López Rodríguez and my advisor's colleague's Ph.D. Student Gabriel Koch Ocker. They helped me generously with the coding materials. I also would like to thank my advisor's colleagues Dr. Eric Shea-Brown and Dr. Brent Doiron, for their valuable suggestions and discussions on my work.

I would like to thank all the academic and administrative members in the Math Dept of the University of Houston. In particular, to Dr. Shanyu Ji, Dr. Ilya Timofeyev, and Ms. Neha Valji.

I thank my fellow graduate students, both those who already left and those still here.

Lastly, I want to dedicate the thesis to my parents. Even Though they are not here with me, I could not have done it without them.

THE IMPACT OF STDP AND CORRELATED ACTIVITY ON NETWORK STRUCTURE

An Abstract of a Dissertation

Presented to

the Faculty of the Department of Mathematics

University of Houston

In Partial Fulfillment

of the Requirements for the Degree

Doctor of Philosophy

By

Changan Liu

May 2017

Abstract

External stimuli shape the network structures of our nervous system. The synaptic connections between neurons are plastic and molded both by spontaneous activity and information they receive from the outside. This is the basis of memory formation and learning. In this dissertation, we study the effects of interactions between neuronal properties and learning rules on neuron network structures. In Chapter 2, we choose EIF (exponential integrate-and-fire) neurons as our neuron model, and show how to use linear response theory to approximate a fundamental descriptor of the interactions between neurons - their spike train cross-covariances. In Chapter 3, we investigate how these cross-covariances along with particular learning rules determine the evolution of synaptic weights in simple two-cell networks, from unidirectionally connected to bidirectionally connected examples. We propose a theoretical way to approximate the evolution of synaptic weights between neurons, and verify that the approximations hold using simulations. We next extend these ideas and approaches to large networks in Chapter 4. The insights we obtained using two-cell networks can help us interpret how synaptic weights evolve in larger networks. We also present a theoretical way to predict the final network structure which is the result of a particular learning rule, and depends on the level of drive and background noise of each neuron in the network.

Contents

CHAPTER 1

Introduction

Our nervous system underlies our thoughts and actions through the electrochemical activity of its constituent neurons. These networks of cells detect, classify, and respond to external stimuli. However, these external stimuli also shape our nervous systems. As our experiences differ, our living environment thus makes each one of us unique. Since the dawn of neuroscience as a modern discipline, one if its main goals has been understanding the physiological basis, and physical mechanisms that underlie learning and memory.

1.1 A brief history of synaptic plasticity

In the early 20th century, the Italian physiologist Ernesto Lugaro introduced the term "plasticity" to describe short- or long-lasting changes in synaptic or cellular physiology caused by a stimulus [24]. The term is now widely used to describe stimulus and activity driven changes in the wiring of neuronal networks. The following is a brief overview of the nearly hundred years of neural plasticity studies. Ralf Gerard used electrical recording in 1930 to find long-lasting depolarization in frog nerves after receiving high-frequency stimuli. This was the first evidence supporting long-lasting electrophysiological changes in response to stimulation. The desire to understand the relationship between neuronal activity and mental function has inspired many early neuroscientists, such as Rafael Lorente de Nó and Karl Lashley. de Nó proved that synaptic transmission only occurs if several synapses are activated, and only then if it "complies with a set of most rigid and exacting conditions" [15]. Lashley suggested that mental function depends on the general, dynamic, adaptive organization of the entire cerebral cortex [36]. In 1949, Karl Lashley's student, Donald Hebb, presented a theoretical mechanism of memory formation in his landmark book " The Organization of Behavior" [16]:

> "When an axon of cell A is near enough to excite a cell B and repeatedly or persistently takes part in firing it, some growth process or metabolic change takes place in one or both cells such that A's efficacy, as one of the cells firing B, is increased."

This idea is sometimes paraphrased as "Neurons that fire together wire together", and is now known as Hebb's rule. Hebb's ideas have strongly influenced the theories of plasticity up to the present.

In 1960's, the most forceful evidence for synaptic plasticity as a mechanism for behavioral learning was provided by Eric Kandel and Ladislav Tauc through an electrophysiological model developed by themselves [22, 23]. They applied stimulus-pairing sequences based on classical behavioral conditioning paradigms to the isolated abdominal ganglion of sea slug *Aplysia depilans*. Their results demonstrated that in certain cells the amplitude of the post-synaptic potential produced by a weak stimulus to one pathway is capable of being facilitated for a prolonged period of time as a result of the repeated and concomitant pairing with a more effective stimulus to another pathway. Later on, Terje Lømo and Timothy V.P. Bliss found that high-frequency stimulation of the perforant path from entorhinal cortex to the dentate gyrus caused long-term potentiation (LTP) of post-synaptic potentials [64, 67], which was also confirmed by Robert M. Douglas and Graham V. Goddard [56]. Besides LTP, Lynch, Dunwiddie and Gribkoff discovered long-term depression (LTD) in response to low-frequency stimulation in the hippocampus at the end of 1970's [28, 63].

Levy and Steward highlighted the importance of the relative timing of pre- and post-synaptic activity [71]. In the late 1990's, Henry Markram and his co-workers demonstrated such spike timing-dependent plasticity (STDP) experimentally by showing that iterative pairs of pre- and post-synaptic spikes can result in either potentiation or depression depending on their relative timing [29]. Later, Bi and Poo

provided a more detailed analysis of the timing dependence [27]. Such experimental studies underlined how the precise timing between pairs of pre- and post-synaptic spikes can govern plasticity, which subserving learning and memory.

1.2 Mathematical models of plasticity

In parallel with this experimental work, the development of the mathematical theory of synaptic plasticity and associated computational approaches have played an important role in our growing understanding of how our nervous system is shaped [30]. Mathematical models have been developed to match experimental observations. In turn theoretical approaches have been used to explain experimentally observed phenomena, and drive computational approaches to simulate the experiments. These models have been tested, validated, and improved by comparing the simulated and experimental data.

Many rate-based plasticity rules were created before the discovery of STDP. Among them, three classic models by Bienenstock, Cooper & Munro (BCM) [21], Oja [19] and Linsker [54], illustrate attempts to capture how synaptic plasticity shapes networks so they can perform computations. The BCM rule predicts that synaptic depression is due to the joint activity between the pre- and post-synaptic neurons, not the competition among synapses. It works well in both the visual cortex and the hippocampus, and it can be shown to correspond to certain abstract learning algorithms [8]. Oja's rule builds on the connection between theories of Hebbian learning

and neural-inspired computations. Both the BCM and Oja's rule can be used to model networks that can perform principal component analysis, and can lead to the emergence of self organizing maps in a layer-by-layer unsupervised learning scheme, such as as those used in models of binocular vision [20]. Linsker' rule explains the emergence of stimulus-selectivity in sensory areas, which is similar to the BCM rule. However, it focuses on orientation selectivity, not ocular dominance. All these rules rely on average firing rates and exclude the discussion of how spiking activity on neuronal timescales affects plasticity.

Different mechanistic models of synaptic plasticity have also been proposed. Calcium-based models have been remarkably influential, and come in two major types: those based on the calcium control hypothesis [61], and those on the assumption of multiple sensors for post-synaptic calcium [31]. The first type is motivated by the experiments illustrating that different post-synaptic calcium levels lead to different plasticity outcomes [61]. The behavior of some of these models depends sensitively on calcium concentration thresholds. The synapse depresses if calcium levels are intermediate while it potentiates if calcium levels are above a threshold. The second type can determine whether synaptic efficiency increases, decreases, or does not change according to a biophysically plausible calcium detection system. Both of these types of model can reproduce STDP that has been observed experimentally. Figure 1.1 shows a comparison between experiments and the second type of model.

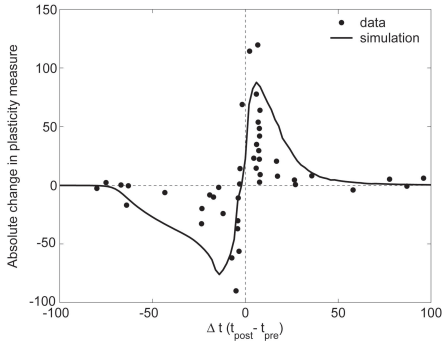

Figure 1.1: The STDP curve generated by the second type of Calcium-based model which can determine the synaptic weights evolution efficiency. From Rubin et al.,2005 [57]. Experimental data points from Bi and Poo,1998 [27].

Donald Hebb postulated in 1949 that a synaptic connection between two neurons is potentiated when a pre-synaptic neuron is repeatedly implicated in the firing of a post-synaptic cell, or, more generally, when a pre- and post-synaptic neuron are active simultaneously. Terrence Sejnowski suggested spike-time correlations as a requirement for synaptic plasticity in 1977 [66]. In 1993, Wulfram Gerstner and colleagues proved that, for a recurrent network to learn spatio-temporal patterns, instead of firing rates, plasticity needs to be based on spike times [70], and, a few years later, proposed spike-timing plasticity models for sound localization [69]. The STDP learning rule have been shown to feed forward artificial neural networks capable of pattern recognition, and have been used to recognize traffic, sound or movement using Dynamic Vision Sensor cameras [9, 65, 49]. Such learning rules can be mapped to equivalent rate-based rules under the assumption of stationary Poisson statistics for the firing times of pre- and postsynaptic neurons [52]. We can also relate STDP to a nonlinear rate model where the weight change depends linearly on the presynaptic rate, but nonlinearly on the postsynaptic rate [21]. There are two ways to achieve

this. One way is to is to implement standard STDP with nearest-neighbor instead of all-to all coupling. This gives a nonlinearity consistent with the BCM rule [32]. The other way is using a triplet STDP rule instead of the standard pair-based rule. The triplet STDP rule can become identical to the BCM rule under certain cases [21].

The timing-based plasticity rules specified the synaptic weight change as a piecewise function of the time lag between pre- and post-synaptic spikes, defining separate windows for potentiation and depression for positive and negative time lags respectively, have the general form:

$$\Delta \mathbf{W}_{\text{post}\leftarrow\text{pre}} = \begin{cases} f_+ \phi(t_{\text{post}} - t_{\text{pre}}), & \text{if } t_{\text{post}} - t_{\text{pre}} \geq 0 \\ -f_- \phi(t_{\text{post}} - t_{\text{pre}}), & \text{if } t_{\text{post}} - t_{\text{pre}} < 0 \end{cases},$$

where $f_\pm$ stands for the amplitudes of synaptic weight change and the function ϕ handles their time dependence. The typical forms of ϕ are exponential functions usually. These models capture the results of pair-based plasticity protocols, and provide an example of theory predicting experimental results in neuroscience. As many other learning rules, this rule can lead to unbounded changes in synaptic amplitudes, and is therefore typically complemented with a hard threshold to prevent runaway potentiation [59]. Alternatively, a sliding potentiation threshold can also prevent such divergence [13]. We use pair-based STDP learning rules throughout this whole dissertation.

1.3 Motivation of this dissertation

Many studies have explored how STDP shapes the distribution of synaptic weights of a group of synaptic connection to a a single neuron [58, 47, 53, 51, 3]. Here, we consider the more challenging problem of understanding how STDP shapes the global structure of a recurrent network of spiking neurons. Related questions have been addressed before in a number of studies [59, 17, 1, 18, 39, 40, 41, 42, 43, 44, 33, 11]. The generally antisymmetric shape of the STDP window, in which reversing the ordering of pre- and postsynaptic spikes reverses the direction of synaptic change, led to the proposal that this synaptic modification rule should eliminate strong recurrent connections between neurons [59, 37]. This idea has been expanded by Kozloski and Cecchi [33] to larger polysynaptic loops in the case of balanced STDP which the magnitudes of potentiation and depression are equal. The case of enhancing recurrent connections through pair-based STDP was also proposed by Song and Abbott [59] and was explored by Clopath and colleagues [11] later in a more complex model. Clopath and her colleagues proposed a STDP model in which the synaptic changes depend on presynaptic spike arrival and the postsynaptic membrane potential, filtered with two different time constants. They use this model to explain the connectivity patterns in cortex with a few strong bidirectional connections. Their plasticity rule lead not only to development of localized receptive fields but also to connectivity patterns that reflect the neural code. An excessively active group of neurons has been shown to decouple from the rest of the network through STDP [1], and in presence of axonal delays, STDP enhances recurrent connections when the neurons fire in a tonic irregular mode [18].

Babadi and Abbott have shown that large network properties can be explained by the effect of STDP on pairwise interactions of Poisson neurons based on the baseline firing rates [4]. They begin with analyzing the vector fields of the synaptic weights for two-cell recurrent symmetric (2 cells with the same baseline firing rate), and asymmetric (with different rates) networks under the influence of balanced and unbalanced (potentiation dominated and depression dominated) Hebbian STDP rules. Based on this analysis, they were able to make predictions about the dynamics of weights in large networks, and found that potentiation dominated STDP rules will generate loops while depression dominated rules will eliminate loops. Moreover, they showed that rightward shifted STDP can generate recurrent connections, and STDP with leftward shift generates loops at higher firing rates but eliminates loops at lower rates. This work provided a clear picture of how local learning rules can shape network dynamics from simple neuron circuits.

Gilson and his colleagues used a theoretical framework based on the assumption that spike trains can be described as Poisson processes, and used this framework to analytically describe the network dynamics and the evolution of the synaptic weights in a series of five papers [39, 40, 41, 42, 43]. They apply STDP to some of the synaptic connections in a network driven by two pools of input spike trains that have homogeneous within-pool firing rates and spike-time correlations. In the first paper, they found that the weights from the more correlated inputs are potentiated. In the second paper, they showed that the presence of fixed excitatory recurrent connections between neurons makes neurons tend to select the same input pool. They showed that, in the absence of external inputs, STDP can nevertheless generate structure

in the network through autocorrelation effects in the third paper. In the fourth paper, they illustrated that, for a network receiving fixed input weights which are stimulated by external spike trains, STDP can lead to both a stabilization of all the neuron firing rates and a robust weight specialization. In the last paper, they showed that a recurrently connected network stimulated by external pools can divide into two groups of neurons under the effect of STDP.

Most of these previous studies were based on the Poisson neuron model. However, while the assumption of a Poisson neuron leads to tractable models, it also does not fully reflect a number of properties of actual neurons. One of the main issues is the noise in neuronal firing. While a Poisson model captures such noise indirectly through the probabilistic nature of the firing of spikes, it does not capture explicitly the internally generated and synaptic noise. Thus it does not provide a mechanistic explanation of neuronal response variability. Spike generation, by itself, is highly reliable and deterministic. However, noise in neural responses is believed to result in part from the fact that synapses are very unreliable [10]. Noise is therefore due to unreliable synapses, or inherited from the input from the rest of the network, and is not due to spike generation. In the integrate-and-fire neuron model, the output is a filtered, thresholded and deterministic function of the input. Thus, the integrate-and-fire model captures many of the qualitative features, and is often used as a starting point for conceptualizing the biophysical behavior of single neurons [62].

There is evidence showing that some cells respond as integrate-and-fire neurons [55]. This implies such model is more close to the real neurons. Here we consider networks built of this general type of neurons - EIF (exponential integrate-and-fire)

neurons [25], which have been shown to match spiking dynamics well in certain cortical areas [7]. We find some new properties for the networks even if the baseline firing rates of the neurons are all the same, which can not be captured by networks of Poisson neurons.

CHAPTER 2

Methods

We consider networks of EIF neurons with the same baseline firing rate but where each cell receives different levels of background noise, which is driven by noise with mean μ and standard deviation σ. The properties of background noise are common to many neurons, so they provide a natural starting point. For fixed baseline firing rate, based on the values of μ and σ, there are two main regimes for EIF neurons: noise driven (higher σ value and lower μ value) and stimulus driven (lower σ value and higher μ value). The spikes of EIF neurons are mainly driven by the noise (σ) in the former regime while the stimulus (μ) is dominant in the latter regime. A neuron is said to be excitable when the direct input, μ results in membrane voltage that is

close to threshold. In this case small fluctuations in membrane voltage, whether due to input or noise internal to the cell, can cause the neuron to fire.

Our goal is to study the impact of STDP rules on the evolution of weights in a network. To do so, we start with networks of two cells. We use linear response theory to determine the cross-covariance function between the cells in the network. It is essential that we require the weights change slowly compared to network dynamics, which provides a separation of time scales (2.3). In turn, this allows us to determine how the weights evolve. Moreover, this also allows us to generalize the approach described in [34] to networks in which the weights are changing by analyzing their cross-covariance functions or phase planes (vector fields), and use these to predict the behavior of large networks. We test our predictions in large networks using both our theoretical framework, and direct numerical simulations.

2.1 The EIF model

All of the the networks we considered are composed of EIF (exponential integrate-and-fire) neurons. The membrane potentials V_i is thus modeled by

$$C_m \frac{dV_i}{dt} = g_L(V_L - V_i) + g_L\psi(V_i) + I_i(t) + f_i(t) \ . \tag{2.1}$$

Here C_m is the membrane capacitance, V_L is the leak reversal potential, and g_L is the membrane conductance.

$$\psi(V_i) = \Delta_T \exp\left[\frac{V_i - V_T}{\Delta_T}\right]$$

is the exponential term. Here V_T is the soft threshold. Δ_T shapes the spiking dynamics of the membrane potential. $I_i(t) = \mu_i + g_L \sigma_i D(\sqrt{(1-c)}\xi_i(t) + \sqrt{c}\xi_c(t))$ is the input term. $D = \sqrt{\frac{2C_m}{g_L}}$, $\xi_i(t)$ models background white noise with mean μ_i and standard deviation σ_i, $\xi_c(t)$ is the external common white noise input, and $c \in [0, 1]$ is the scaling parameter. When $c = 0$ the neurons in the network receive independent background white noise input. When $c = 1$ this background noise is identical in all cells. Here we choose to use the EIF neuron model because it accurately predicts the statistical features of spike trains for a large class of pyramidal neurons [35].

A post–synaptic input current is generated whenever a presynaptic cell spikes. We assume the synaptic kernels are exponential, and thus have the form:

$$\mathbf{J}_{ij}(t) = \mathbf{W}_{ij}\mathcal{H}(t - \tau_D)\exp\left[-\frac{t - \tau_D}{\tau_S}\right].$$

Here $\mathcal{H}$ is the heaviside step function, τ_D is the synaptic delay, τ_S is the synaptic time constant. The matrix $\mathbf{W}$ defines the synaptic weights, and the entry $\mathbf{W}_{ij}$ denotes the weight of the directed connection from neuron j to neuron i. Therefore, $y_j(t) = \Sigma_k \delta(t - t_{j,k})$ is the output spike train of cell j, then the synaptic current in cell i generated by the spiking of cell j is given by $f_i(t) = \Sigma_j(\mathbf{J}_{ij} * y_j)(t)$.

A Poisson neuron is completely described by its firing rate [60]. However, the dynamics and response of the EIF neuron are governed by parameters that capture the physiological properties of the cell. Here we will concentrate on two parameters, the mean μ and standard deviation σ of the input. These two parameters both affect the firing rate, and the variability of the neuron's output [38]. The same firing rate can be achieved for different μ and σ values (Figure 2.1). The variability in the output is not the same however. The statistics of the spike trains can be different according to the μ and σ values (Figure 2.2). Moreover, CV (coefficient of variation, the ratio of the standard deviation σ to the mean μ, $\frac{\sigma}{\mu}$) can vary even if the firing rate stays the same. As we will see below, this makes STDP in such networks more subtle.

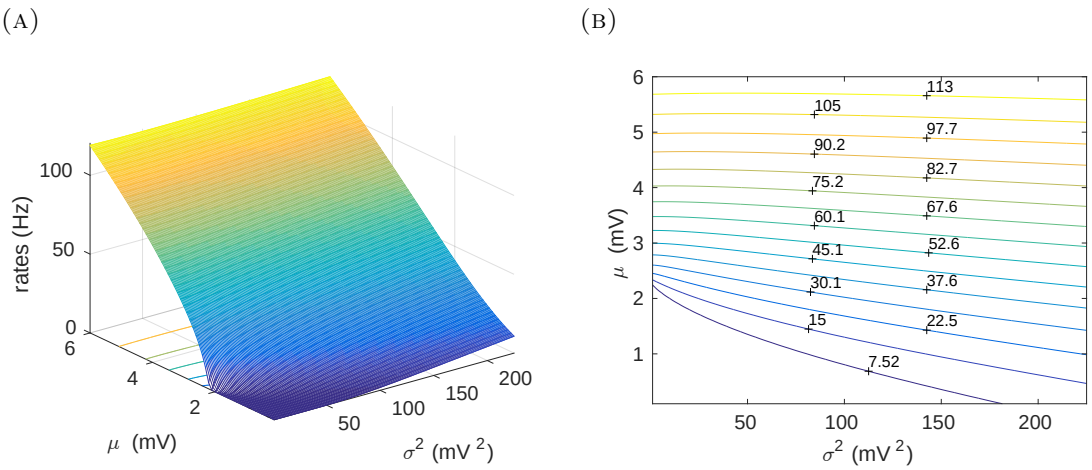

Figure 2.1: **Different μ-σ values can attain the same baseline firing rate. (A)** Changes of baseline firing rate according to μ and σ values. **(B)** Bottom of (A), illustrating that different μ and σ values can attain the same baseline firing rate.

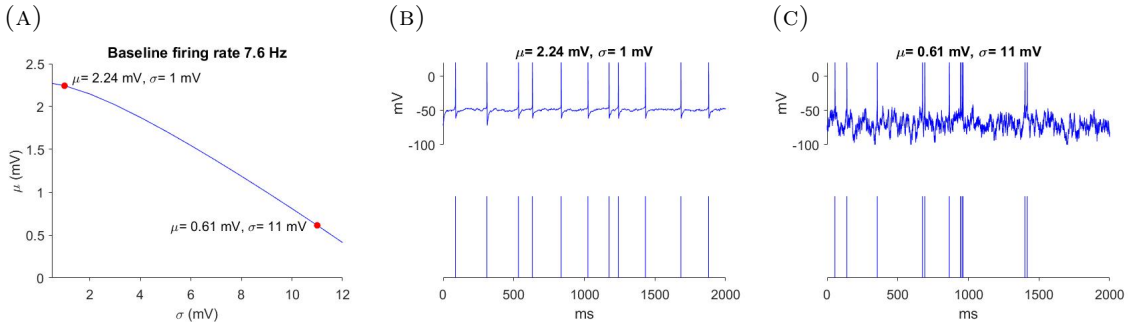

Figure 2.2: **Neurons with the same baseline firing rate can have different firing statistics. (A)** Different μ and σ values can attain the same baseline firing rate 7.6 Hz. **(B)** EIF neurons with the same baseline firing rate 7.6 Hz and higher μ will generate more regular spike train. **(C)** Neurons with lower μ will generate less regular spike train.

In Table 2.1, we choose 5 different μ-σ pairs that lead to the same baseline firing rate 7.6(Hz) as an example. Besides μ and σ, other parameters can also affect the rates, such as the spiking dynamics shaping parameter Δ_T in the exponential term $\psi(V_i)$. Higher Δ_T causes more rapid spike onset, and leads to higher firing rates. However, the impact of these other parameters is expected to be small compared to μ and σ, the parameters that are the focus of our study.

Pair index	μ (mV)	σ^2 (mV^2)	Fano factor	Baseline firing rate (Hz)
1	1.37	49	0.77	7.6
2	1.19	64	0.81	
3	1	81	0.84	
4	0.81	100	0.88	
5	0.61	121	0.91	

Table 2.1: 5 different μ-σ pairs that attain the same baseline firing rate 7.6(Hz). Red row is our baseline setting for the neuron model.

We take the red pair as our baseline setting. Table 2.1 thus shows that to obtain the same baseline firing rate when we increase σ, we need to lower μ.

2.2 The Hebbian STDP rule

To study how plasticity shapes the structure of the network, we use a well-known model of STDP [69], which has been supported by experimental evidence starting with that of Bi and Poo in 1998 [27], and followed by other studies [72, 2, 68]. If we denote by s the time difference between the pre- and post-synaptic spikes

$$s = t_{post} - t_{pre} = t_j - t_i \ ,$$

then we can define a Hebbian STDP rule by

$$\Delta \mathbf{W}_{ji}(s) = \begin{cases} \mathbf{W}^0_{ji} \mathcal{H}(W^{max} - \mathbf{W}_{ji}) L(s) \ , & \text{if } s \geq 0 \\ \mathbf{W}^0_{ji} \mathcal{H}(\mathbf{W}_{ji}) L(s) \ , & \text{if } s < 0 \end{cases} \ , \tag{2.2}$$

where

$$L(s) = \begin{cases} f_+ e^{-\frac{|s|}{\tau_+}} \ , & \text{if } s \geq 0 \\ -f_- e^{-\frac{|s|}{\tau_-}} \ , & \text{if } s < 0 \end{cases} \ .$$

Here $\mathcal{H}(x)$ is the Heaviside function, $f_+ > 0$ and $f_- > 0$ are the amplitudes of

potentiation and depression respectively, τ_+ and τ_- are the time constants, W^{max} is the upper bound of the synaptic weights and $\mathbf{W}^0$ is the binary adjacency matrix of the network, enforcing that STDP rule can only modify connections that exist in the network structure.

We also consider an Anti-Hebbian STDP rule, which is similar to the Hebbian STDP rule and the only difference is the potentiation and depression sides are reversed. We use these rules in a number of examples we describe below, although our approach is applicable to any other pairwise STDP rules.

2.3 Weight change dynamics

We can denote the spiking output of a neuron i by

$$\mathbf{y}_i(t) = \sum_{i=1}^{n_i} \delta(t - t_i) \ . \tag{2.3}$$

According to [52, 37, 44, 3], we can build the bridge from the joint statistics of $\mathbf{y}_i(t)$ and $\mathbf{y}_j(t)$ to the evolution of synaptic weights. The learning rule given in Eq.(2.2) governs the changes of the synaptic weight $\mathbf{W}_{ji}$ (from neuron i to neuron j). Let $\Delta_T \mathbf{W}_{ji}$ be the total change in the related synaptic weight during a time interval of length T. This weight change is calculated by summing the contributions of input

(i) and output (j) spikes occurring in the time interval $[t, t+T]$. We have

$$\Delta_T \mathbf{W}_{ji} = \int_t^{t+T} \int_t^{t+T} \Delta\mathbf{W}_{ji}(t_2 - t_1)\mathbf{y}_j(t_2)\mathbf{y}_i(t_1)dt_2dt_1 \ .$$

Let $s = t_2 - t_1$, $\langle\cdot\rangle$ denote the trial average, then the trial-averaged rate of synaptic weight change is

$$\frac{\langle\Delta_T \mathbf{W}_{ji}\rangle}{T} = \frac{1}{T}\int_t^{t+T} \int_{t-t_1}^{t+T-t_1} \Delta\mathbf{W}_{ji}(s)\langle\mathbf{y}_j(t_1+s)\mathbf{y}_i(t_1)\rangle dsdt_1 \ . \tag{2.4}$$

The trial-averaged spike train cross-covariance $\mathbf{C}_{ji}(s)$ is

$$\mathbf{C}_{ji}(s) = \frac{1}{T}\int_t^{t+T} \langle\mathbf{y}_j(t_1+s)\mathbf{y}_i(t_1)\rangle dt_1 - r_i r_j \ ,$$

where r_j and r_i are the stationary firing rates for neuron j and i respectively. Using this term in Eq.(2.4), we get

$$\frac{\langle\Delta_T \mathbf{W}_{ji}\rangle}{T} = \int_{t-t_1}^{t+T-t_1} \Delta\mathbf{W}_{ji}(s)(\mathbf{C}_{ji}(s) + r_j r_i)ds \ . \tag{2.5}$$

We define the width $\mathcal{W}$ of the learning rule $\Delta\mathbf{W}_{ji}(s)$ and let $T \gg \mathcal{W}$. Then most of the contributions to the weights evolution of the learning rule should be inside the interval $[-\mathcal{W}, \mathcal{W}]$. Thus, we can extend the integration over s in Eq.(2.5) to run from $-\infty$ to $+\infty$. We require the amplitude of individual changes in the synaptic weights to be small ($f_\pm \ll W^{max}$). So the value of $\mathbf{W}_{ji}$ do not change much in the time interval of length T. Thus T separates the time scale $\mathcal{W}$ from the time scale of

the learning dynamics, which allows us to approximate the left-hand side of Eq.(2.5) by the rate of change $\frac{d\mathbf{W}_{ji}}{dt}$:

$$\begin{aligned}\frac{d\mathbf{W}_{ji}}{dt} &= \int_{-\infty}^{+\infty} \Delta\mathbf{W}_{ji}(s)(\mathbf{C}_{ji}(s) + r_j r_i)ds \\ &= \underbrace{\int_{-\infty}^{+\infty} \Delta\mathbf{W}_{ji}(s)\mathbf{C}_{ji}(s)ds}_{1} + \underbrace{r_j r_i \int_{-\infty}^{+\infty} \Delta\mathbf{W}_{ji}(s)ds}_{2} \ . \end{aligned} \tag{2.6}$$

For fixed learning rule and neuron properties of the networks, part 2 of Eq.(2.6) is a constant. Part 1 is illustrated in Figure 2.3.

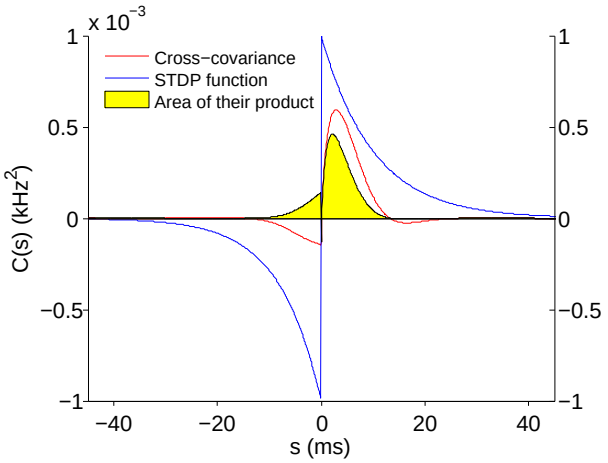

Figure 2.3: **Illustration for Part 1 of Eq.(2.6).** Cross-covariance (red curve), together with the STDP rule (blue curve) define the weight change dynamics (yellow region). These quantities are used to obtain the theoretical weight change dynamics. The yellow region is the integral (area) of the product of cross-covariance and learning rule, which stands for Part 1 of Eq.(2.6). It contributes the weights evolution.

2.4 Approximating cross-covariances using linear response theory

We will briefly introduce an approximation method to estimate the pairwise spike train cross-covariances $\mathbf{C}_{ij}(s)$ using a synaptic weight matrix $\mathbf{W}$ [5, 6, 34, 48]. We consider the Fourier transform of a spike train (Eq.(2.3)),

$$\tilde{\mathbf{y}}_i(\omega) = \int_{-\infty}^{\infty} \mathbf{y}_i(t) e^{-2\pi i \omega t} dt \ ,$$

where ω is frequency. Assuming the synaptic weights, $\mathbf{W}_{ij}$ are weak, we can approximate the spike response from neuron i (Eq.(2.1)) as:

$$\tilde{\mathbf{y}}_i(\omega) \approx \tilde{\mathbf{y}}_i^0(\omega) + \tilde{A}_i(\omega)\left(\sum_{j=1}^{N} \tilde{\mathbf{J}}_{ij}(\omega)\tilde{\mathbf{y}}_j(\omega) \right) . \tag{2.7}$$

Here $\tilde{A}_i(\omega)$ is Fourier transform of the linear response [12] of the post-synaptic neuron i, measuring how strongly modulations in synaptic currents at frequency ω are transferred into modulations of instantaneous firing rate about a background state $\tilde{\mathbf{y}}_i^0(\omega)$. The function $\tilde{\mathbf{J}}_{ij}(\omega)$ is the Fourier transform of a synaptic filter. Eq.(2.7) is a linear approximation for how a neuron integrates and transforms a realization of synaptic input into a spike train.

Following [5, 6, 34], we use this linear approximation to estimate the Fourier transform of $\mathbf{C}_{ij}(s)$, written as $\tilde{\mathbf{C}}_{ij}(\omega) =< \tilde{\mathbf{y}}_i(\omega)\tilde{\mathbf{y}}_j^*(\omega) >$. Here $\tilde{\mathbf{y}}^*$ denotes the

conjugate transpose. This yields the following matrix equation:

$$\tilde{\mathbf{C}}(\omega) \approx (\mathbf{I} - \tilde{\mathbf{K}}(\omega))^{-1}\tilde{\mathbf{C}}^{0}(\omega)(\mathbf{I} - \tilde{\mathbf{K}}^{*}(\omega))^{-1} \ , \tag{2.8}$$

where $\tilde{\mathbf{K}}(\omega)$ is an interaction matrix defined by $\tilde{\mathbf{K}}_{ij}(\omega) = \tilde{A}_i(\omega)\tilde{\mathbf{J}}_{ij}(\omega)$. We can compute $\tilde{A}_i(\omega)$ using standard methods based on using a Fokker-Planck equation to describe the probability distribution of a neuron's membrane potential [45, 46]. The diagonal matrix $\tilde{\mathbf{C}}^{0}(\omega)$ is the auto-spectra in the absence of synaptic coupling, with elements $\tilde{\mathbf{C}}^{0}_{ii}(\omega) =< \tilde{\mathbf{y}}^{0}_{i}(\omega)\tilde{\mathbf{y}}^{0*}_{i}(\omega) >$, and $\mathbf{I}$ is the identity matrix. From Eq.(2.8), we can recover the matrix of spike train cross-covariance functions $\mathbf{C}(s)$ through inverse Fourier transformation. Thus, Eq.(2.8) gives us an estimate of the statistics of pairwise spiking activity in the full network given its architecture.

For the parameter of correlated input $c > 0$, let $\mathbf{C}^{ext}$ be the covariance matrix of the common external input ($g_L\sigma_i D\sqrt{c}\xi_c(t)$ for neuron i) for all the neurons in a network, we have

$$\mathbf{C}^{ext}_{ii} = \mathrm{Cov}(g_L\sigma_i D\sqrt{c}\xi_c(t), g_L\sigma_i D\sqrt{c}\xi_c(t)) = \mathrm{Var}(g_L\sigma_i D\sqrt{c}\xi_c(t)) = cg_L^2D^2\sigma_i^2 \ ,$$
$$\mathbf{C}^{ext}_{ij} = \mathrm{Cov}(g_L\sigma_i D\sqrt{c}\xi_c(t), g_L\sigma_j D\sqrt{c}\xi_c(t)) = cg_L^2D^2\sigma_i\sigma_j \ .$$

The full array of cross-spectra in the network can then be approximated by

$$\tilde{\mathbf{C}}(\omega) \approx (\mathbf{I} - \tilde{\mathbf{K}}(\omega))^{-1}(\tilde{\mathbf{C}}^{0}(\omega) + \tilde{\mathbf{A}}(\omega)\mathbf{C}^{ext}\tilde{\mathbf{A}}^{*}(\omega))(\mathbf{I} - \tilde{\mathbf{K}}^{*}(\omega))^{-1} \ , \tag{2.9}$$

where $\tilde{\mathbf{A}}(\omega)$ is a diagonal matrix containing the Fourier transform of linear response

functions of each neuron ($\tilde{A}_i(\omega)$s).

Examples comparing theoretical and simulated cross-covariances of simple circuits with two neurons are in Sections 3.1.1 and 3.1.2.

CHAPTER 3

Results for simple circuits

In this chapter we first study the evolution of synaptic weights in a system of two mutually coupled neurons. We apply the theoretical approach described in the previous section, and confirm the results numerically. Insights gained from the simple system of two neurons allow us to understand how features of the linear response function together with the shape of the STDP function together determine the evolution of synaptic weights.

3.1 Cross-covariances and learning for two-cell networks

We first study the cross-covariances and evolution of synaptic weights in particular two-cell networks. We then generalize the approach to larger networks in the following chapter.

3.1.1 Two EIF neurons with one directed connection

The connectivity in a network of two EIF neurons with a synaptic connection from cell 1 to cell 2 (Figure 3.1), is described by the weight matrix

$$\mathbf{W} = \begin{pmatrix} 0 & 0 \\ \mathbf{W}_{21} & 0 \end{pmatrix} .$$

Figure 3.1: **Connected 2 EIF neurons with just one connection from cell 1 to cell 2.**

For this case, we have $\mathbf{J}_{12}(t) = 0$, $\mathbf{K}_{12}(t) = 0$ and $\tilde{\mathbf{K}}_{12} = 0$. Thus,

$$\tilde{\mathbf{K}} = \begin{pmatrix} 0 & 0 \\ \tilde{\mathbf{K}}_{21} & 0 \end{pmatrix}$$

with $\tilde{\mathbf{K}}_{21} = \tilde{A}_2\tilde{\mathbf{J}}_{21}$. We therefore have, $(\mathbf{I}-\tilde{\mathbf{K}})^{-1} = (\mathbf{I}+\tilde{\mathbf{K}})$, and similarly, $(\mathbf{I}-\tilde{\mathbf{K}}^*)^{-1} = (\mathbf{I}+\tilde{\mathbf{K}}^*)$.

The cross-spectrum matrix of the two processes is therefore given by Eq.(2.8),

$$\begin{aligned}
\begin{pmatrix} \tilde{\mathbf{C}}_{11} & \tilde{\mathbf{C}}_{12} \\ \tilde{\mathbf{C}}_{21} & \tilde{\mathbf{C}}_{22} \end{pmatrix} &\approx (\mathbf{I}+\tilde{\mathbf{K}}) \begin{pmatrix} \tilde{\mathbf{C}}^0_{11} & 0 \\ 0 & \tilde{\mathbf{C}}^0_{22} \end{pmatrix} (\mathbf{I}+\tilde{\mathbf{K}}^*) \\
&= \begin{pmatrix} 1 & 0 \\ \tilde{\mathbf{K}}_{21} & 1 \end{pmatrix} \begin{pmatrix} \tilde{\mathbf{C}}^0_{11} & 0 \\ 0 & \tilde{\mathbf{C}}^0_{22} \end{pmatrix} \begin{pmatrix} 1 & \tilde{\mathbf{K}}^*_{21} \\ 0 & 1 \end{pmatrix} \\
&= \begin{pmatrix} \tilde{\mathbf{C}}^0_{11} & \tilde{\mathbf{K}}^*_{21}\tilde{\mathbf{C}}^0_{11} \\ \tilde{\mathbf{K}}_{21}\tilde{\mathbf{C}}^0_{11} & |\tilde{\mathbf{K}}_{21}|^2\tilde{\mathbf{C}}^0_{11} + \tilde{\mathbf{C}}^0_{22} \end{pmatrix} .
\end{aligned}$$

Thus, $\tilde{\mathbf{C}}_{21} \approx \tilde{\mathbf{K}}_{21}\tilde{\mathbf{C}}^0_{11} = \tilde{A}_2\tilde{\mathbf{J}}_{21}\tilde{\mathbf{C}}^0_{11}$, and $\tilde{\mathbf{C}}_{12} \approx (\tilde{A}_2\tilde{\mathbf{J}}_{21})^*\tilde{\mathbf{C}}^0_{11}$. We can therefore use inverse Fourier transforms to recover the cross-covariances, $\mathbf{C}_{12}(t) \approx \mathcal{F}^{-1}(\tilde{\mathbf{C}}_{12})(t)$ and $\mathbf{C}_{21}(t) \approx \mathcal{F}^{-1}(\tilde{\mathbf{C}}_{21})(t)$.

These equations show that the cross-covariances are determined by the linear response function, $A_i(t)$, the synaptic kernel $\mathbf{J}_{ij}(t)$, as well as the uncoupled auto-covariance $\mathbf{C}^0_{11}$. This is shown in Figure 3.2. This dependence can be presented schematically as:

$$\begin{aligned}
&\text{Linear response} \;+\; \text{Synaptic kernel} \;+\; \text{Uncoupled auto-covariance} \\
&\qquad\qquad \rightarrow \;\text{Cross-covariances} \; . \qquad\qquad (3.1)
\end{aligned}$$

In Figure 3.2, we show the linear response function, $A_2(t)$, the synaptic kernel, $\mathbf{J}_{21}(t)$, the uncoupled auto-covariance, $\mathbf{C}^0_{11}$, and the matched cross-covariance, $\mathbf{C}_{21}(t)$. As we have shown, the first three functions (panels A–C) can be combined to obtain an approximation of the fourth (panel D). In Figure 3.2D, the red curve represents this theoretical result obtained using Eq.(2.8), while the blue curve is obtained using direct simulations of the stochastic differential equation Eq.(2.1). We use the same color assignments to distinguish theoretical and simulation results below.

The dynamics of synaptic weights given by Eq.(2.6) is determined by the cross-covariances, and the learning rule. This is illustrated in Figure 3.3. Note that a change in synaptic weights affects the firing rate. In turn, this can affect the cross-correlation, and the further evolution of the weights. We therefore need to recompute the rates and linear responses for each update of synaptic weights. Thus this is a closed loop - unlike in the Poisson neuron case.

In sum, we can complement the heuristic rule expressed in Eq.(3.1) by

$$\text{Cross-covariance} \;+\; \text{Learning rule} \;\rightarrow\; \text{Synaptic weight changes}\;.$$

Figure 3.3A shows the theoretical cross-covariance, $\mathbf{C}_{21}(t)$. Figure 3.3B shows the balanced Hebbian STDP rule ($f_+ = f_-$ and $\tau_+ = \tau_-$ in Eq.(2.2)). The peak of the cross-covariance is in the positive time domain. This is the potentiation side of the balanced Hebbian STDP rule (See Figure 2.3). Due to the shape of the cross-covariance and the learning rule, the synaptic weight $\mathbf{W}_{21}$ will be potentiated (Figure 3.3C).

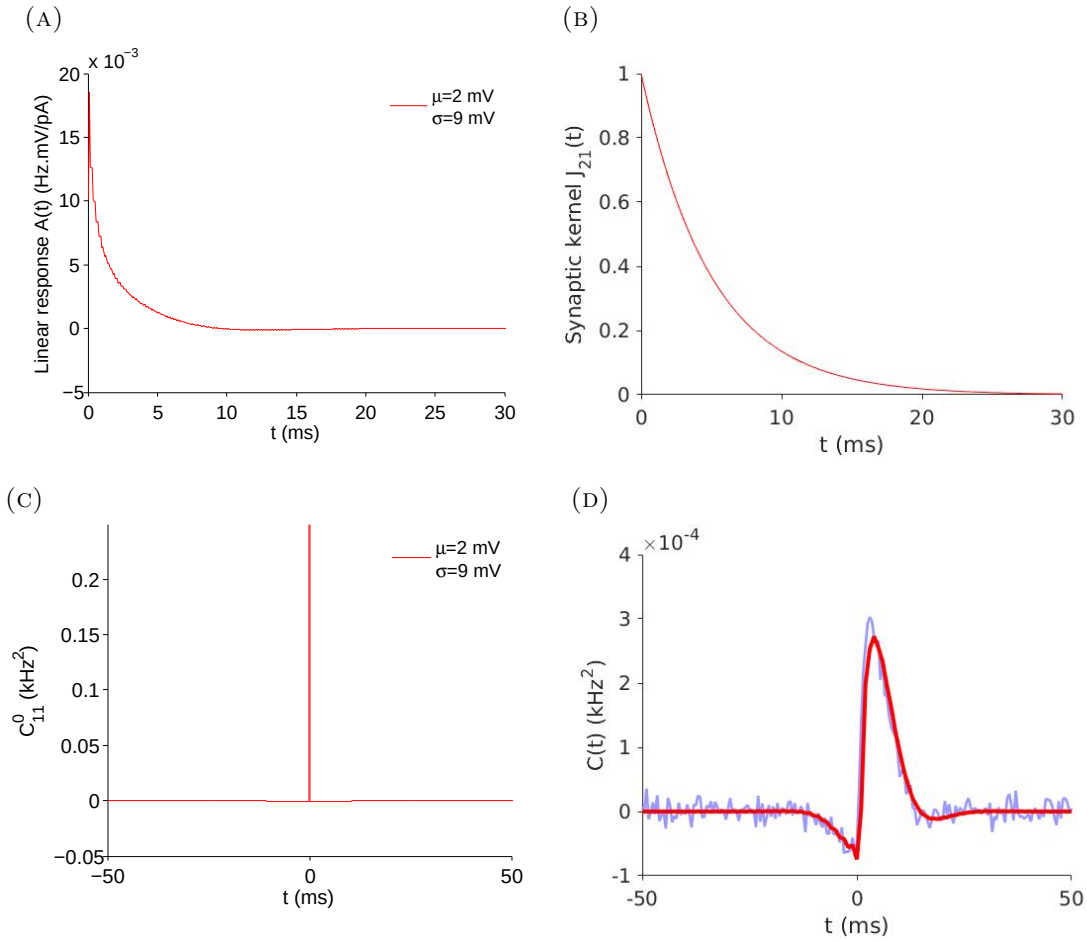

Figure 3.2: **A theoretical approximation of the cross-covariances.** The baseline firing rate is about 27 Hz for the two cells when $\mu = 2$ mV and $\sigma = 9$ mV. $\mathbf{W}_{21} = 1\ \mu\text{A/cm}^2$. **(A)** The linear response function, $A_2(t)$. **(B)** The synaptic kernel, $\mathbf{J}_{21}(t)$. **(C)** The auto-covariance for uncoupled cells, $\mathbf{C}^0_{11}$. **(D)** Matched cross-covariance $\mathbf{C}_{21}(t)$. The smooth red curve shows he theoretical results, while the blue curve shows the results of simulations. Here we use the spike trains with length of 10^7 ms and bin size of 0.5 ms for computing the simulated cross-covariance.

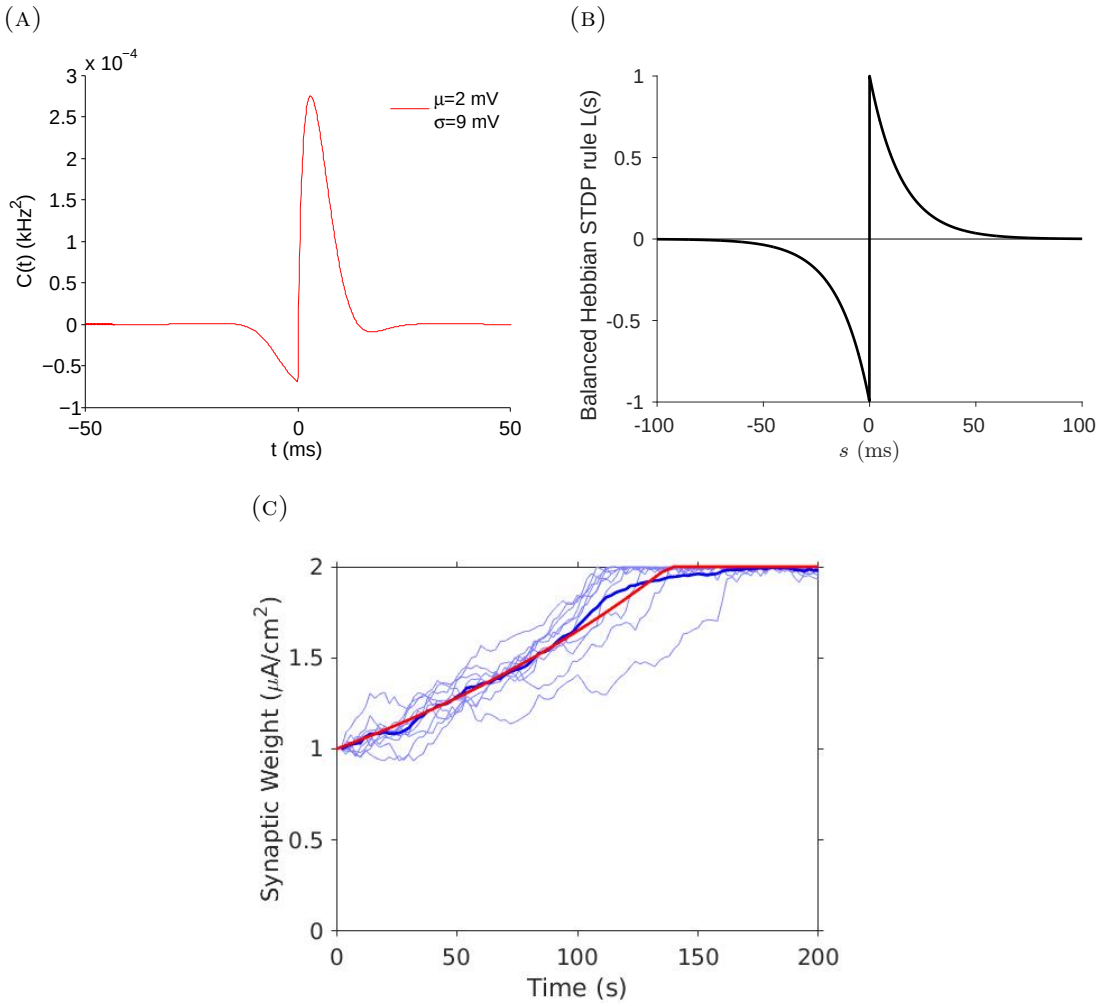

Figure 3.3: **The relation between cross-covariances and learning.** The baseline firing rate is about 27 Hz for the two cells with $\mu = 2$ mV and $\sigma = 9$ mV. **(A)** Theoretical cross-covariance $\mathbf{C}_{21}(t)$. **(B)** Balanced Hebbian STDP rule ($\Delta\mathbf{W}$). **(C)** A comparison of the theoretical (red) and simulated (blue) evolution of the synaptic weight $\mathbf{W}_{21}$. The light blue curves are obtained from 10 realizations of the system. The thick blue curve is the average of these 10 simulations.

3.1.2 Two EIF neurons with recurrent connections

For the network formed by two EIF neurons with recurrent connections shown in Figure 3.4, we have the synaptic weight matrix

$$\mathbf{W} = \begin{pmatrix} 0 & \mathbf{W}_{12} \\ \mathbf{W}_{21} & 0 \end{pmatrix} .$$

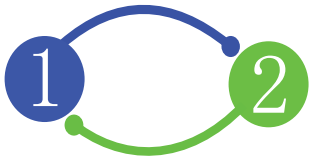

Figure 3.4: **Two EIF neurons with recurrent connections.**

In this case,

$$\tilde{\mathbf{K}} = \begin{pmatrix} 0 & \tilde{\mathbf{K}}_{12} \\ \tilde{\mathbf{K}}_{21} & 0 \end{pmatrix}$$

with $\tilde{\mathbf{K}}_{21} = \tilde{A}_2\tilde{\mathbf{J}}_{21}$ and $\tilde{\mathbf{K}}_{12} = \tilde{A}_1\tilde{\mathbf{J}}_{12}$.

Similarly,

$$(\mathbf{I} - \tilde{\mathbf{K}})^{-1} = \frac{1}{1 - \tilde{\mathbf{K}}_{12}\tilde{\mathbf{K}}_{21}}(\mathbf{I} + \tilde{\mathbf{K}}) \ , \quad \text{and} \quad (\mathbf{I} - \tilde{\mathbf{K}}^*)^{-1} = \frac{1}{1 - \tilde{\mathbf{K}}^*_{12}\tilde{\mathbf{K}}^*_{21}}(\mathbf{I} + \tilde{\mathbf{K}}^*) \ ,$$

and so,

$$\begin{aligned}
\begin{pmatrix} \tilde{\mathbf{C}}_{11} & \tilde{\mathbf{C}}_{12} \\ \tilde{\mathbf{C}}_{21} & \tilde{\mathbf{C}}_{22} \end{pmatrix} &\approx \frac{1}{(1-\tilde{\mathbf{K}}_{12}\tilde{\mathbf{K}}_{21})(1-\tilde{\mathbf{K}}_{12}^*\tilde{\mathbf{K}}_{21}^*)}(\mathbf{I}+\tilde{\mathbf{K}})\begin{pmatrix} \tilde{\mathbf{C}}_{11}^0 & 0 \\ 0 & \tilde{\mathbf{C}}_{22}^0 \end{pmatrix}(\mathbf{I}+\tilde{\mathbf{K}}^*) \\
&= \frac{1}{|1-\tilde{\mathbf{K}}_{12}\tilde{\mathbf{K}}_{21}|^2}\begin{pmatrix} 1 & \tilde{\mathbf{K}}_{12} \\ \tilde{\mathbf{K}}_{21} & 1 \end{pmatrix}\begin{pmatrix} \tilde{\mathbf{C}}_{11}^0 & 0 \\ 0 & \tilde{\mathbf{C}}_{22}^0 \end{pmatrix}\begin{pmatrix} 1 & \tilde{\mathbf{K}}_{21}^* \\ \tilde{\mathbf{K}}_{12}^* & 1 \end{pmatrix} \\
&= \frac{1}{|1-\tilde{\mathbf{K}}_{12}\tilde{\mathbf{K}}_{21}|^2}\begin{pmatrix} \tilde{\mathbf{C}}_{11}^0+|\tilde{\mathbf{K}}_{12}|^2\tilde{\mathbf{C}}_{22}^0 & \tilde{\mathbf{K}}_{21}^*\tilde{\mathbf{C}}_{11}^0+\tilde{\mathbf{K}}_{12}\tilde{\mathbf{C}}_{22}^0 \\ \tilde{\mathbf{K}}_{21}\tilde{\mathbf{C}}_{11}^0+\tilde{\mathbf{K}}_{12}^*\tilde{\mathbf{C}}_{22}^0 & |\tilde{\mathbf{K}}_{21}|^2\tilde{\mathbf{C}}_{11}^0+\tilde{\mathbf{C}}_{22}^0 \end{pmatrix}.
\end{aligned}$$

This implies

$$\tilde{\mathbf{C}}_{12} \approx \frac{\tilde{\mathbf{K}}_{21}^*\tilde{\mathbf{C}}_{11}^0+\tilde{\mathbf{K}}_{12}\tilde{\mathbf{C}}_{22}^0}{|1-\tilde{\mathbf{K}}_{12}\tilde{\mathbf{K}}_{21}|^2} = \frac{(\tilde{A}_2\tilde{\mathbf{J}}_{21})^*\tilde{\mathbf{C}}_{11}^0+\tilde{A}_1\tilde{\mathbf{J}}_{12}\tilde{\mathbf{C}}_{22}^0}{|1-\tilde{A}_1\tilde{\mathbf{J}}_{12}\tilde{A}_2\tilde{\mathbf{J}}_{21}|^2}$$

and

$$\tilde{\mathbf{C}}_{21} \approx \frac{\tilde{\mathbf{K}}_{21}\tilde{\mathbf{C}}_{11}^0+\tilde{\mathbf{K}}_{12}^*\tilde{\mathbf{C}}_{22}^0}{|1-\tilde{\mathbf{K}}_{12}\tilde{\mathbf{K}}_{21}|^2} = \frac{\tilde{A}_2\tilde{\mathbf{J}}_{21}\tilde{\mathbf{C}}_{11}^0+(\tilde{A}_1\tilde{\mathbf{J}}_{12})^*\tilde{\mathbf{C}}_{22}^0}{|1-\tilde{A}_1\tilde{\mathbf{J}}_{12}\tilde{A}_2\tilde{\mathbf{J}}_{21}|^2}\ .$$

We can rewrite these expressions as geometric series,

$$\frac{1}{1-\tilde{\mathbf{K}}_{12}\tilde{\mathbf{K}}_{21}} = \sum_{k=0}^{\infty}(\tilde{\mathbf{K}}_{12}\tilde{\mathbf{K}}_{21})^k\ , \quad \frac{1}{1-\tilde{\mathbf{K}}_{12}^*\tilde{\mathbf{K}}_{21}^*} = \sum_{l=0}^{\infty}(\tilde{\mathbf{K}}_{12}^*\tilde{\mathbf{K}}_{21}^*)^l\ ,$$

to obtain

$$\begin{aligned}\frac{1}{|1-\tilde{\mathbf{K}}_{12}\tilde{\mathbf{K}}_{21}|^2} &= \frac{1}{(1-\tilde{\mathbf{K}}_{12}\tilde{\mathbf{K}}_{21})(1-\tilde{\mathbf{K}}_{12}^*\tilde{\mathbf{K}}_{21}^*)} \\ &= \left(\sum_{k=0}^{\infty}(\tilde{\mathbf{K}}_{12}\tilde{\mathbf{K}}_{21})^k\right)\left(\sum_{l=0}^{\infty}(\tilde{\mathbf{K}}_{12}^*\tilde{\mathbf{K}}_{21}^*)^l\right) \\ &= \sum_{k,l=0}^{\infty}(\tilde{\mathbf{K}}_{12}\tilde{\mathbf{K}}_{21})^k(\tilde{\mathbf{K}}_{12}^*\tilde{\mathbf{K}}_{21}^*)^l \ .\end{aligned}$$

This leads to, for example,

$$\tilde{\mathbf{C}}_{12} \approx \sum_{k,l=0}^{\infty}(\tilde{\mathbf{K}}_{12}\tilde{\mathbf{K}}_{21})^k(\tilde{\mathbf{K}}_{12}^*\tilde{\mathbf{K}}_{21}^*)^l((\tilde{A}_2\tilde{\mathbf{J}}_{21})^*\tilde{\mathbf{C}}_{11}^0 + \tilde{A}_1\tilde{\mathbf{J}}_{12}\tilde{\mathbf{C}}_{22}^0) \ , \tag{3.2}$$

and similar expression for $\tilde{\mathbf{C}}_{21}$. These expressions can be interpreted in terms of paths through the graph which is in this case composed of just two cells [34].

When $k = 0$ and $l = 0$, we obtain the first term of this series, $(\tilde{A}_2\tilde{\mathbf{J}}_{21})^*\tilde{\mathbf{C}}_{11}^0 + \tilde{A}_1\tilde{\mathbf{J}}_{12}\tilde{\mathbf{C}}_{22}^0$. But $(\tilde{A}_2\tilde{\mathbf{J}}_{21})^*\tilde{\mathbf{C}}_{11}^0$ is just the cross-correlation, $\tilde{\mathbf{C}}_{12}$, in the unidirectionally coupled network of two EIF neurons discussed in Section 3.1.1. Similarly, $\tilde{A}_1\tilde{\mathbf{J}}_{12}\tilde{\mathbf{C}}_{22}^0$ is the cross-correlation $\tilde{\mathbf{C}}_{12}$ of the mirror image of this network formed by a single connection from cell 2 to cell 1. The cross-covariance is determined by this leading term when coupling is not too strong (See Figure 3.5). The other terms may matter if coupling is strong. This implies that the cross-covariances in a two-cell recurrent networks are approximately the sum of the cross-covariances of two unidirectionally coupled networks, which has already been noted by Ostojic and Brunel [50], as well as Trousdale [34], et al.

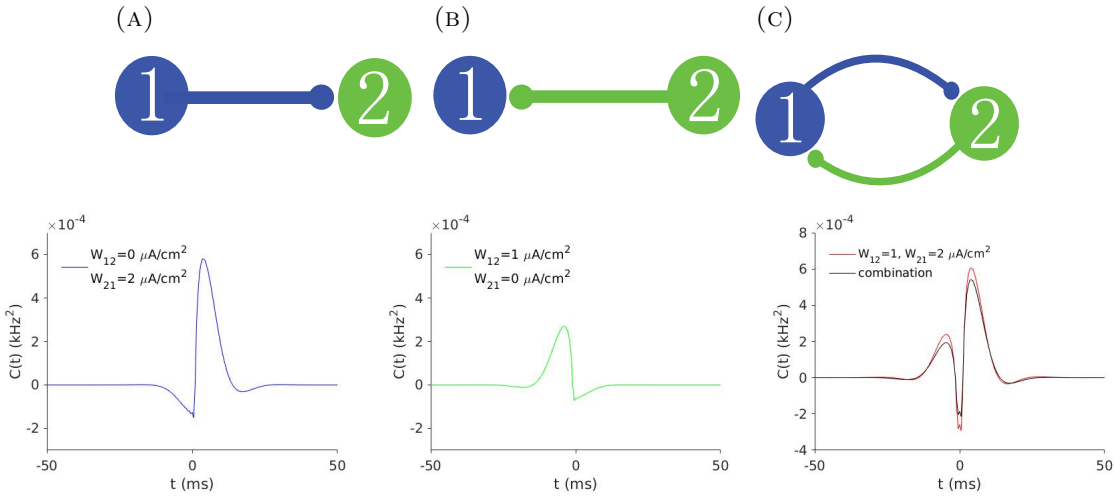

Figure 3.5: **Using leading order term to approximate the cross-covariances in two-cell recurrent networks. (A)** Cross-covariance for the two-cell network with a synaptic connection from cell 1 to cell 2. **(B)** Cross-covariance for the two-cell network with a synaptic connection from cell 2 to cell 1. **(C)** The red curve is the cross-covariance of the full circuit, while the sum of the cross-covariances in (A) and (B) is shown in black.

The top row of Figure 3.5 shows the two halves, and the full two-cell network: with only a synaptic connection from cell 1 to cell 2 (A); with a connection from cell 2 to cell 1 (B); the recurrent network (C). The bottom row shows the corresponding cross-covariances. Figure 3.5C bottom, shows that the cross-covariance of the full two-cell network (red) is well approximated by the sum of the two cross-covariances corresponding to the unidirectional networks (black). It is important to also note that this type of decomposition does not always work, for example when coupling is too strong.

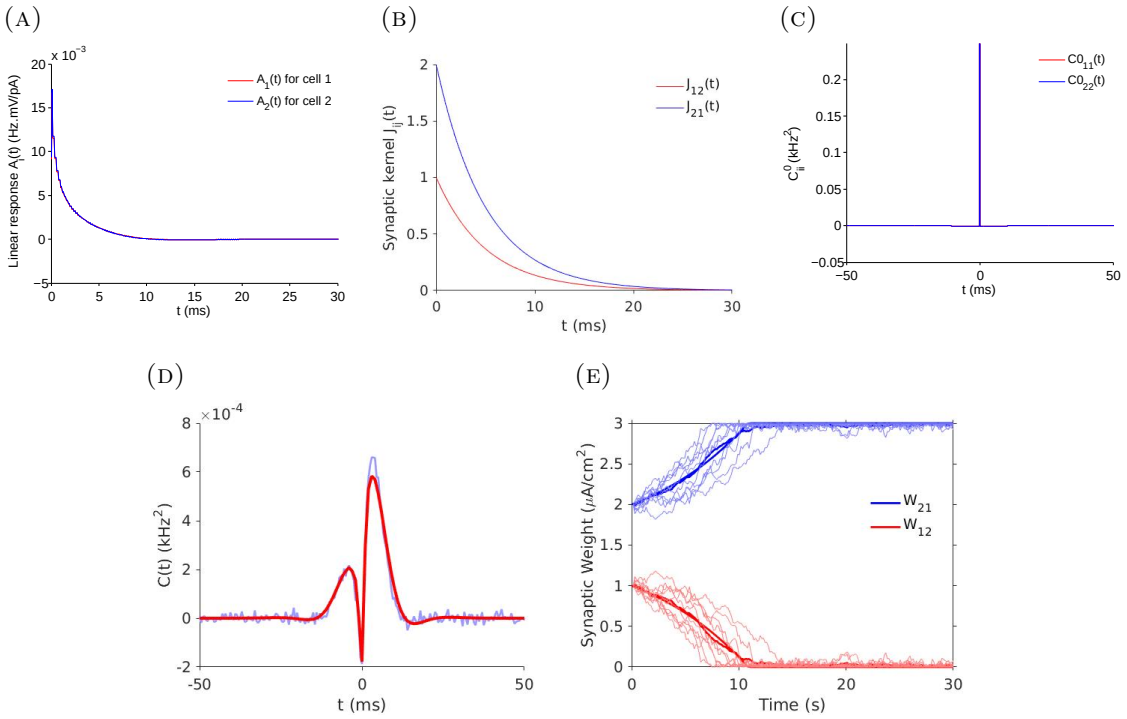

Figure 3.6: **Cross-covariance and learning under balanced Hebbian STDP rule for two-cell recurrent network. (A)** Here the red and blue curves are the linear response functions $A_1(t)$ and $A_2(t)$, respectively. **(B)** The red and blue curves are the synaptic kernels $\mathbf{J}_{12}(t)$ and $\mathbf{J}_{21}(t)$, respectively. **(C)** The red and blue curves are uncoupled auto-covariances $\mathbf{C}_{11}^0$ and $\mathbf{C}_{22}^0$, respectively. **(D)** Theoretical (red) and numerically (blue) obtained cross-covariance $\mathbf{C}_{21}(t)$. **(E)** Compared synaptic weights change curves. Red and blue curves correspond to $\mathbf{W}_{12}$ and $\mathbf{W}_{21}$, respectively. The thin curves again represent individual realizations.

Figure 3.6A shows the linear response functions $A_1(t)$ and $A_2(t)$. These are the same as the intrinsic properties of the two cells are equal – we chose the same parameters for this example. Figure 3.6B shows the synaptic kernels $\mathbf{J}_{12}(t)$ and $\mathbf{J}_{21}(t)$. The amplitude of $\mathbf{J}_{21}(t)$ is bigger than that of $\mathbf{J}_{12}(t)$, since $\mathbf{W}_{21} = 2\ \mu\text{A/cm}^2$ is greater than $\mathbf{W}_{12} = 1\ \mu\text{A/cm}^2$. Figure 3.6C shows the uncoupled auto-covariances, $\mathbf{C}_{11}^0$ and $\mathbf{C}_{22}^0$. These are again equal since the two cells are identical. Figure 3.6D

compares the cross-covariance $\mathbf{C}_{21}(t)$ obtained from simulations (blue) and theory (red). The peak with the higher amplitude is in the positive time domain, which is on the potentiation side of our Hebbian STDP rule (Figure 3.3B). With a symmetric learning rule this implies that potentiation of $\mathbf{W}_{21}$ is dominant, which will lead to an increase in $\mathbf{W}_{21}$, while $\mathbf{W}_{12}$ will decrease in time. Figure 3.6E shows $\mathbf{W}_{12}$ and $\mathbf{W}_{21}$ obtained using theory and simulations with a symmetric Hebbian STDP rule.

The asymmetry of the cross-covariances seen in Figure 3.5 and 3.6 is due to the different initial weights of the two synaptic connections. Asymmetric cross-covariances can also occur when the connection weights and firing rates are equal, but the intrinsic properties, as determined by the parameters μ and σ, differ between the cells. This is illustrated in Figure 3.7.

Here we fixed the baseline firing rate of both cells at 27 Hz. This occurs both when $\mu = 2$ mV and $\sigma = 9$ mV, and when $\mu = 2.37$ mV and $\sigma = 5$ mV (note that firing rates can be equal for different μ and σ values, as shown in Figure 2.1 and Table 2.1). We also set both synaptic weights to 2 μA/cm^2. We consider two cases: two cells with the same and two cells with different setting of the parameters μ and σ. When we use $\mu = 2$ mV and $\sigma = 9$ mV for both cells we have symmetric cross-covariances (Figure 3.7B). With $\mu = 2$ mV and $\sigma = 9$ mV for cell 1 and $\mu = 2.37$ mV and $\sigma = 5$ mV for cell 2 we see that the amplitude of the linear response function for cell 2 ($A_2(t)$ (blue)) is larger than that for cell 1 (Figure 3.7D). This means that, even when the baseline firing rates are equal, the cell with lower σ (or higher μ value) will have a linear response function of bigger amplitude. That is, lower noise makes a cell more sensitive to its inputs, and hence a larger peak in the linear response.

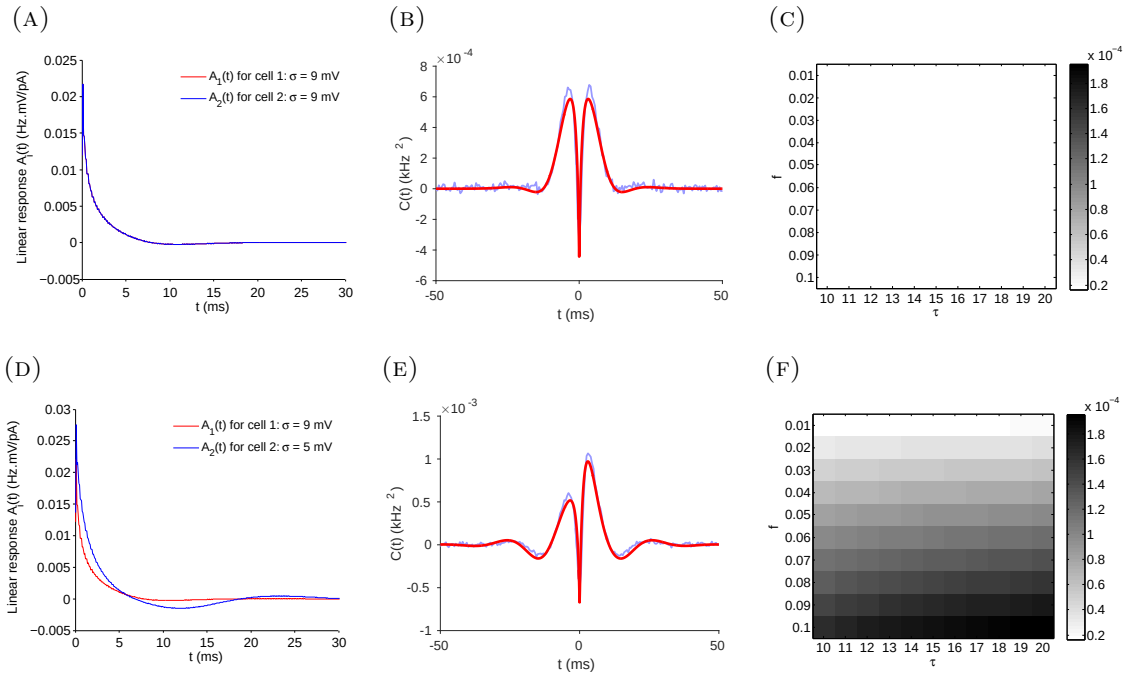

Figure 3.7: **Different intrinsic properties of neurons lead to asymmetric cross-covariances, and, in turn, affect the evolution of synaptic weights. (A,D)** Linear response functions for the two cells with the same setting and different setting respectively. **(B,E)** cross-covariance $\mathbf{C}_{21}(t)$ for the two cells with the same setting and different setting respectively. **(C,F)** Integrals of the product of cross-covariances $\mathbf{C}_{21}(t)$ and different learning rules for the two cells with the same setting and different setting respectively.

This difference in linear responses breaks the symmetry of the cross-covariances. With equal synaptic weights, $A_2(t)$ governs the peak of $\mathbf{C}_{21}(t)$ (spike times of cell 1 as reference) in the positive time domain while $A_1(t)$ controls the peak in the negative time domain. The amplitude of $A_2(t)$ is bigger than that of $A_1(t)$ implying the amplitude of the peak in the positive time domain will be bigger than that in the negative time domain. This leads to the asymmetry of the cross-covariances which is apparent in Figure 3.7E.

The shape of the cross-covariances affects the evolution of the synaptic weights. In the right column of Figure 3.7, we show the integrals of the product of corresponding cross-covariances and different learning rules. Here we used a balanced leaning rule with $f = f_+ = f_-$, $\tau = \tau_+ = \tau_-$, and varied f and τ. For symmetric cross-covariance, the integral is always 0. However, for asymmetric cross-covariances, it changes with f and τ. We can see that the integral increases with f and τ (Figure 3.7F). This implies that the learning rule with bigger amplitude (f) and broader shape (τ) will make the synaptic weight changes more sensitive to the cross-covariance.

In this case, under fixed baseline firing rate, the differences in the properties of the individual cells result in an asymmetric cross-covariance, and thus impact the evolution of their coupling weights according to the applied learning rule. Cross-covariances and learning rules shape the network structure together, and both are important here. However, the Poisson neuron model does not exhibit this behavior, as the properties of this neuron are determined by the baseline firing rate only.

3.1.3 Two EIF neurons with recurrent connections and common input

In a recurrent two-cell network with common input to the two cells, Eq.(2.9), gives the uncoupled auto-spectrum as:

$$\begin{aligned}\tilde{\mathbf{C}}^0 + \tilde{\mathbf{A}}\mathbf{C}^{ext}\tilde{\mathbf{A}}^* &= \begin{pmatrix} \tilde{\mathbf{C}}^0_{11} & 0 \\ 0 & \tilde{\mathbf{C}}^0_{22} \end{pmatrix} + cg_L^2D^2 \begin{pmatrix} \tilde{A}_1 & 0 \\ 0 & \tilde{A}_2 \end{pmatrix} \begin{pmatrix} \sigma_1^2 & \sigma_1\sigma_2 \\ \sigma_2\sigma_1 & \sigma_2^2 \end{pmatrix} \begin{pmatrix} \tilde{A}_1^* & 0 \\ 0 & \tilde{A}_2^* \end{pmatrix} \\ &= \begin{pmatrix} \tilde{\mathbf{C}}^0_{11} + cg_L^2D^2\sigma_1^2|\tilde{A}_1|^2 & cg_L^2D^2\sigma_1\sigma_2\tilde{A}_1\tilde{A}_2^* \\ cg_L^2D^2\sigma_1\sigma_2\tilde{A}_2\tilde{A}_1^* & \tilde{\mathbf{C}}^0_{22} + cg_L^2D^2\sigma_2^2|\tilde{A}_2|^2 \end{pmatrix}.\end{aligned}$$

Therefore,

$$\begin{aligned}&\begin{pmatrix} \tilde{\mathbf{C}}_{11} & \tilde{\mathbf{C}}_{12} \\ \tilde{\mathbf{C}}_{21} & \tilde{\mathbf{C}}_{22} \end{pmatrix} \\ \approx\ & \frac{1}{|1-\tilde{\mathbf{K}}_{12}\tilde{\mathbf{K}}_{21}|^2} \\ & \begin{pmatrix} 1 & \tilde{\mathbf{K}}_{12} \\ \tilde{\mathbf{K}}_{21} & 1 \end{pmatrix} \begin{pmatrix} \tilde{\mathbf{C}}^0_{11} + cg_L^2D^2\sigma_1^2|\tilde{A}_1|^2 & cg_L^2D^2\sigma_1\sigma_2\tilde{A}_1\tilde{A}_2^* \\ cg_L^2D^2\sigma_1\sigma_2\tilde{A}_2\tilde{A}_1^* & \tilde{\mathbf{C}}^0_{22} + cg_L^2D^2\sigma_2^2|\tilde{A}_2|^2 \end{pmatrix} \begin{pmatrix} 1 & \tilde{\mathbf{K}}^*_{21} \\ \tilde{\mathbf{K}}^*_{12} & 1 \end{pmatrix} \\ =\ & \frac{1}{|1-\tilde{\mathbf{K}}_{12}\tilde{\mathbf{K}}_{21}|^2} \begin{pmatrix} \tilde{\mathbf{C}}^0_{11} + |\tilde{\mathbf{K}}_{12}|^2\tilde{\mathbf{C}}^0_{22} + cg_L^2D^2P_1 & \tilde{\mathbf{K}}^*_{21}\tilde{\mathbf{C}}^0_{11} + \tilde{\mathbf{K}}_{12}\tilde{\mathbf{C}}^0_{22} + cg_L^2D^2P_2 \\ \tilde{\mathbf{K}}_{21}\tilde{\mathbf{C}}^0_{11} + \tilde{\mathbf{K}}^*_{12}\tilde{\mathbf{C}}^0_{22} + cg_L^2D^2P_3 & |\tilde{\mathbf{K}}_{21}|^2\tilde{\mathbf{C}}^0_{11} + \tilde{\mathbf{C}}^0_{22} + cg_L^2D^2P_4 \end{pmatrix},\end{aligned}$$

where

$$P_1 = \sigma_1^2|\tilde{A}_1|^2 + \sigma_1\sigma_2\tilde{A}_2\tilde{A}_1^*\tilde{\mathbf{K}}_{12} + \sigma_1\sigma_2\tilde{A}_1\tilde{A}_2^*\tilde{\mathbf{K}}_{12}^* + \sigma_2^2|\tilde{A}_2|^2|\tilde{\mathbf{K}}_{12}|^2 \ ,$$

$$P_2 = \sigma_1^2|\tilde{A}_1|^2\tilde{\mathbf{K}}_{21}^* + \sigma_1\sigma_2\tilde{A}_2\tilde{A}_1^*\tilde{\mathbf{K}}_{12}\tilde{\mathbf{K}}_{21}^* + \sigma_1\sigma_2\tilde{A}_1\tilde{A}_2^* + \sigma_2^2|\tilde{A}_2|^2\tilde{\mathbf{K}}_{12} \ ,$$

$$P_3 = \sigma_1^2|\tilde{A}_1|^2\tilde{\mathbf{K}}_{21} + \sigma_1\sigma_2\tilde{A}_2\tilde{A}_1^* + \sigma_1\sigma_2\tilde{A}_1\tilde{A}_2^*\tilde{\mathbf{K}}_{21}\tilde{\mathbf{K}}_{12}^* + \sigma_2^2|\tilde{A}_2|^2\tilde{\mathbf{K}}_{12}^* \ ,$$

$$P_4 = \sigma_1^2|\tilde{A}_1|^2|\tilde{\mathbf{K}}_{21}|^2 + \sigma_1\sigma_2\tilde{A}_2\tilde{A}_1^*\tilde{\mathbf{K}}_{21}^* + \sigma_1\sigma_2\tilde{A}_1\tilde{A}_2^*\tilde{\mathbf{K}}_{21} + \sigma_2^2|\tilde{A}_2|^2 \ .$$

Thus,

$$\tilde{\mathbf{C}}_{12} \approx \frac{(\tilde{A}_2\tilde{\mathbf{J}}_{21})^*\tilde{\mathbf{C}}_{11}^0 + \tilde{A}_1\tilde{\mathbf{J}}_{12}\tilde{\mathbf{C}}_{22}^0 + cg_L^2D^2P_2}{|1 - \tilde{A}_1\tilde{\mathbf{J}}_{12}\tilde{A}_2\tilde{\mathbf{J}}_{21}|^2}$$

and

$$\tilde{\mathbf{C}}_{21} \approx \frac{\tilde{A}_2\tilde{\mathbf{J}}_{21}\tilde{\mathbf{C}}_{11}^0 + (\tilde{A}_1\tilde{\mathbf{J}}_{12})^*\tilde{\mathbf{C}}_{22}^0 + cg_L^2D^2P_3}{|1 - \tilde{A}_1\tilde{\mathbf{J}}_{12}\tilde{A}_2\tilde{\mathbf{J}}_{21}|^2} \ .$$

Common input thus modifies the uncoupled cross-spectrum $\tilde{\mathbf{C}}^0$ and therefore increases the uncoupled auto-covariances. These will lead to an increase in the amplitude in the cross-covariances compared with the ones without common input.

Similar as Eq.(3.2), we can rewrite $\tilde{\mathbf{C}}_{12}$ in the form of series,

$$\tilde{\mathbf{C}}_{12} \approx \sum_{k,l=0}^{\infty}(\tilde{\mathbf{K}}_{12}\tilde{\mathbf{K}}_{21})^k(\tilde{\mathbf{K}}_{12}^*\tilde{\mathbf{K}}_{21}^*)^l((\tilde{A}_2\tilde{\mathbf{J}}_{21})^*\tilde{\mathbf{C}}_{11}^0 + \tilde{A}_1\tilde{\mathbf{J}}_{12}\tilde{\mathbf{C}}_{22}^0 + cg_L^2D^2P_2) \ .$$

The leading term in this series is $(\tilde{A}_2\tilde{\mathbf{J}}_{21})^*\tilde{\mathbf{C}}^0_{11} + \tilde{A}_1\tilde{\mathbf{J}}_{12}\tilde{\mathbf{C}}^0_{22} + cg_L^2D^2P_2$. In this leading term, the summand $(\tilde{A}_2\tilde{\mathbf{J}}_{21})^*\tilde{\mathbf{C}}^0_{11}$ is just the cross-covariance $\tilde{\mathbf{C}}_{12}$ of the network formed by two EIF neurons with a synaptic connection from cell 1 to cell 2, but without common input. $\tilde{A}_1\tilde{\mathbf{J}}_{12}\tilde{\mathbf{C}}^0_{22}$ is $\tilde{\mathbf{C}}_{12}$ of the network for reversed case (connection from cell 2 to cell 1 without common input). The last summand, $cg_L^2D^2P_2$, contains the term $cg_L^2D^2\sigma_1\sigma_2\tilde{A}_1\tilde{A}_2^*$, which is the cross-covariance $\tilde{\mathbf{C}}_{12}$ between cell 1 and cell 2 with common input in the absence of synaptic connections between the cells.

Thus, we can approximate the cross-covariances of a recurrent, two-cell network with common input by combining the cross-covariances of two unidirectional circuits, and one with common input (See Figure 3.8).

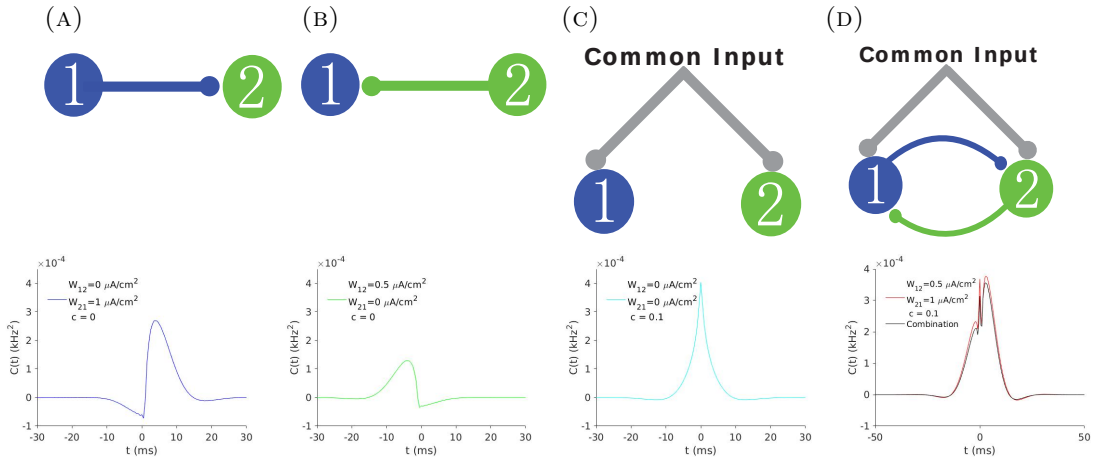

Figure 3.8: **Approximation of the cross-covariances in a two-cell recurrent network with common input. (A)** Cross-covariance of two-cell network with a synaptic connection from cell 1 to cell 2. **(B)** Cross-covariance of two-cell network with a synaptic connection from cell 2 to cell 1. **(C)** Cross-covariance of two-cell network without connections, but with common input to both cells. **(D)** Red curve is the cross-covariances of two-cell recurrent network with common input. The black curve is the combination of cross-covariances in (A), (B) and (C).

Figure 3.8 is similar to the Figure 3.5 in the previous section. The figure illustrates that in a two-cell recurrent network with common input, we can also use the cross-covariances of simpler, uni-directional circuits, along with the cross-covariance generated by the common input to approximate the full cross-covariance.

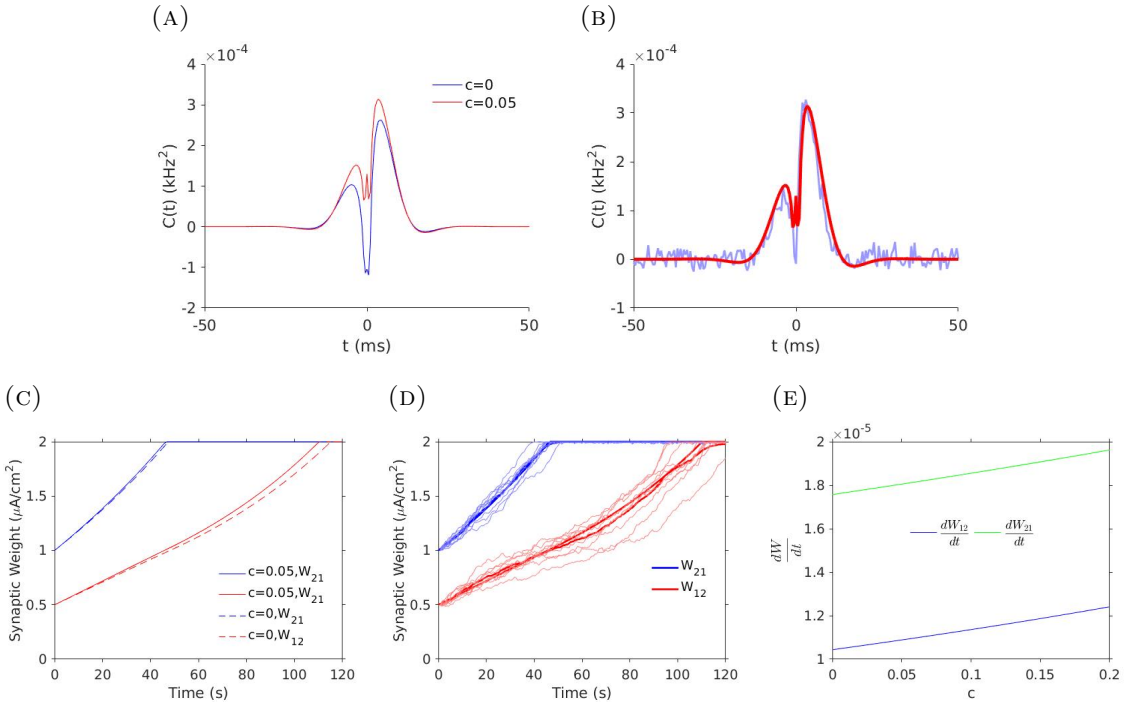

Figure 3.9: **Cross-covariances and synaptic weight dynamics under balanced Hebbian STDP in a two-cell, recurrently coupled network with common input. (A)** Cross-covariances between the cells with (red) and without (blue) common input. **(B)** Comparison of cross-covariance with common input (red curve in (A)) obtained analytically and numerically. **(C)** Theoretical weight changes for two-cell recurrent network with (solid lines) and without (dash lines) common input. **(D)** Matched weight changes for two-cell recurrent network with common input (solid lines in (C)). **(E)** The first iteration of $\frac{dW}{dt}$ for two-cell recurrent network according to c value.

Figure 3.9A shows the cross-covariances for two-cell recurrent network with (red) and without (blue) common input. Here we set $c = 0.05$. We can see that the cross-covariance of the case with common input has bigger amplitude. And this change in cross-covariance will affect the learning according to the learning rule. For the same learning rule, cross-covariance with bigger amplitude will lead to faster learning. Figure 3.9B shows that the cross-covariance obtained using Eq.(2.9) is a good approximation to those obtained from direct simulations. Figure 3.9C shows the theoretical weight changes for two-cell recurrent network with (solid lines) and without (dash lines) common input under the same potentiation dominated Hebbian STDP rule (here we set $f_+ = 0.005, f_- = 0.004$ and $\tau_+ = \tau_-$). We can see that the solid lines reach the boundaries (maximal synaptic weights) faster. This implies the learning speed of networks with common input is faster than that without common input under the same learning rule. Figure 3.9D is the weight changes for two-cell recurrent network with common input (solid lines in bottom left) got by Eq.(2.6) and direct simulations. In Figure 3.9E, we plot the first iteration of $\frac{dW}{dt}$ according to change of c by fixing the initial network structure and learning rule. We can see that both $\frac{dW_{12}}{dt}$ and $\frac{dW_{21}}{dt}$ increase with c. This implies that increase common input will make changes in the weights faster.

3.2 The effects of cross-covariances and learning rules

We have shown that the cross-covariances determine the evolution of weights in networks. Eq.(2.6) shows that to approximate weight change dynamics requires computing the cross-covariances, and using them in conjunction with the learning rules. We next illustrate the effects of these two components separately.

We consider a two-cell recurrent network with identical cells, equal weights ($W_{12} = W_{21} = 2$ (μA/cm^2)) and baseline firing rates (about 27 Hz). We choose 6 different $\mu - \sigma$ pairs which result in the same baseline firing rate with σ ranging from 3 mV to 8 mV. The corresponding linear response functions and cross-covariances are shown in Figure 3.10. The linear response functions of network with pair for lower σ value (or higher μ value) have more oscillation, which is reflected in the corresponding cross-covariances. What's more, the cross-covariances with lower σ value (or higher μ value) have bigger amplitude. This is again due to the higher sensitivity of less noisy cells to input.

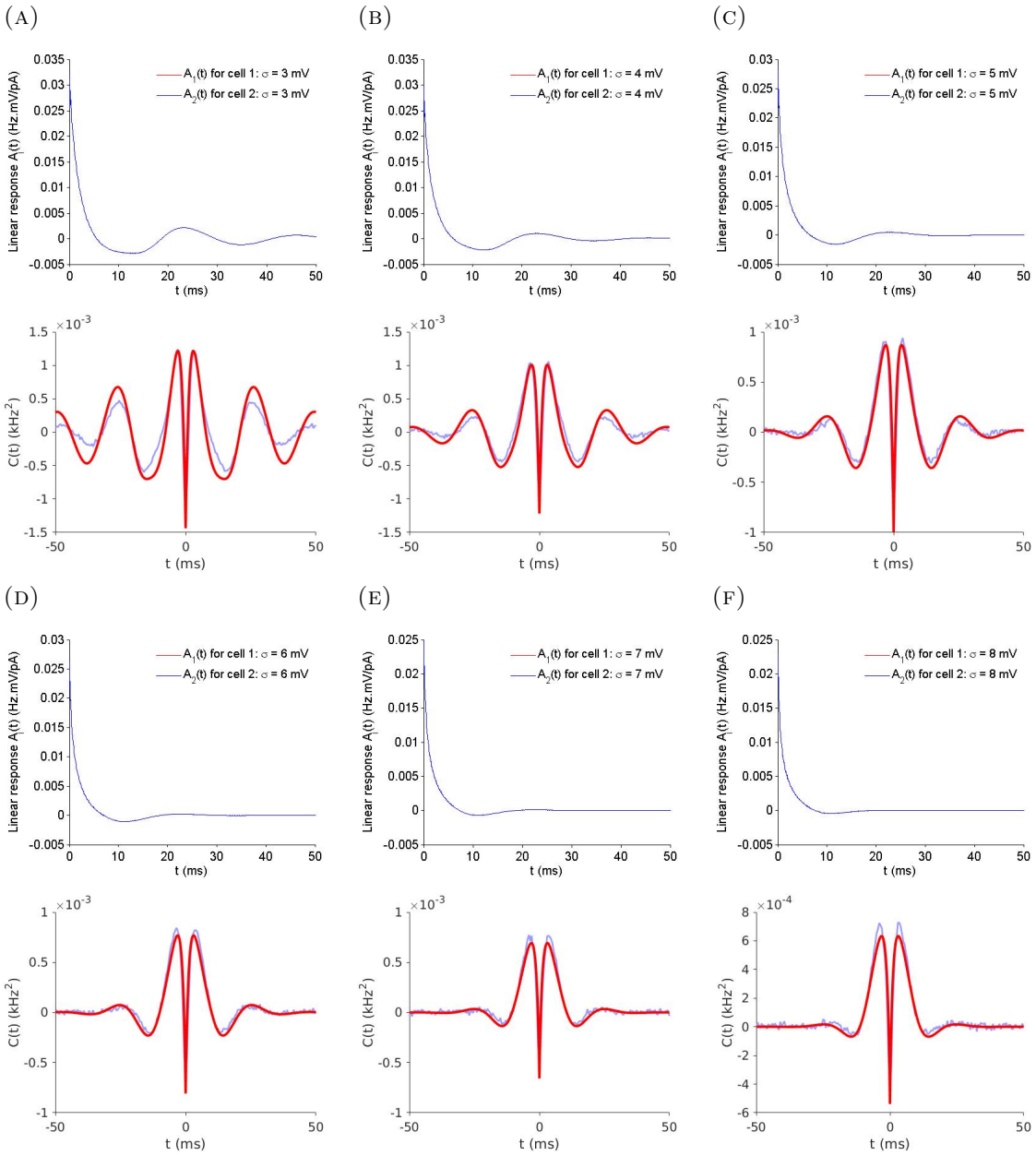

Figure 3.10: **The linear response functions and cross-covariances for two-cell recurrent networks with same baseline firing rate but different $\mu - \sigma$ settings. (A-F)** Linear response functions (top) and cross-covariances (bottom) for two-cell recurrent networks with σ varying from 3 mV to 8 mV. For the cross-covariances, blue lines show the results of simulation, while the red lines show the theoretical predictions.

We use a balanced Hebbian STDP rule for the networks (see Figure 3.11).

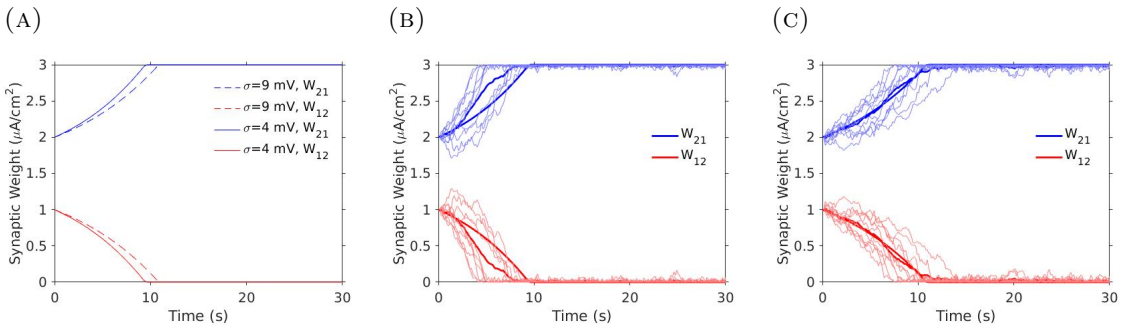

Figure 3.11: **Weights changes in two-cell recurrent networks with different σ value but same baseline firing rate.** The fixed baseline firing rate is about 27 Hz. We set $W_{12} = 1$ (μA/cm^2) and $W_{21} = 2$ (μA/cm^2) initially. **(A)** Theoretical weight changes for two-cell recurrent networks with $\sigma = 4$ (solid lines) and 9 mV (dash lines) respectively. **(B)** Comparison of numerically and theoretically obtained weight change dynamics for $\sigma = 4$ mV (solid lines in (A)). **(C)** Comparison of numerically and theoretically obtained weight change dynamics for $\sigma = 9$ mV (dash lines in (A)).

Figure 3.11A shows the evolution of the weights predicted by Eq.(2.6). Figure 3.11B shows the synaptic weight changes for $\sigma = 4$ mV while Figure 3.11C is for $\sigma = 9$ mV. Weight changes are faster in the network with lower σ value (or higher μ value), even thought the rates in both cases are equal. As we have discussed above, this is due to the higher amplitude of their cross-covariances when direct input dominates. A more obvious example is shown in Figure 3.12.

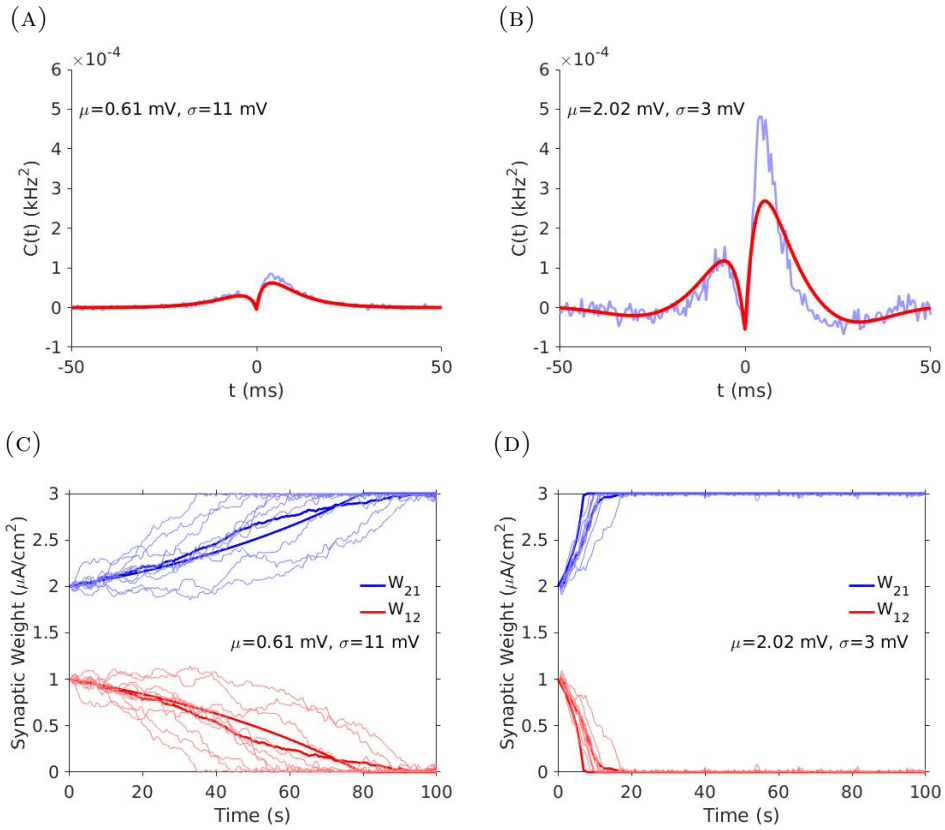

Figure 3.12: **Another example for weights changes in two-cell recurrent networks with different σ value but same baseline firing rate.** Here the fixed baseline firing rate is about 7.6 Hz. **(A)** Comparison of numerically and theoretically obtained cross-covariance for $\sigma = 11$ mV. **(B)** Comparison of numerically and theoretically obtained cross-covariance for $\sigma = 3$ mV. **(C)** Comparison of numerically and theoretically obtained weight change dynamics for $\sigma = 11$ mV. **(D)** Comparison of numerically and theoretically obtained weight change dynamics for $\sigma = 3$ mV.

To illustrate the effects of different learning rules we compare a balanced (symmetric), and asymmetric Hebbian STDP rules in a network with $\sigma = 9$ mV. The results are shown in Figure 3.13, while the corresponding phase planes (vector fields) are shown in Figure 3.14. We chose the same initial weights in these simulations. Under a symmetric learning rule, one of the weights is potentiated, while the other

depressed. However, under asymmetric learning rule, both of them are potentiated. Thus different learning rules can lead to different network dynamics.

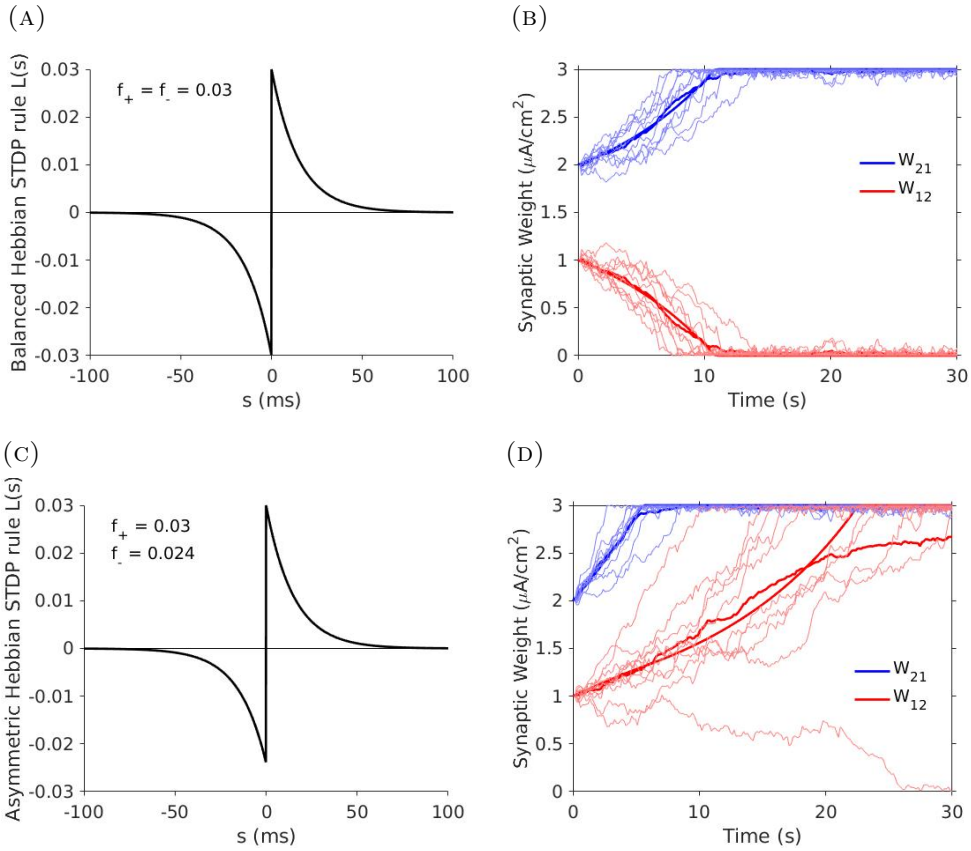

Figure 3.13: **Effects for different learning rules. (A)** Symmetric (balanced) Hebbian STDP function we choose. **(B)** Compared weight changes for two-cell recurrent network under the learning rule in (A). **(C)** Asymmetric (potentiation dominated) Hebbian STDP function we choose. **(D)** Compared weight changes for two-cell recurrent network under the learning rule in (C).

For a two-cell recurrent network, according to Eq.(2.6), the following system of equations governs the evolution of the weights,

$$\begin{cases} \frac{d\mathbf{W}_{12}}{dt} = \int_{-\infty}^{+\infty} \Delta\mathbf{W}_{12}(s)(\mathbf{C}_{12}(s) + r_1 r_2)ds \\ \frac{d\mathbf{W}_{21}}{dt} = \int_{-\infty}^{+\infty} \Delta\mathbf{W}_{21}(s)(\mathbf{C}_{21}(s) + r_2 r_1)ds \end{cases} .$$

The phase planes for two-cell recurrent networks (like Figure 3.14) are obtained using these equations. For an initial value of the weights $(\mathbf{W}_{12}, \mathbf{W}_{21})$, the related phase plane shows what values will $(\mathbf{W}_{12}, \mathbf{W}_{21})$ attain under certain learning rule. Here we follow the idea of Babadi and Abbott [4] in analyzing the phase planes.

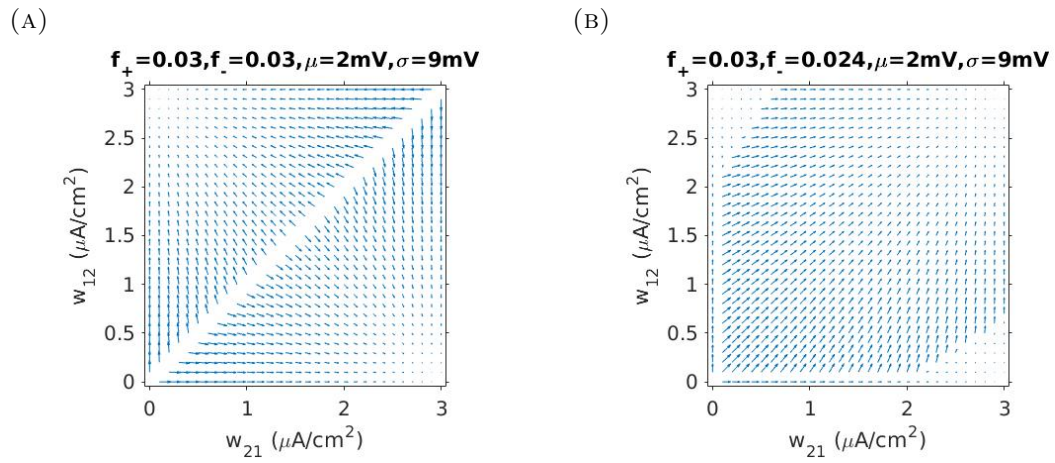

Figure 3.14: **Phase planes for Figure 3.13. (A)** Phase plane under balanced (symmetric) Hebbian STDP rule (Figure 3.13A). There are two stable fixed points, (3,0) and (0,3). **(B)** Phase plane under asymmetric Hebbian STDP rule (Figure 3.13C). There are three stable fixed points, (3,0), (0,3) and (3,3).

Here we set the upper bound of the synaptic weights at 3 (μA/cm^2). Figure 3.14A shows the phase plane in the case of a balanced (symmetric) Hebbian STDP rule while Figure 3.14B is for asymmetric learning rule. In the balanced case, there are two stable fixed points (3,0) and (0,3), while the unstable fixed points are on the diagonal line. Almost all initial weight values result in trajectories that are driven to these two fixed points. In the asymmetric case, a new stable fixed point at (3,3) emerges. For the parameters we chose, most initial weights will result in trajectories that converge to this point. This explains the different dynamics of the weights under these two leaning rule. Initially we set the weights $(\mathbf{W}_{12}, \mathbf{W}_{21}) = (1, 2)$, under symmetric learning rule, they will go to fixed point (0,3) (Figure 3.13B). However, under asymmetric learning rule, they go to fixed point (3,3) (Figure 3.13D). This implies that the asymmetric learning rule leads to a asymmetric final state, while the symmetric learning rule leads to a symmetric final state.

We next illustrate the effects of the shapes of cross-covariances. We begin with the case of unequal baseline firing rates for different networks. Here we apply asymmetric Hebbian STDP rule on the two-cell recurrent networks. The cells from the two networks have the same μ value (μ=2 mV) but different levels of noise (σ=9 and 20 mV respectively). In this case, cells with σ=9 mV have baseline firing rate about 27 Hz, while cells with σ=20 mV have baseline firing rate about 52 Hz. The results are shown in Figure 3.15 while the corresponding phase planes are in Figure 3.16.

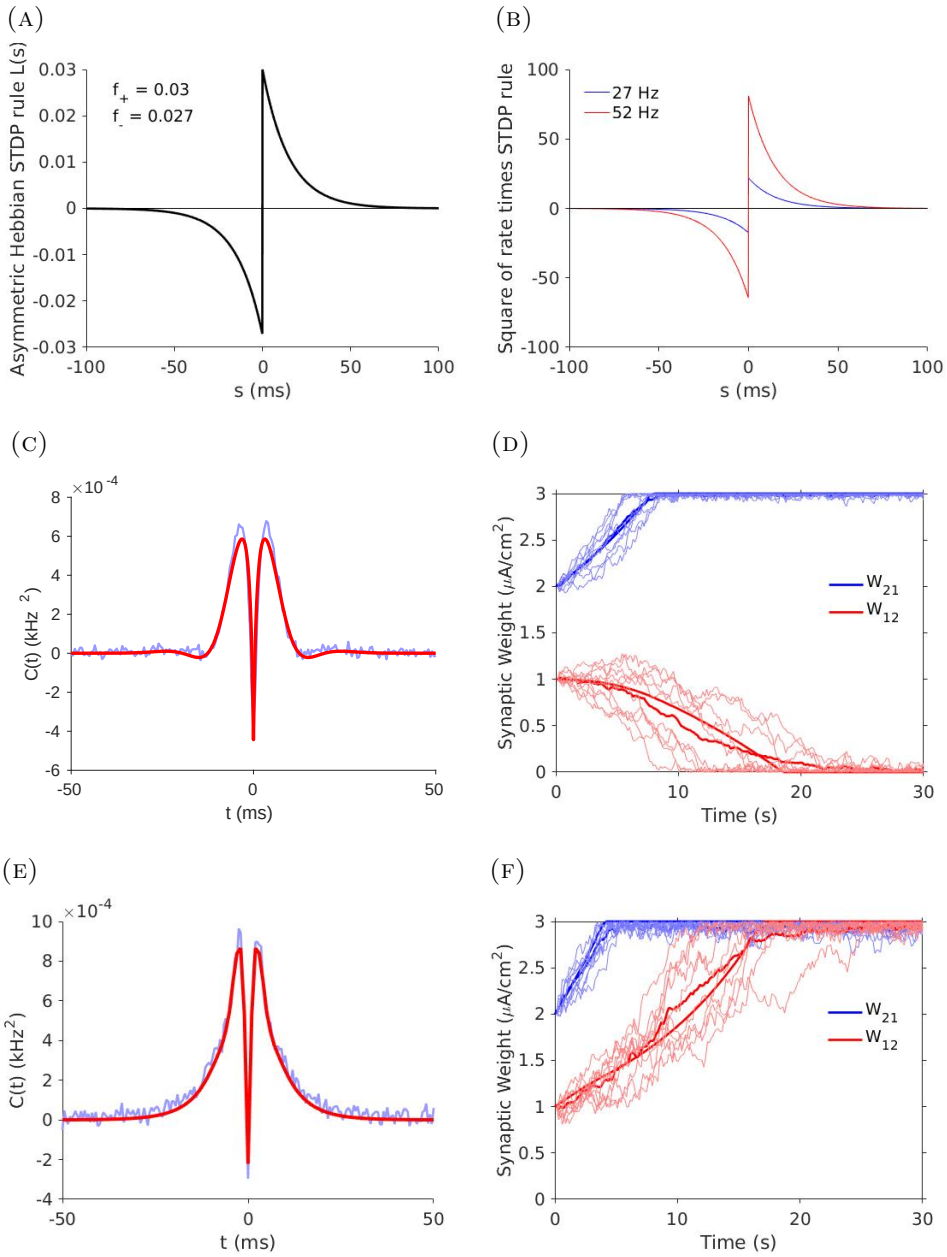

Figure 3.15: **Effects for different cross-covariances under different baseline firing rates. (A)** The selected asymmetric (potentiation dominated) Hebbian STDP function. **(B)** Square of baseline firing rate times learning rule in (A) ($r_i r_j L(s)$ and $r_i = r_j$ in Eq.(3.3)) for $\sigma = 9$ mV (blue) and $\sigma = 20$ mV (red) respectively. **(C)** Compared cross-covariances for $\sigma = 9$ mV. **(D)** Compared weights changes curves for $\sigma = 9$ mV under the learning rule in (A). **(E)** Compared cross-covariances for $\sigma = 20$ mV. **(F)** Compared weights changes curves for $\sigma = 20$ mV under the learning rule in (A).

Figure 3.15B shows that square of baseline firing rate times learning rule ($r_i r_j L(s)$ and $r_i = r_j$ in Eq.(3.3)) for $\sigma = 9$ mV (blue) and $\sigma = 20$ mV (red) respectively. When the difference of the baseline firing rates is large, the difference of these products ($r_i r_j L(s)$) is also large, as is the difference of the integrals of the products. These difference will be reflected in the evolution of the synaptic weights. Figure 3.15C illustrates the case $\sigma = 9$ mV while Figure 3.15E shows the case $\sigma = 20$ mV. Here we can see that the shape of the cross-covariance with higher sigma value is broader under fixing μ value. Figure 3.15D and F are for the corresponding weights changes curves. For the same learning rule, we have different dynamics for these two networks: one weight is potentiated while another is depressed for lower σ value; both of the weights are potentiated for higher σ value. Here the difference of network dynamics is mainly due to the different baseline firing rates. We will show that we can also get different network dynamics under same learning rule and fixed baseline firing rate (Figure 3.20).

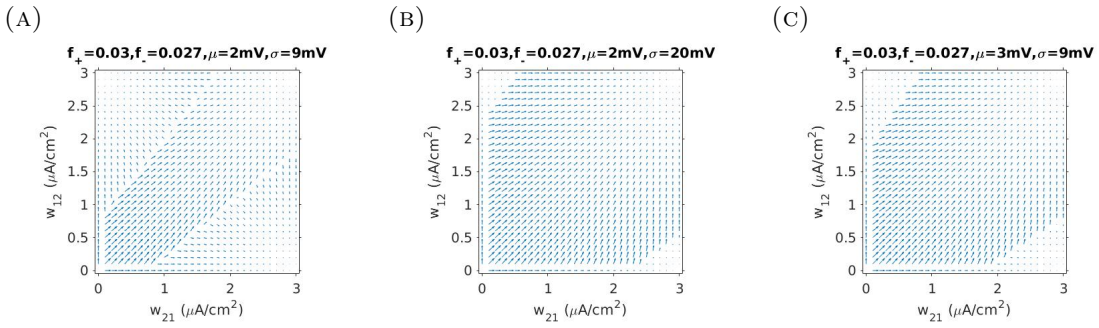

Figure 3.16: **Phase planes related to Figure 3.15. (A)** Phase plane for $\sigma = 9$ mV under the learning rule in Figure 3.15A. **(B)** Phase plane for $\sigma = 20$ mV under the learning rule in Figure 3.15A. **(C)** Phase plane for $\sigma = 9$ mV and $\mu = 3$ mV under the learning rule in Figure 3.15A.

Figure 3.16A shows the phase plane when noise is smaller, that is $\sigma = 9$ mV, while Figure 3.16B is for higher σ ($\sigma = 20$ mV) under the same asymmetric learning rule. We can see that these two phase planes have the same stable fixed points (3,0), (0,3) and (3,3). However, the region of initial weights which converge to the fixed point (3,3) for bigger σ is much larger than that for smaller σ. Thus, under this same asymmetric learning rule, the initial weights $(\mathbf{W}_{12}, \mathbf{W}_{21}) = (1, 2)$ will go to the fixed point (0,3) in the low σ case (Figure 3.15C), and to the fixed point (3,3) for higher σ (Figure 3.15E). The main reason is the baseline firing rates. For $\mu = 2$ mV and $\sigma = 9$ mV, the baseline firing rate is about 27 Hz. It becomes to about 52 Hz for $\mu = 2$ mV and $\sigma = 20$ mV. In Figure 3.16C, we fix $\sigma = 9$ mV and increase μ from 2 mV to 3 mV. In this case, the baseline firing rate is about 52 Hz. We obtain a similar phase plane as in Figure 3.16B. Increasing the baseline firing rate will increase the basin of attraction for the fixed point (3,3).

We next use an analytical approach to understand these observations. According to Section 2.2, for simplification, we can rewrite the Hebbian STDP learning (Eq.(2.2)) rule as

$$L(s) = \begin{cases} \mathbf{W}_{ij}^0 \mathcal{H}(W^{max} - \mathbf{W}_{ij}) f_+ e^{-\frac{|s|}{\tau_+}} , & \text{if } s \geq 0 \\ \mathbf{W}_{ij}^0 \mathcal{H}(\mathbf{W}_{ij})(-f_-) e^{-\frac{|s|}{\tau_-}} , & \text{if } s < 0 \end{cases} .$$

For the recurrent connected two cells i and j ($i \leftrightarrow j$), the two weights $\mathbf{W}_{ij}$ and

$\mathbf{W}_{ji}$ always exist initially. So we have $\mathbf{W}_{ij}^0 = \mathbf{W}_{ji}^0 = 1$. Then

$$L(s) = \begin{cases} \mathcal{H}(W^{max} - \mathbf{W}_{ij}) f_+ e^{-\frac{s}{\tau_+}} , & \text{if } s \geq 0 \\ -\mathcal{H}(\mathbf{W}_{ij}) f_- e^{\frac{s}{\tau_-}} , & \text{if } s < 0 \end{cases} .$$

The theoretical weight changes due to the learning rule is

$$\begin{aligned} \frac{d\mathbf{W}_{ij}}{dt} &= \int_{-\infty}^{+\infty} L(s)(\mathbf{C}_{ij}(s) + r_i r_j) ds \qquad (3.3) \\ &= \int_{-\infty}^{+\infty} L(s)\mathbf{C}_{ij}(s) ds + r_i r_j \int_{-\infty}^{+\infty} L(s) ds \\ &= \underbrace{f_+ \int_0^{+\infty} \mathcal{H}(W^{max} - \mathbf{W}_{ij}) e^{-\frac{s}{\tau_+}} \mathbf{C}_{ij}(s) ds}_{A} - \underbrace{f_- \int_{-\infty}^{0} \mathcal{H}(\mathbf{W}_{ij}) e^{\frac{s}{\tau_-}} \mathbf{C}_{ij}(s) ds}_{B} \\ &\quad + \underbrace{r_i r_j \int_{-\infty}^{+\infty} L(s) ds}_{C} \\ &= A - B + C . \end{aligned}$$

3.2.1 Symmetric learning rules

For the symmetric (balanced) Hebbian STDP learning rule, that is when $f_+ = f_-$ and $\tau_+ = \tau_-$ in Eq.(2.2), we have $\int_{-\infty}^{+\infty} L(s) ds = 0$ and $C = 0$ in Eq.(3.3). In this case, if $\mathbf{W}_{ij} = \mathbf{W}_{ji}$ initially, we have $\mathbf{C}_{ij}(s) = \mathbf{C}_{ji}(s)$ and both of them are symmetric with respect to the zero time axis ($s = 0$). Therefore, $A = B$ and $\frac{d\mathbf{W}_{ij}}{dt} = 0$ in Eq.(3.3), which implies that both synaptic weights will not change (See Figure

3.14A where the diagonal consists of unstable fixed points). However, if the initial synaptic weights are not equal, *e.g.* $\mathbf{W}_{ij} > \mathbf{W}_{ji}$, the amplitude of the peak of $\mathbf{C}_{ij}(s)$ in the positive time domain (potentiation side of the learning rule) will be larger than that in the negative time domain (depression side of the learning rule). We therefore obtain an asymmetric cross-covariance which drives the change in synaptic weight for this case. In this case, $A > B$, $\frac{d\mathbf{W}_{ij}}{dt} > 0$ in Eq.(3.3) and $\mathbf{W}_{ij}$ increases while $\mathbf{W}_{ji}$ decreases (note $\mathbf{C}_{ji}(s) = \mathbf{C}_{ij}(-s)$). Therefore, larger initial weights are potentiated and smaller initial weights depressed.

3.2.2 Asymmetric learning rules

We next consider one type of asymmetric learning rules, the potentiation dominated Hebbian STDP learning rules. The key difference between such rules and the symmetric rules is that $\int_{-\infty}^{+\infty} L(s)ds > 0$ and thus $C > 0$ in Eq.(3.3).

We can compute the term C explicitly.

$$C = r_i r_j \left[f_+ \int_0^{+\infty} \mathcal{H}(W^{max} - \mathbf{W}_{ij}) e^{-\frac{s}{\tau_+}} ds - f_- \int_{-\infty}^{0} \mathcal{H}(\mathbf{W}_{ij}) e^{\frac{s}{\tau_-}} ds \right] .$$

The learning rules modify the weights when $0 < \mathbf{W}_{ij} < W^{max}$, *i.e.* when $\mathcal{H}(W^{max} - \mathbf{W}_{ij}) = \mathcal{H}(\mathbf{W}_{ij}) = 1$. In this case,

$$C = r_i r_j \left(f_+ \int_0^{+\infty} e^{-\frac{s}{\tau_+}} ds - f_- \int_{-\infty}^{0} e^{\frac{s}{\tau_-}} ds \right) = r_i r_j (f_+ \tau_+ - f_- \tau_-) .$$

Note that the magnitudes of cross-covariances we considered are around $10^{-4} \sim 10^{-3}$ (kHz^2), while the baseline firing rates (r_i, r_j) are around $10 \sim 20$ (Hz). For the learning rules such that

$$f_+\tau_+ - f_-\tau_- \neq 0 \ ,$$

we have

$$|C| \gg |A| \ \text{ and } \ |C| \gg |B| \ .$$

If we choose a potentiation dominated Hebbian STDP learning rule by setting $f_+ > f_-$ and $\tau_+ = \tau_- = \tau$ in Eq.(2.2), for fixed baseline firing rates of all the neurons $(r_i = r_j = r)$ in the networks, we have

$$C = r^2\tau(f_+ - f_-) > 0 \ ,$$

and thus contribution from C in Eq.(3.3) is positive for all such networks.

When $\mathbf{W}_{ij} = \mathbf{W}_{ji}$, $A > B$ for $f_+ > f_-$, even if both of $\mathbf{C}_{ij}(s)$ and $\mathbf{C}_{ji}(s)$ are symmetric with respect to the zero time axis ($s = 0$). In addition, $C > 0$, $\frac{d\mathbf{W}_{ij}}{dt} > 0$ and both of $\mathbf{W}_{ij}$ and $\mathbf{W}_{ji}$ will be potentiated. This implies that (W^{max}, W^{max}) is a fixed point (Figure 3.14B).

When the two weights are not equal, the larger will be potentiated. The smaller one, if the difference between it and the bigger one is not large (the cross-covariances does not change much compared to the case of equal synaptic weights), we may

have $A - B + C > 0$ for $f_+ > f_-$ and $C > 0$. In this case, the weaker synaptic weight also gets potentiated. With fixed neuron properties (σ and μ), the basin of attraction of the stable fixed point (W^{max}, W^{max}) in the phase plane is determined by the difference between f_+ and f_-. The larger this difference, the larger the basin of attraction.

If we fix the potentiation dominated learning rule and increase the baseline firing rates of both cells (r_i and r_j) by increasing σ or μ, part C can increase dramatically, and make a larger contribution, or even dominate in Eq.(3.3). Both of the initial weights will be potentiated due to the high positive C value. This leads to the increase of the basin of attraction for the stable fixed point (W^{max}, W^{max}) in the phase plane (Figure 3.16).

We can also build the potentiation dominated Hebbian STDP learning rules by setting $f_+ = f_- = f$ and $\tau_+ > \tau_-$ in Eq.(2.2). In this case, for fixed baseline firing rate (r) of all the neurons in the networks, we have

$$C = r^2 f(\tau_+ - \tau_-) > 0$$

is also a positive constant.

With a fixed baseline firing rate, the cross-covariances between neurons will not change much when varying μ and σ (for fixed weights between neurons). The changes in cross-covariances will change the values of A and B a bit. However, comparing with the high positive constant C, such changes are very small and affect the phase planes of the weights only a little. This means the basin of attraction in the phase

planes are mainly determined by the C value for such potentiation dominated learning rules (Figure 3.17).

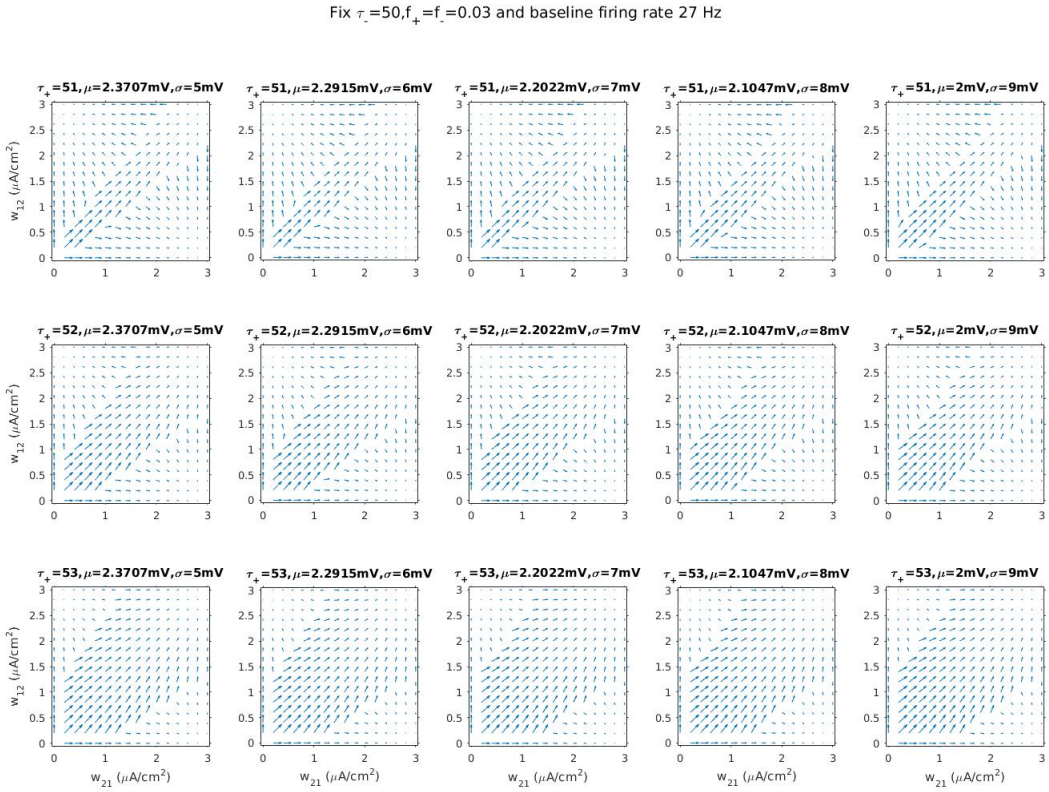

Figure 3.17: **Phase planes for small differences between τ_+ and τ_-.**

The different rows of Figure 3.17 show that phase planes change little when we vary μ and σ (change the cross-covariances). The small differences are in the boundaries of different basins of attraction.

If the difference between τ_+ and τ_- in the potentiation dominated learning rule is sufficiently large, then C will dominate the changes in weights, so that $\frac{d\mathbf{W}_{ij}}{dt}$ can never be negative, no matter how the cross-covariances change. In this case, initial $(W_{12}, W_{21}) = (a, 0)$ will go to $(W^{max}, 0)$, initial $(W_{12}, W_{21}) = (0, b)$ will go to $(0, W^{max})$ and initial $(W_{12}, W_{21}) = (a, b)$ will go to (W^{max}, W^{max}) with $a, b > 0$ (Figure 3.18).

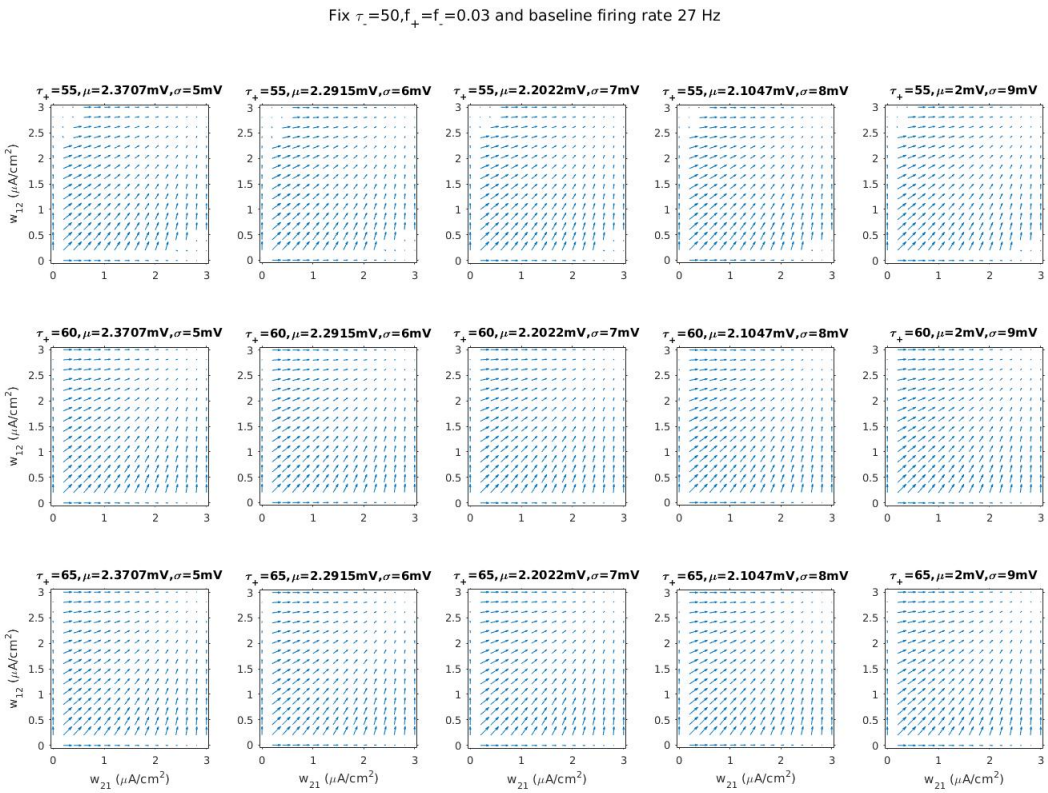

Figure 3.18: **Phase planes for big differences between τ_+ and τ_-.**

For fixed baseline firing rate (r), if we want to increase the effect of cross-covariances, we need to decrease the effect of part C:

$$C = r^2(f_+\tau_+ - f_-\tau_-) \ .$$

The direct way is setting the learning rule so that

$$C = r^2(f_+\tau_+ - f_-\tau_-) = 0 \iff f_+\tau_+ = f_-\tau_- \ .$$

Here we fix f_- and τ_-, and we change f_+ and τ_+ to make sure that $f_+\tau_+ = f_-\tau_-$. Note that here we ignore the balanced (symmetric) case: $f_+ = f_-$ and $\tau_+ = \tau_-$. Then we check the phase planes by varying μ and σ (change the cross-covariances under the same baseline firing rate). They are illustrated in Figure 3.19.

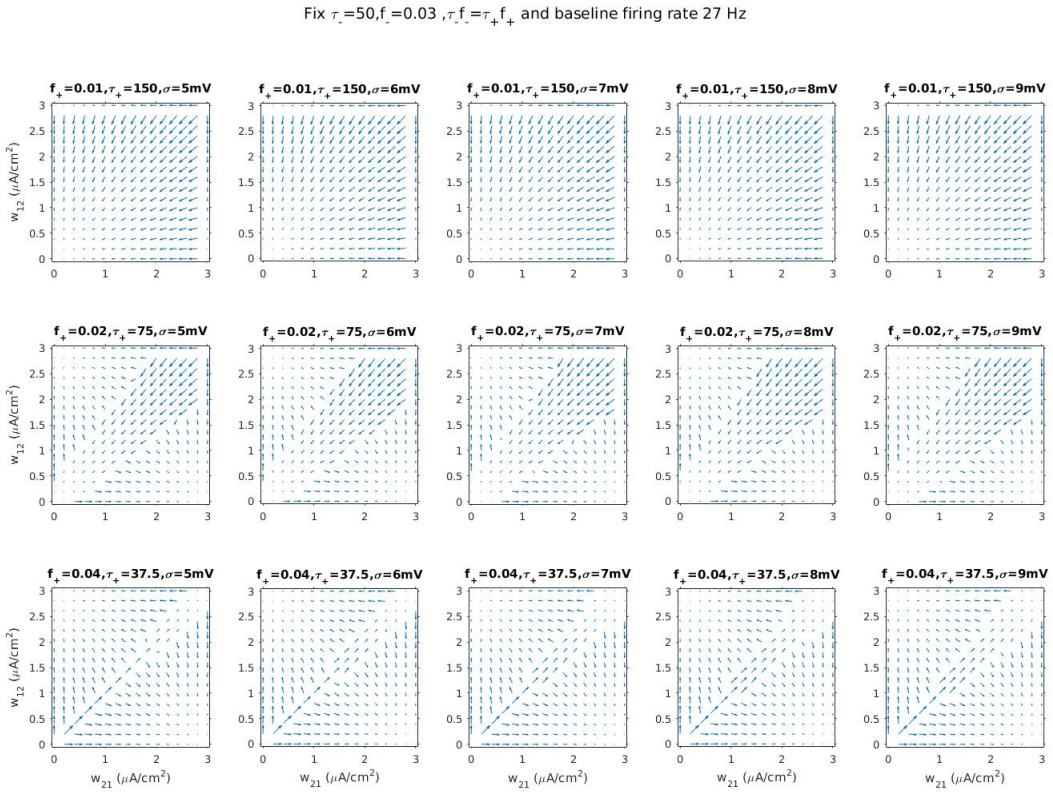

Figure 3.19: **Phase planes for setting the integral of learning rule to be 0.**

From the middle and bottom rows of Figure 3.19, the changes in the phase planes are much more obvious. This implies the effect of cross-covariances is larger. Here we use the the parameters of bottom row left one and right one of Figure 3.19 as an example (Figure 3.20), which shows that cross-covariances can change the network dynamics for fixed baseline firing rate under such learning rules. We can see that the properties of the cells (μ and σ) can affect the cross-covariances, and therefor can affect the dynamics of the weights in the network. However, this only happens when the term C is not big compared with A and B in Eq.(3.3).

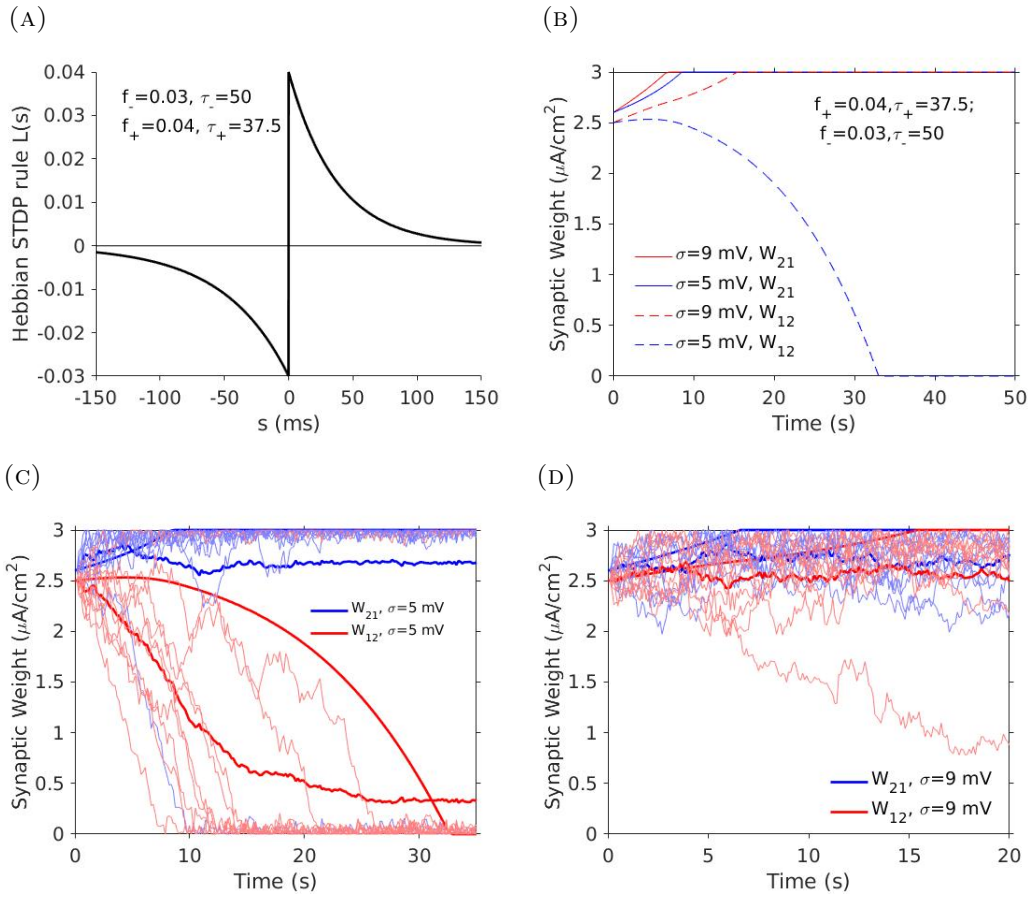

Figure 3.20: **Cross-covariances can affect network dynamics for the same baseline firing rate. (A)** Selected learning rule with the parameter in Figure 3.19. **(B)** Theoretical weights changes for $\sigma = 5$ mV and $\sigma = 9$ mV under the learning rule in (A) respectively. **(C)** Compared weights changes for $\sigma = 5$ mV. **(D)** Compared weights changes for $\sigma = 9$ mV.

CHAPTER 4

Results for larger networks

In the previous section, we studied how STDP together with the properties of spike train cross-covariances determine the evolution of synaptic weights in networks of two neurons. In this chapter we will generalize these ideas, and examine the evolution of weights in larger networks. For demonstration we simulate networks of put to 100 EIF neurons, although our conclusions and approach hold more generally.

4.1 Different μ-σ settings have different weight change speeds

In Section 3.2, we showed that, with a fixed baseline firing rate and with a balanced STDP learning rule, for two coupled neurons with different levels of drive (μ) and background noise (σ), the synaptic weights can change at different rates. Similar results hold in larger networks, and we have consequences for their global connectivity structure.

The different intrinsic properties of the cells (μ-σ settings) affect the cross-covariances between the spike trains of synaptically connected pairs of cells in the network (See Figure 3.10). This in turn leads to distinct dynamics of synaptic weights, as governed by the learning rule. Here we choose μ-σ settings shown in Table 2.1. The cross-covariances of two-cell recurrent networks for these 5 different parameter values are shown in the following Figure 4.1A. We also show the balanced Hebbian STDP learning rule we use in the simulations (Figure 4.1B; By "balanced" we again mean that $f_+ = f_-$ and $\tau_+ = \tau_-$ in Eq.(2.2)). Note that the baseline firing rates in Figure 3.10 (about 27 Hz) and 4.1A (about 7.6 Hz) are different. We can see that there are more oscillations for higher baseline firing rates case.

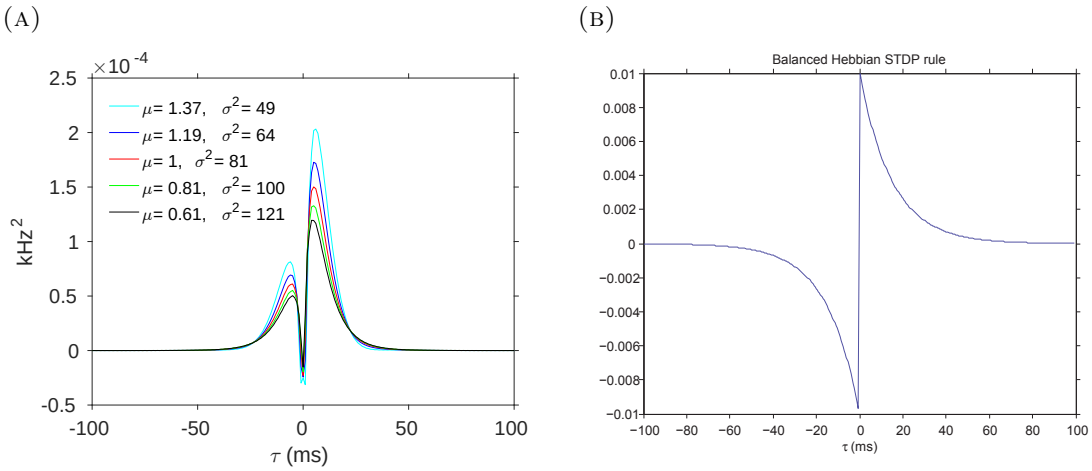

Figure 4.1: **The cross-covariance functions of two-cell recurrent networks for the 5 pairs of parameters shown in Table 2.1 and the balanced Hebbian STDP rule. (A)** Cross-covariances for two-cell recurrent networks with 5 pairs of parameters. **(B)** The graph of the function defining the balanced Hebbian STDP learning rule we choose.

Despite different initial weights, Figure 4.1A is similar to Figure 3.10: given equal firing rates, neurons with lower noise (σ), and higher drive (μ) are more susceptible to inputs. Thus the cross-covariance functions for pairs of such neurons have higher amplitudes than for other pairs subject to higher background noise. As we have argued in the previous chapter, give the same STDP rule (*e.g.* the one in Eq.(2.6)), we can predict that the synaptic weights will change faster in networks with higher drive, and lower noise. The weight dynamics in a two-cell network under a balanced Hebbian STDP rule for 3 different pairs of parameters are shown in Figure 4.2.

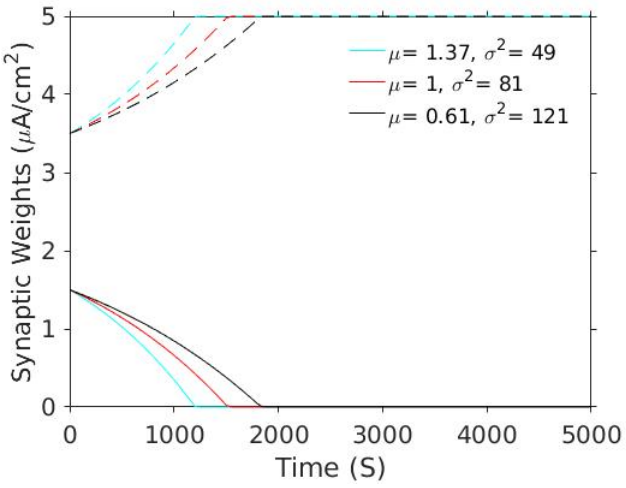

Figure 4.2: **The evolution of synaptic weights for three different pairs of parameter values specifying intrinsic properties of cells.** Results are obtained using the theory developed in Section 2.3.

As in Figure 3.11A, we can see that the synaptic weights in the less noisy networks (with lower σ) reach the boundaries faster (See Figure 4.2).

We next built a network of ten all–to–all connected cells. We again used the five different parameter sets described above, and let the synaptic weights in the network evolve according to the same balanced Hebbian STDP rule describe above. We used the same initial synaptic weight matrix for all these networks (Figure 4.3A), and obtained the same steady state (Figure 4.3B) after a transient period. Here the initial synaptic weight matrix is generated randomly. The dynamics of synaptic weights for 3 parameter sets are shown in Figure 4.4.

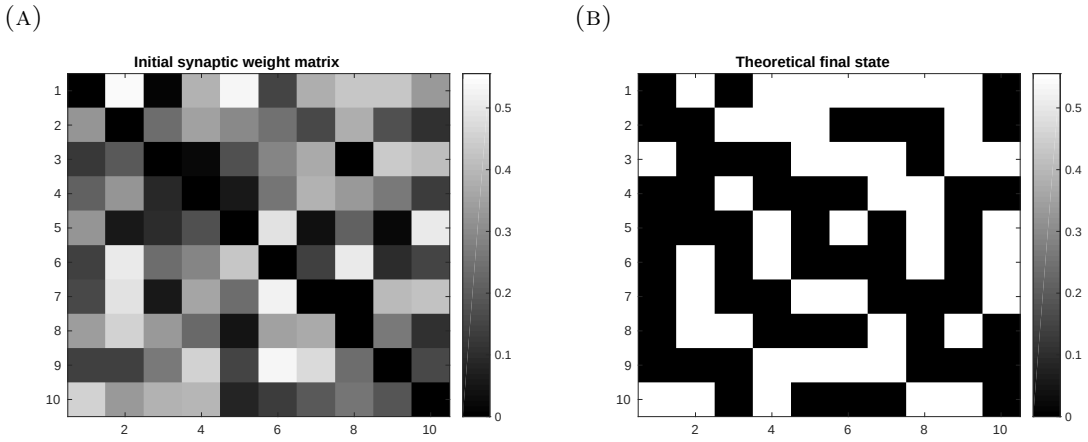

Figure 4.3: **The initial synaptic weight matrix and the theoretical steady state for all the 5 μ-σ pairs. (A)** The initial synaptic weight matrix. **(B)** The theoretical steady state of the weight matrix after learning. This final state is the same for each of the five parameter settings we used.

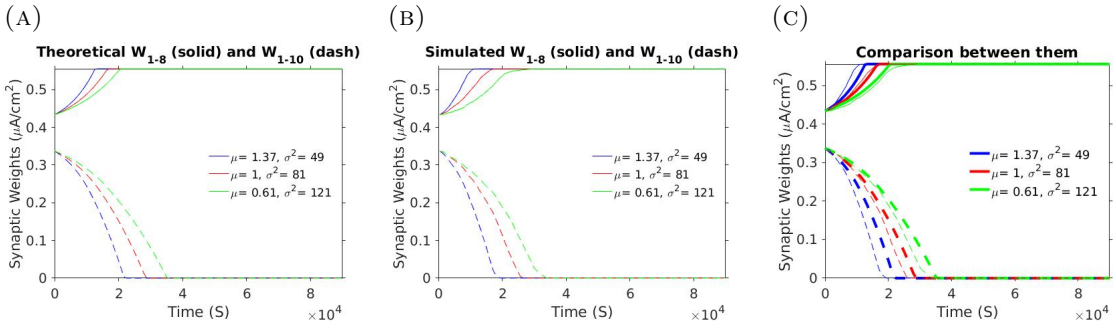

Figure 4.4: **The evolution of synaptic weights for three different parameter settings. (A)** The dynamics of the synaptic weights obtained using the theory developed in Section 2.3. **(B)** The dynamics of the synaptic weights for the same parameter values as in (A) obtained by direct simulation of the network and averaging over 10 realizations. **(C)** The comparison between the dynamics of the synaptic weights obtained by theory ((A)) and simulation ((B)). The thick curves are from (A) while the thin curves are from (B).

In this example the main effect of the different parameter settings is the speed at which the final state is reached. Networks with less background noise (lower σ) reach the final state faster than those with higher levels of noise, but the same baseline firing rate. This verifies our prediction and generalizes our results in Section 3.2.

4.2 Weight dynamics depend on individual neuron properties

As discussed in Section 3.1.2 (Figure 3.7), we know that, for the same baseline firing rate, different properties of individual cells, *i.e* different values of the parameters μ and σ, in a two-cell recurrent network affect spike train cross-covariances. In Section 3.2, we can show that learning rules can magnify the effect of cross-covariances on weight change dynamics. Here we will examine how these two factors affect the dynamics of synaptic weight changes in larger networks.

4.2.1 Balanced Hebbian STDP case

As in the previous section we examine weight changes under a balanced Hebbian STDP rule. As we have shown in Section 3.2 this implies that the cross-covariances dominate the evolution of synaptic weights. We begin by analyzing the phase planes (vector fields) of two-cell, recurrent networks with each neuron with different parameter settings. We will then use the properties found in two-cell networks to understand

the dynamics observed in larger networks.

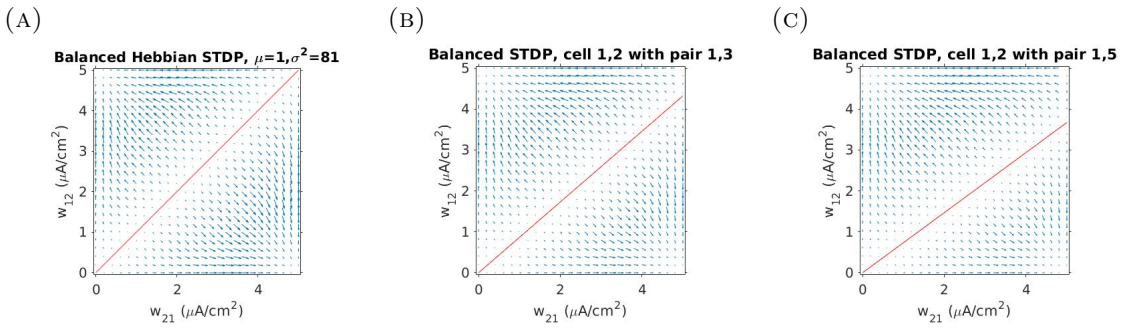

Figure 4.5: **Phase planes for synaptic weights in two-cell, recurrent networks under balanced Hebbian STDP.** In all cases we refer to the parameter numbering used in Table 2.1. We use an upper bound on the weights corresponding to $W^{max} = 5\ \mu\text{A/cm}^2$. **(A)** Phase plane with both cells having the same parameters (setting 3). **(B)** Phase plane with parameter setting 1 for cell 1 and setting 3 for cell 2. **(C)** Phase plane with parameter setting 1 for cell 1 and setting 5 for cell 2.

Phase planes of two-cell network for three parameter settings from Table 2.1 under a balanced Hebbian STDP rule are shown in Figure 4.5. When the two cells have the same parameter setting (Figure 4.5A), the phase plane is symmetric. The diagonal consists of unstable equilibria. The two stable fixed points ($\mathbf{W}_{21}$,$\mathbf{W}_{12}$)=(5,0) and ($\mathbf{W}_{21}$,$\mathbf{W}_{12}$)=(0,5) are attracting and have symmetric basins. This is a consequence of the shapes of the learning rule and the cross-covariance (both of them are symmetric). We can therefore predict that, for a network with cells with the same parameter setting under balanced Hebbian STDP rule, if all the initial synaptic weights are generated randomly, half of them will be potentiated while the other half will be depressed.

When we consider a network of two cells with different parameter settings (Figure 4.5B and C) this symmetry is broken. The line of unstable fixed points is tilted toward the axis corresponding to the weight of the connection from the cell with higher drive (μ) to the cell with higher noise (σ). This implies that the basin of attraction of the fixed point ($\mathbf{W}_{21}$,$\mathbf{W}_{12}$)=(0,5) is larger than the basin of ($\mathbf{W}_{21}$,$\mathbf{W}_{12}$)=(5,0). The outgoing synapses of the neuron with higher noise values (parameter settings 3 and 5 in Table 2.1) are more likely to be potentiated, while the incoming synapses are likely to weaken. Conversely, outgoing synapses from the neuron with higher drive value (setting 1 in Table 2.1) are more likely to weaken and its incoming synapses are more likely to be potentiated.

We therefore predict that for a network consisting of different groups of cells sharing the same initial baseline firing rate, but with different individual properties, under balanced Hebbian STDP rule, the synaptic weights of the connections from cells with lower drive (lower μ) and higher noise (higher σ) to cells with higher drive and lower noise will be potentiated. The synaptic weights of the connections from cells with higher drive to those with lower drive will weaken. These synapses can eventually be pruned if the lower bound is set to 0.

We next examine the dynamics of synaptic weights in a network of 100 cells with all–to–all connectivity. We again use a balanced Hebbian STDP rule. The network consists of two groups composed of cells with indices 1-50 (Group 1), and 51-100 (Group 2), respectively. Cells in the two groups have the same baseline firing rates, and share the same intrinsic properties with those within the group, but not with those in the different group. That is the values of the parameters μ and σ differ

between the two groups. As a result we can split the synaptic weight matrix into four quarters corresponding to connections within and between these two groups. We will use two examples to illustrate how our phase plan analysis can be used to predict weight dynamics in a larger network.

Example 4.2.1. We use parameter set 3 for cells in the Group 1 (indices 1-50), and set 1 for cells in Group 2 (indices 51-100). The initial synaptic weight matrix is generated randomly, and it is shown in Figure 4.6.

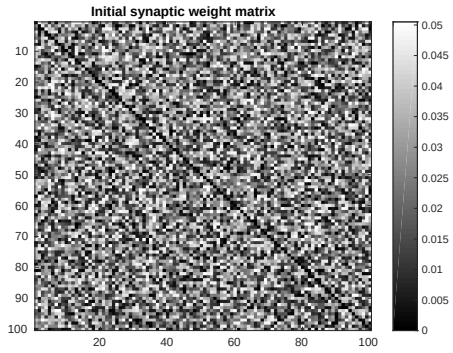

Figure 4.6: **The initial synaptic weight matrix of 100-cell dense network.**

The final state of the synaptic weights in the network is shown in Figure 4.7 obtained both using our theoretical approach, and direct simulations of the network of EIF neurons. The two approaches give quantitatively similar results. As predicted by our simulation of the two cell recurrent network, the bottom-left quarter (the weights corresponding to connections from higher noise neurons (parameter set 3) to lower noise neurons (parameter set 1)), is lighter than the top-right quarter after training. This indicates that these weights are bigger. We quantify this effect further below. The comparison of weight dynamics is in Figure 4.8.

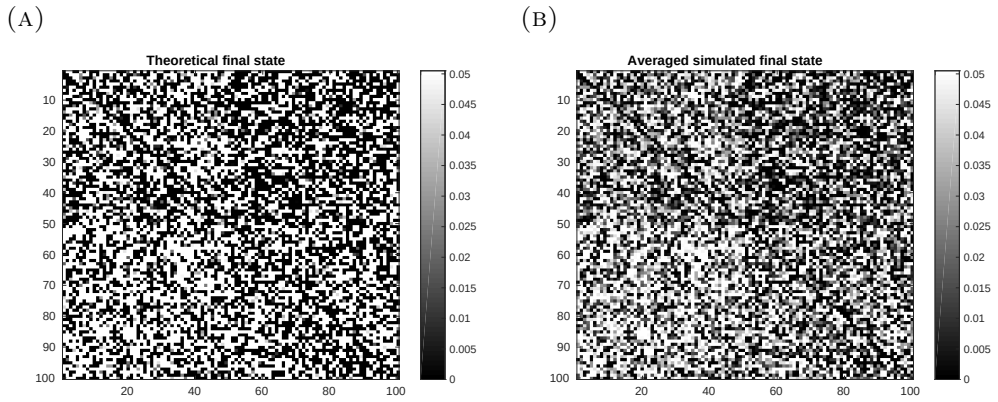

Figure 4.7: **The steady states for 100-cell dense network consisting of two groups (Example 4.2.1). (A)** The steady state obtained using the theoretical prediction as described in Section 2.3. **(B)** The steady state obtained from direct simulations using the same initial weights as in (A). The final state was averaged over 10 realizations.

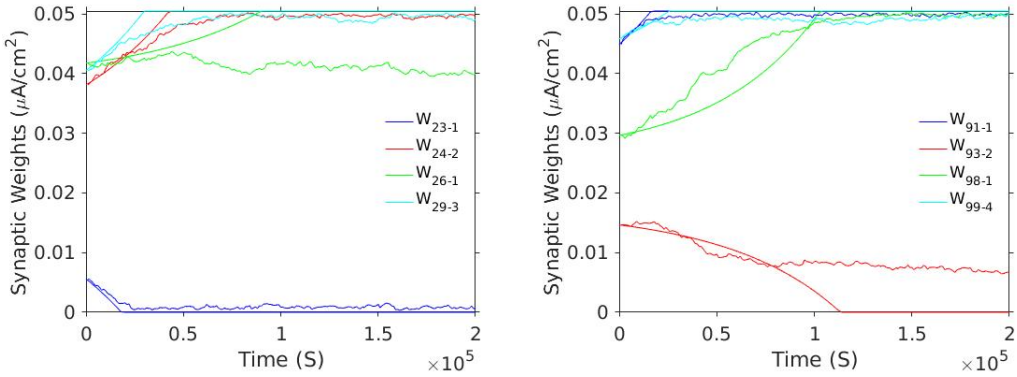

Figure 4.8: **Comparison of theoretically and computationally obtained synaptic weight dynamics in a large network.** Here we show the results with the parameter settings discussed in Example 4.2.1. The smooth curves represent theoretical results, while the jagged curves represent the average obtained from 10 realizations of the network of EIF neurons.

To quantify this difference we compute the mean synaptic weight for each of the four types of connections between and within the groups in the final state of the network. These are shown in Table 4.1 with the standard error of the averaged simulated final states obtain using bootstrap statistics (boot() function in R with 1000 replicates).

group 1: pair 3(strong noise) group 2: pair 1(weak noise)	**mean weights(μA/cm^2)**		**standard error**
	theory	**simulation**	
strong-strong(top-left)	0.025	0.025	0.00039
weak-strong(top-right)	0.020	0.020	0.00040
strong-weak(bottom-left)	0.030	0.030	0.00039
weak-weak(bottom-right)	0.025	0.025	0.00040

Table 4.1: The mean weights in each of the four quarters of the synaptic weights matrix for Example 4.2.1.

We again observe that the mean synaptic weight for the strong-weak (noise level) connections (bottom-left quarter of the synaptic weight matrix) is higher than that for weak-strong connections (top-right quarter) for both theoretical and simulated final states. The mean weights for strong-strong (top-left quarter) connections and weak-weak connections(bottom-right quarter) are very close. Moreover, the theory and simulation results agree closely.

Example 4.2.2. For this example we set the parameters for cells in Group 1 (indices 1-50) according to setting 3, for cells in Group 2 (indices 51-100) according to setting 5 in Table 2.1. The initial synaptic weight matrix is the same as Example 4.2.1 (Figure 4.6). Note that the results do not depend on the initial weight matrix. The theoretically obtained final state, and that obtained by direct simulation of the network are shown in the following Figure 4.9. We use the same balanced STDP rule discussed in the previous section.

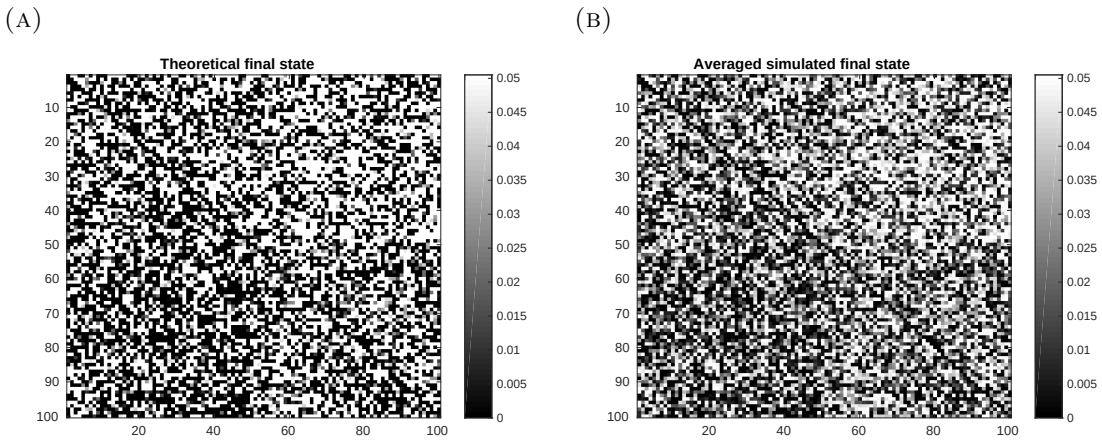

Figure 4.9: **The theoretical and simulated final steady states for 100-cell network with two groups of cells described in Example 4.2.2. (A)** The final state of the synaptic weight matrix obtained using our theoretical approach. **(B)** The same final state obtained using simulations and averaging over 10 realizations.

The final weight matrix in this example has a different structure, as weights of connections from high noise neurons (setting 5) to low noise neurons become stronger than weights from low noise to high noise neurons. There is again a good comparison between the theory and simulations, as show in Figure 4.10. The means of the four quarters of the synaptic weights matrix are in the following Table 4.2.

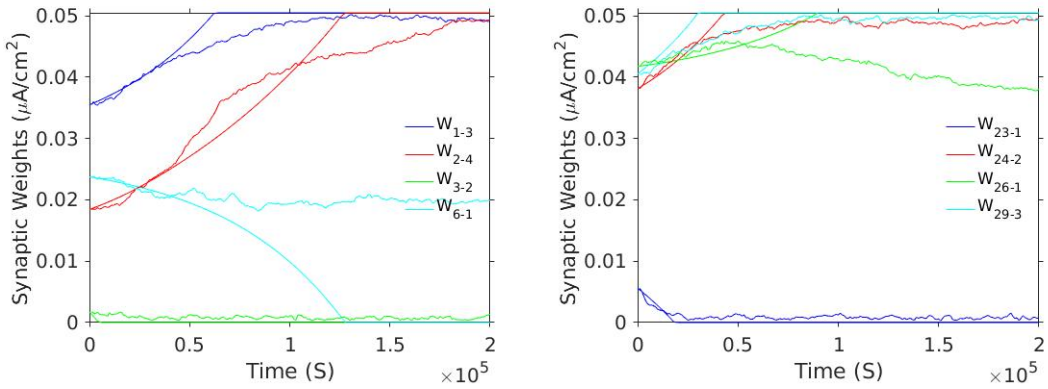

Figure 4.10: **The comparison of the evolution of selected weights in a 100-cell network of all–to–all coupled cells with parameter setting as discussed in Example 4.2.2.** Smooth curves are theoretical results, while jagged curves represent the average over 10 realizations.

group 1: pair 3(weak noise) group 2: pair 5(strong noise)	**mean weights(μA/cm^2)**		**standard error**
	theory	**simulation**	
weak-weak(top-left)	0.025	0.025	0.00041
strong-weak(top-right)	0.030	0.030	0.00040
weak-strong(bottom-left)	0.020	0.020	0.00039
strong-strong(bottom-right)	0.025	0.025	0.00041

Table 4.2: The mean weights in each of the four quarters of the synaptic weights matrix for Example 4.2.2.

Here we show that the mean weight of connections from neurons with strong background noise to those with weak niose (strong-weak, top-right quarter) is higher than that of weak-strong connections (bottom-left quarter), both in the case of the final state obtained theoretically and by simulations. The mean weights of weak-weak connections (top-left quarter) and strong-strong connections (bottom-right quarter)

are in the same level. Moreover, all the theoretical mean weights are close to their related simulated ones.

These two examples agree with the conclusions of our two-cell, recurrent network in the beginning of this section : the synaptic weights of the connections from cells with lower drive (lower μ) and higher internal noise (higher σ) to those with higher drive (higher μ) and lower lower internal noise(lower σ) are potentiated, while weights in the opposite direction are typically weakened under a balanced Hebbian STDP rule. This is due to the difference in the size of basins of attraction of the fixed points for the two different types of cells.

4.2.2 Balanced Anti-Hebbian STDP case

Here we ask what is the effect of a balanced Anti-Hebbian STDP rule mentioned in Section 2.2 on the evolution of synaptic weights in larger networks. This rule is defined by the following weight change function:

$$\Delta \mathbf{W}_{ji}(s) = \begin{cases} \mathbf{W}_{ji}^0 \mathcal{H}(\mathbf{W}_{ji}) L(s) \ , & \text{if } s \geq 0 \\ \mathbf{W}_{ji}^0 \mathcal{H}(W^{max} - \mathbf{W}_{ji}) L(s) \ , & \text{if } s < 0 \end{cases} ,$$

where

$$L(s) = \begin{cases} -f_- e^{-\frac{|s|}{\tau_+}} \ , & \text{if } s \geq 0 \\ f_+ e^{-\frac{|s|}{\tau_-}} \ , & \text{if } s < 0 \end{cases} .$$

The rule is similar to the Hebbian STDP rule defined in Eq.(2.2), but it reverses the windows of potentiation and depression. As with the the balanced Hebbian STDP rule, this rule also leads to a cancellation of part C in Eq.(3.3) so that the cross-covariances control the weight evolution.

Similar as the balanced Hebbian case, fixing the learning rule as balanced Anti-Hebbian STDP rule, we study the phase planes for two-cell recurrent networks with each neuron in different parameter (μ-σ) settings firstly.

Phase planes of two-cell network for three parameter settings from Table 2.1 under a balanced Anti-Hebbian STDP rule are shown in Figure 4.11.

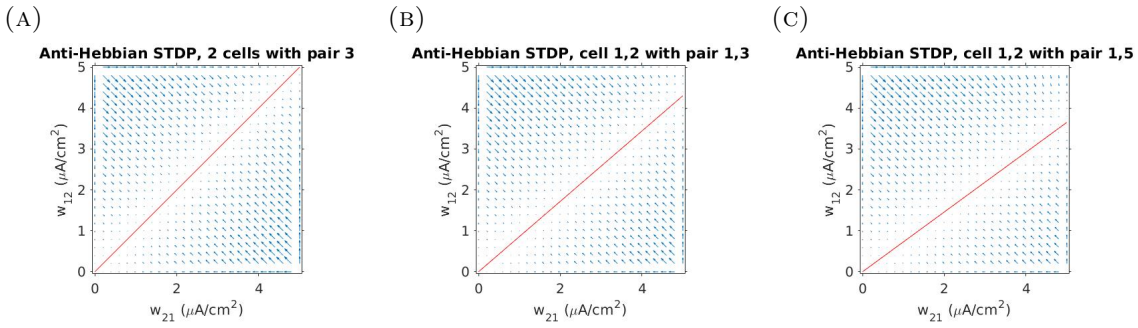

Figure 4.11: **Phase planes for synaptic weights in two-cell, recurrent network under balanced Anti-Hebbian STDP rule.** In all cases we refer to the parameter numbering used in Table 2.1. We use an upper bound on the weights corresponding to $W^{max} = 5$ μA/cm^2. **(A)** Phase plane with both cells having the same parameters (setting 3). **(B)** Phase plane with parameter setting 1 for cell 1 and setting 3 for cell 2. **(C)** Phase plane with parameter setting 1 for cell 1 and setting 5 for cell 2.

Since the Anti-Hebbian STDP rule differs from the Hebbian STDP rule in the that potentiation side and depression side are reversed, we obtain the same phase planes as Figure 4.5, but with reversed time flow. This means that all arrows are now reversed (see Figure 4.11), and therefore all initial conditions converge to the line of fixed points.

For the two cells with the same parameter (μ-σ) setting (Figure 4.11A), the phase plane is also symmetric. We can make a prediction that, for a network with cells of the same parameter setting, under balanced Anti-Hebbian STDP rule, if all the initial weights are generated randomly, they will attain the same value or similar values finally.

Additionally, for the two cells with different parameter settings (Figure 4.11B and C), the line of equilibrium (stable fixed points) is tilted toward the axis corresponding to the weight of the connection from the cell with higher drive (μ) to the cell with higher noise (σ). This implies that the outgoing synapses of the neuron with higher noise (parameter settings 3 and 5 in Table 2.1) are more likely to weaken, while its incoming synapses are likely to be potentiated. Conversely, outgoing synapses from the neuron with higher drive (setting 1 in Table 2.1) are more likely to be potentiated and its incoming synapses are more likely to weaken.

As in the previous section we can use these observations to examine the evolution of synaptic weights in networks composed of different groups of cells with the same baseline firing rates, but different levels of drive and noise. Under a balanced Anti-Hebbian STDP rule, the weights of synaptic connections from cells with higher noise to those with lower noise will weaken. The weights going of synapses in the opposite

direction will be potentiated. We verify this prediction in the following example.

Example 4.2.3. For this example we set the parameters for cells in Group 1 (indices 1-50) according to setting 1, for cells in Group 2 (indices 51-100) according to setting 5 in Table 2.1. The initial synaptic weight matrix is the same as previous two examples (Figure 4.6). Under balanced Anti-Hebbian STDP rule, the theoretically obtained final state, and that obtained by direct simulation of the network are shown in the following Figure 4.12.

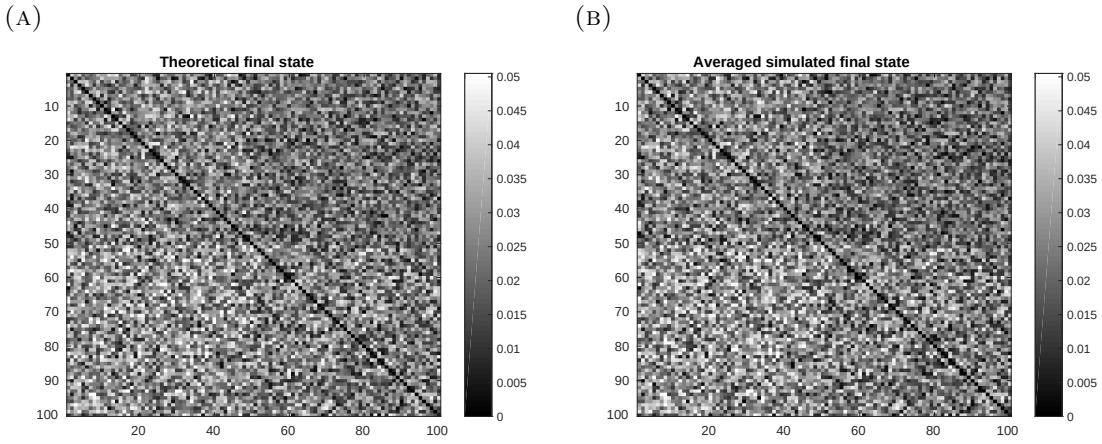

Figure 4.12: **The theoretical and simulated final steady states for 100-cell network with two groups of cells described in Example 4.2.3. (A)** The final state of the synaptic weight matrix obtained using our theoretical approach. **(B)** The same final state obtained using simulations and averaging over 10 realizations.

We can see that, the final weight matrix in this example has a different structure, as weights of connections from lower noise neurons to higher noise neurons (bottom-left quarter) become stronger than weights from higher noise to lower noise neurons (top-right quarter). The results look similar as Example 4.2.1, but with reversed

parameter (μ-σ) settings according to the reversed sides of potentiation and depression in the learning rules. There is again a good comparison between the theory and simulations, as show in Figure 4.13. The means of the four quarters of the synaptic weights matrix are in the following Table 4.3.

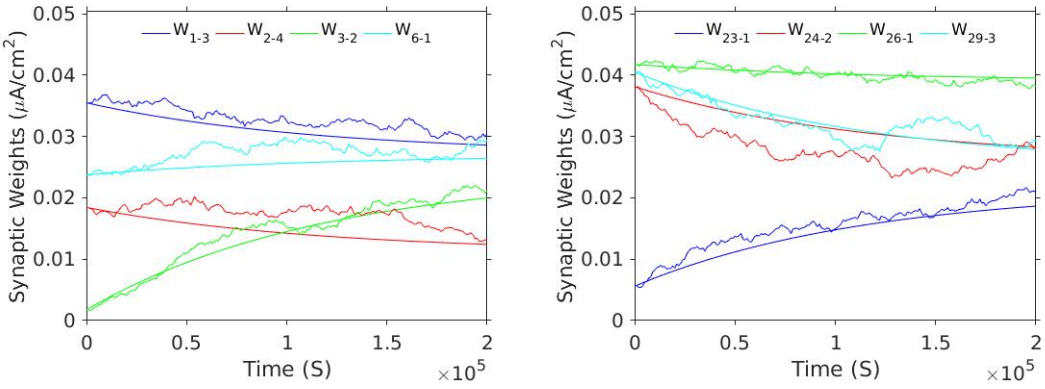

Figure 4.13: **The comparison of the evolution of selected weights in a 100-cell network of all–to–all coupled cells with parameter setting as discussed in Example 4.2.3.** Smooth curves are theoretical results, while jagged curves represent the average over 10 realizations.

group 1: pair 1(weak noise) group 2: pair 5(strong noise)	**mean weights(μA/cm^2)**		**standard error**
	theory	**simulation**	
weak-weak(top-left)	0.025	0.025	0.00022
strong-weak(top-right)	0.020	0.020	0.00019
weak-strong(bottom-left)	0.028	0.028	0.00023
strong-strong(bottom-right)	0.025	0.025	0.00022

Table 4.3: The mean weights in each of the four quarters of the synaptic weights matrix for Example 4.2.3.

Here we show that the mean weight of connections from neurons with strong background noise to those with weak niose (strong-weak, top-right quarter) is lower

than that of weak-strong connections (bottom-left quarter), both in the case of the final state obtained theoretically and by simulations. The mean weights of weak-weak connections (top-left quarter) and strong-strong connections (bottom-right quarter) are in the same level. Moreover, all the theoretical mean weights are close to their related simulated ones.

This example demonstrates that, under balanced Anti-Hebbian STDP rules, weights of connection from cells with higher internal noise (σ) to those with lower noise will weaken, while weights of connections in the opposite direction are potentiated. This agrees with our predictions.

4.3 Internal cell properties can lead to differences in synaptic weight evolution

We next consider a network of neurons with the same parameter setting μ-σ, and therefore the same baseline firing rates. We then compare the dynamics of synaptic weights for different parameter settings, but same baseline firing rates. We use the potentiation dominated Hebbian STDP rule and set $f_+ = A \cdot f_-$ and $\tau_+ = \tau_-$ with $A > 1$. Again, our network initially has all–to–all connectivity. In this case, the term denoted by C in Eq.(3.3) is bigger than 0, and hence firing rates will affect the weight change in addition to the effect of cross-covariances. We will show that, the cross-covariances can still affect the evolution of the synaptic weights in this case.

As in the previous sections, we start by analyzing the phase planes for two-cell networks first. These are shown for parameter settings 1 and 5, under potentiation dominated Hebbian STDP with $A = 1.5$ in Figure 4.14.

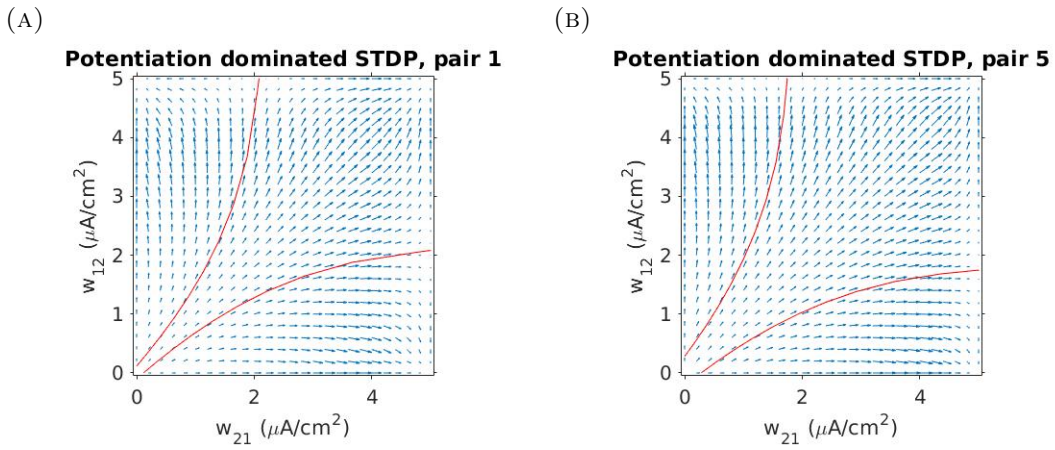

Figure 4.14: **The phase planes of synaptic weights in a two-cell, recurrent network under a potentiation dominated STDP rule. (A)** Phase plane for the parameter setting 1. **(B)** Phase plane for the parameter setting 5.

The phase planes show that, in this case there are three fixed points: $(\mathbf{W}_{21},\mathbf{W}_{12})$=(5,0), (0,5) and (5,5). All thee fixed points are stable. However, the basin of attraction of the stable fixed point corresponding to equal final weights, $(\mathbf{W}_{21}, \mathbf{W}_{12}) = (5, 5)$ is larger for parameter setting 5 than for setting 1. Thus, we can predict that networks of identical cells with higher noise (σ) under potentiation dominated Hebbian STDP rule will exhibit more recurrent connections – and more connections overall – after in the final state. We illustrate that this conclusion holds in the following examples.

Example 4.3.1. We use the potentiation dominated Hebbian STDP rule ($f_+ = 1.05 \cdot f_-$ and $\tau_+ = \tau_-$), and we begin with a small network of 10 all–to–all connected cells for direct observation. We will show the results hold for large networks (networks of 100 all–to–all connected cells, Example 4.3.3). We want to examine networks of cells with different internal properties (parameter settings). The initial synaptic weight matrix is fixed for all networks here, which is shown in Figure 4.3A. For the networks of neurons with parameter setting 1 and 5, the theoretically obtained final states, and those obtained by direct simulation are shown in the following Figure 4.15

Figure 4.15 shows that, after training, there are more white blocks in the synaptic weight matrices of the second row. This means, there are more potentiated weights in the network of neurons with parameter setting 5 than those for parameter setting 1. Therefore the network of cells with higher noise (parameter setting 5) get more recurrently connected cells. There is also a good comparison between the theory and simulations, as show in Figure 4.16.

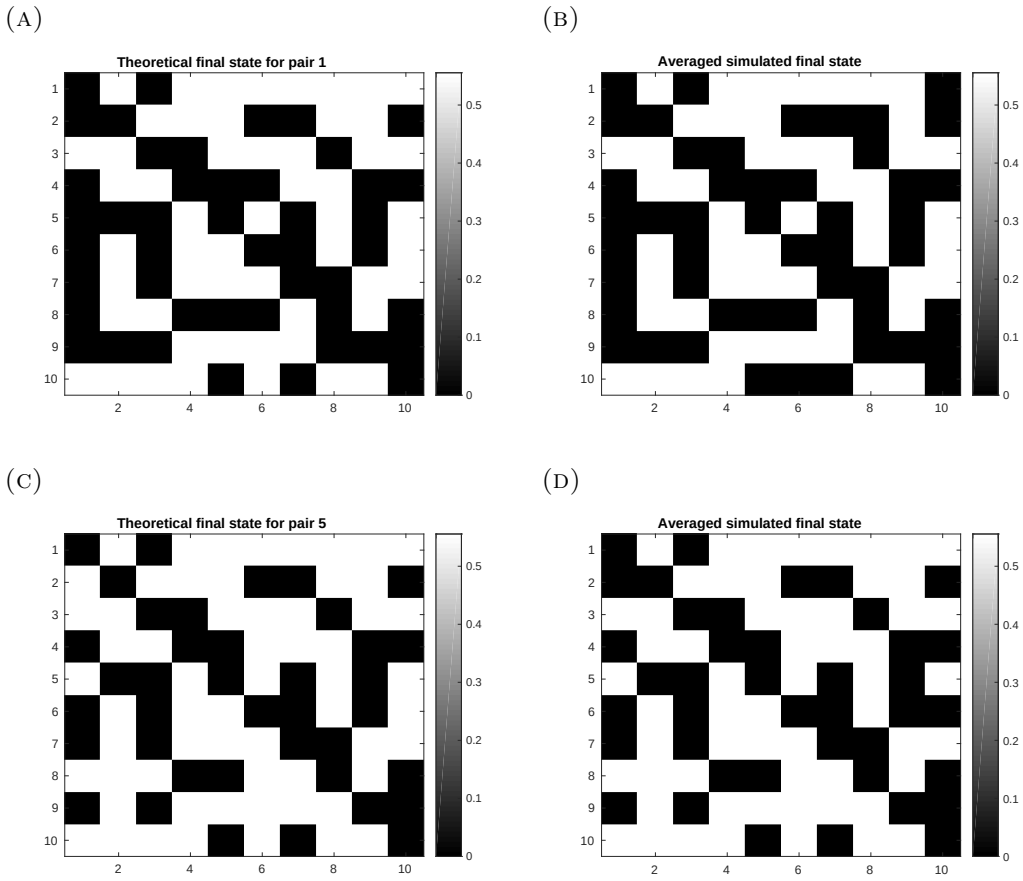

Figure 4.15: **The theoretical and simulated final steady states for 10-cell network under potentiation dominated learning rule described in Example 4.3.1. (A)** The final state of the synaptic weight matrix with parameter setting 1 obtained using our theoretical approach. **(B)** The final state corresponding to (A) obtained using simulations and averaging over 10 realizations. **(C)** The final state of the synaptic weight matrix with parameter setting 5 obtained using our theoretical approach. **(D)** The final state corresponding to (C) obtained using simulations and averaging over 10 realizations.

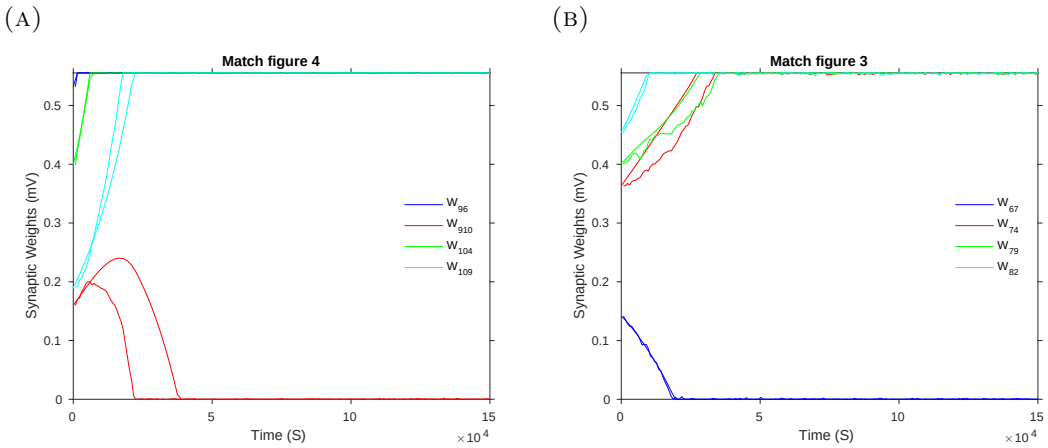

Figure 4.16: **The comparison of the evolution of selected weights in a 10-cell network of all–to–all coupled cells with parameter setting as discussed in Example 4.3.1.** Smooth curves are theoretical results, while jagged curves represent the average over 10 realizations. **(A)** For network of identical cells with parameter setting 1. **(B)** For network of identical cells with parameter setting 5.

Example 4.3.2. Here we use the potentiation dominated Hebbian STDP rule by setting $f_+ = 1.05 \cdot f_-$, and again, $\tau_+ = \tau_-$. Then we apply the rule on the same network of 10 all–to–all connected cells as Example 4.3.1. For the networks of neurons with parameter setting 1 and 5, the theoretically obtained final states, and those obtained by direct simulation are shown in the following Figure 4.17 and Figure 4.18 respectively, together with comparison of the evolution of selected weights between the theory and simulations.

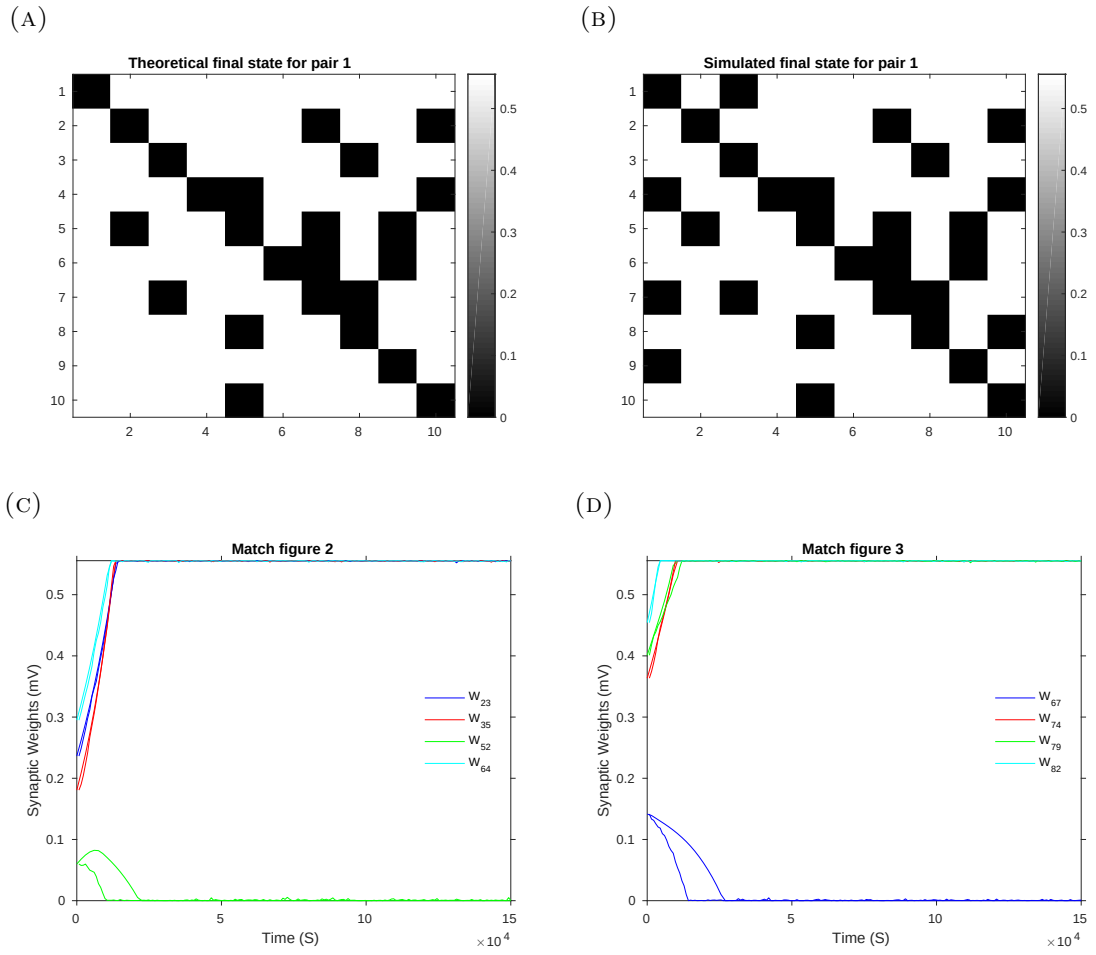

Figure 4.17: **The final steady states and the comparison of the evolution of selected weights for 10-cell network with parameter setting 1 in Example 4.3.2. (A)** The final state of the synaptic weight matrix with parameter setting 1 obtained using our theoretical approach. **(B)** The final state corresponding to (A) obtained using simulations and averaging over 10 realizations. **(C,D)** The comparison of the evolution of selected weights for parameter setting 1. Smooth curves are theoretical results, while jagged curves represent the average over 10 realizations.

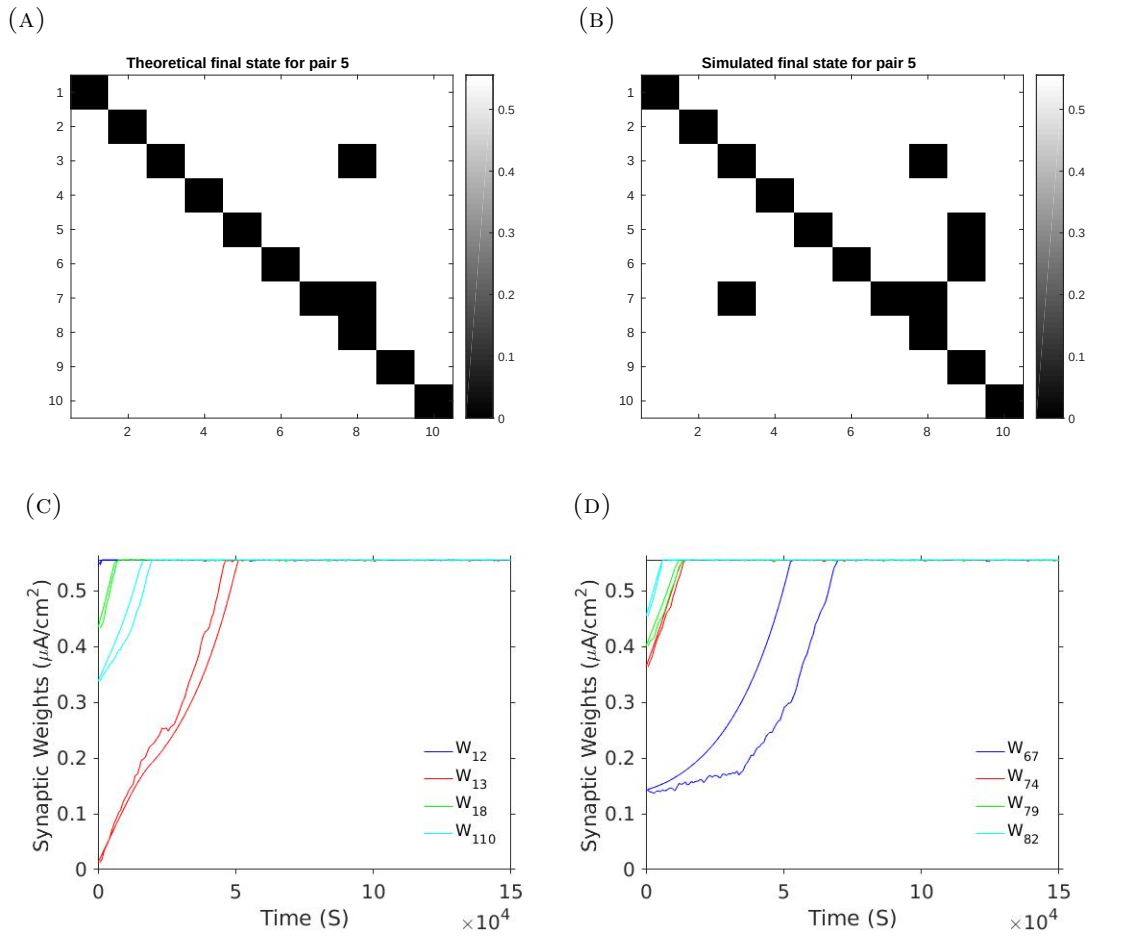

Figure 4.18: **The final steady states and the comparison of the evolution of selected weights for 10-cell network with parameter setting 5 in Example 4.3.2. (A)** The final state of the synaptic weight matrix with parameter setting 5 obtained using our theoretical approach. **(B)** The final state corresponding to (A) obtained using simulations and averaging over 10 realizations. **(C,D)** The comparison of the evolution of selected weights for parameter setting 5. Smooth curves are theoretical results, while jagged curves represent the average over 10 realizations.

By comparing the first row of Figure 4.17 and that of Figure 4.18, we can get the same conclusion as Example 4.3.1. Additionally, we observe that there are more potentiated weights for higher A value (which controls the tendency of potentiation) of the potentiation dominated Hebbian STDP rule through comparing Example 4.3.1 and Example 4.3.2.

Example 4.3.3. Here we consider two networks of 100 cells with all–to–all connectivity and with parameter setting 1 and 5 respectively. Their initial synaptic weight matrices are the same as Figure 4.6. We then apply the potentiation dominated STDP rule ($f_+ = 1.005 \cdot f_-$) on them. The theoretically obtained final states, and those obtained by direct simulation are shown in the Figure 4.19.

Although this is not obvious from inspection, there are more white dots, *i.e.* synaptic connections that have strengthened, in the final states of the network when we use parameter setting 5 (Figure 4.19C and D) than when we use parameter setting 1 (Figure 4.19A and B). This implies the former one have more potentiated weights. The comparison between the theory and simulations is shown in Figure 4.20. The means of the synaptic weights matrices are in the following Table 4.4.

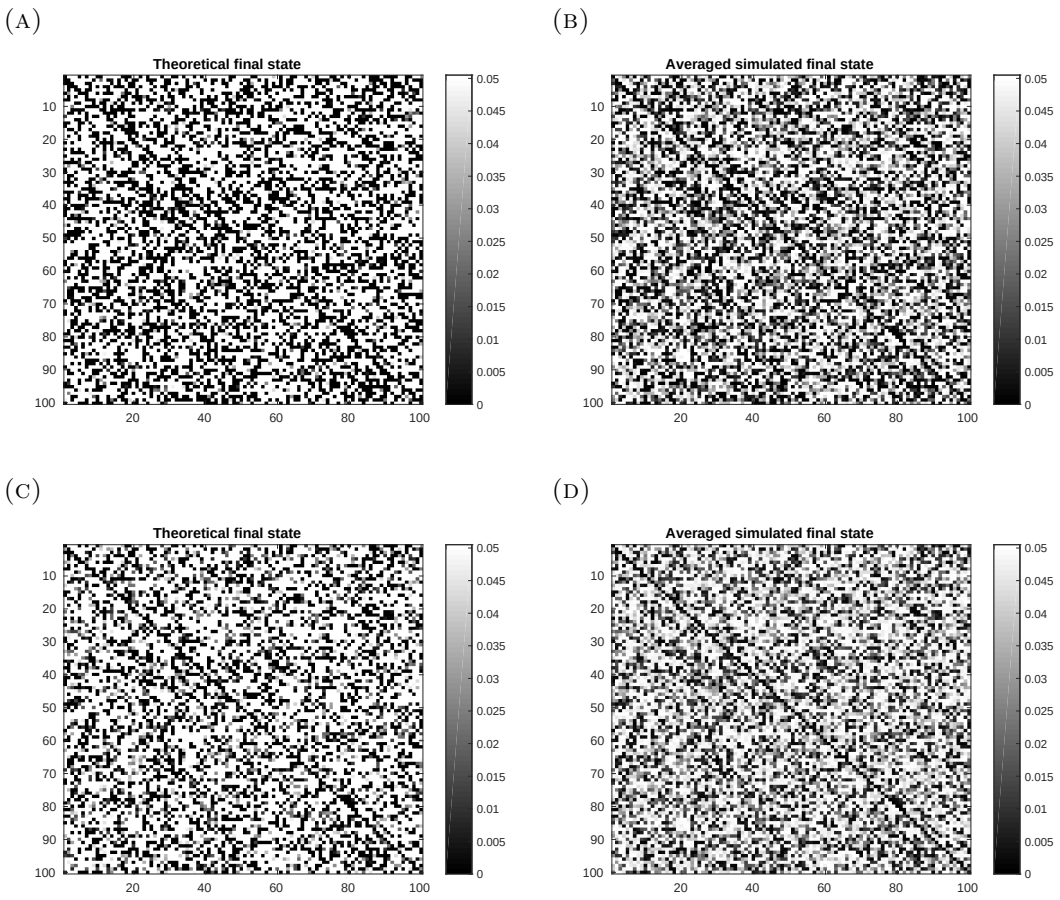

Figure 4.19: **The theoretical and simulated final steady states for 10-cell network under potentiation dominated learning rule described in Example 4.3.3. (A)** The final state of the synaptic weight matrix with parameter setting 1 obtained using our theoretical approach. **(B)** The same final state as (A) obtained using simulations and averaging over 10 realizations. **(C)** The final state of the synaptic weight matrix with parameter setting 5 obtained using our theoretical approach. **(D)** The same final state as (C) obtained using simulations and averaging over 10 realizations.

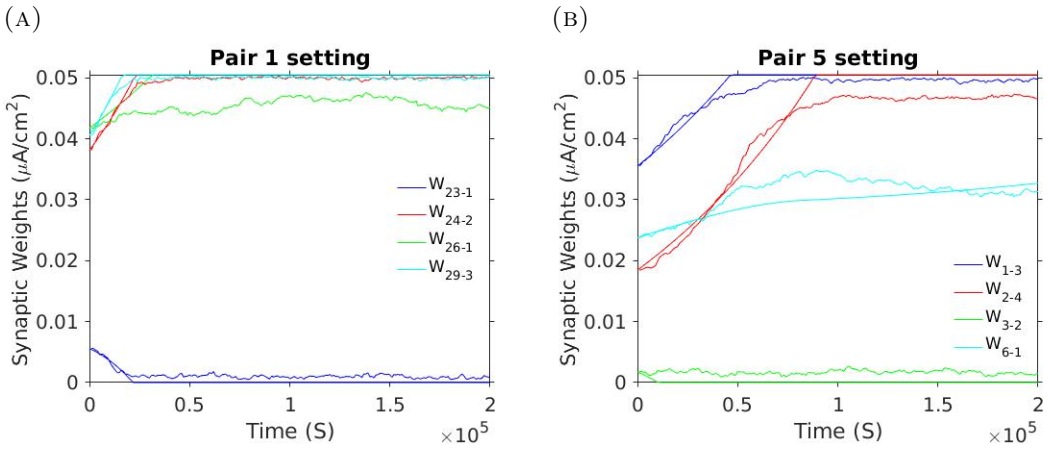

Figure 4.20: **The comparison of the evolution of selected weights in a 100-cell network of all–to–all coupled cells with parameter settings as discussed in Example 4.3.3.** Smooth curves are theoretical results, while jagged curves represent the average over 10 realizations. **(A)** For network of identical cells with parameter setting 1. **(B)** For network of identical cells with parameter setting 5.

Network parameter setting	**mean weights (μA/cm^2)**		**standard error**
	theory	**simulation**	
Setting 1	0.030	0.029	0.00021
Setting 5	0.033	0.033	0.00019

Table 4.4: The means weights of the final states of the synaptic weights matrices for Example 4.3.3

We can see that, for both theoretical and simulated final states, the mean of the synaptic weights matrix for the network of neurons with higher noise (σ, parameter setting 5) is bigger than that for lower noise (parameter setting 1).

These three examples above can verify our prediction that, under potentiation

dominated Hebbian STDP rule, the synaptic weights of the networks of the neurons with higher noise (σ, or lower drive μ) are more likely to strengthen than those of the reversed case, even though all the neurons of all the different networks have the same baseline firing rate.

4.4 Predict the steady state under balanced Hebbian STDP rule

Here we consider an ideal case: for some particular learning rules, we can predict the steady state of a network after training just by giving its initial synaptic weight matrix.

We apply balanced Hebbian STDP rule on 10-cell (with all-to-all connections) networks of all the neurons with the same parameter setting in one network. The initial synaptic weight matrices are the same for all networks and it is shown in Figure 4.3A.

According to Eq.(2.6), we compute the matrices of $\frac{d\mathbf{W}_{ji}}{dt}$ at the beginning of the training (the first iteration for updating the weights under balanced Hebbian STDP rule) for the networks of neurons with different parameter settings. We then define a transformation of the matrices of $\frac{d\mathbf{W}_{ji}}{dt}$ by replacing positive $\frac{d\mathbf{W}_{ji}}{dt}$ value with 1 and negative $\frac{d\mathbf{W}_{ji}}{dt}$ value with 0.

We find that, through the transformation we defined, the matrices of $\frac{d\mathbf{W}_{ji}}{dt}$ are

identical for all the 5 networks of neurons with the 5 parameter settings (μ-σ in Table 2.1, same setting for the neurons in the same network). We show it in Figure 4.21, compared with the theoretical steady states of the synaptic weight matrices for the 5 networks after training (they are also identical).

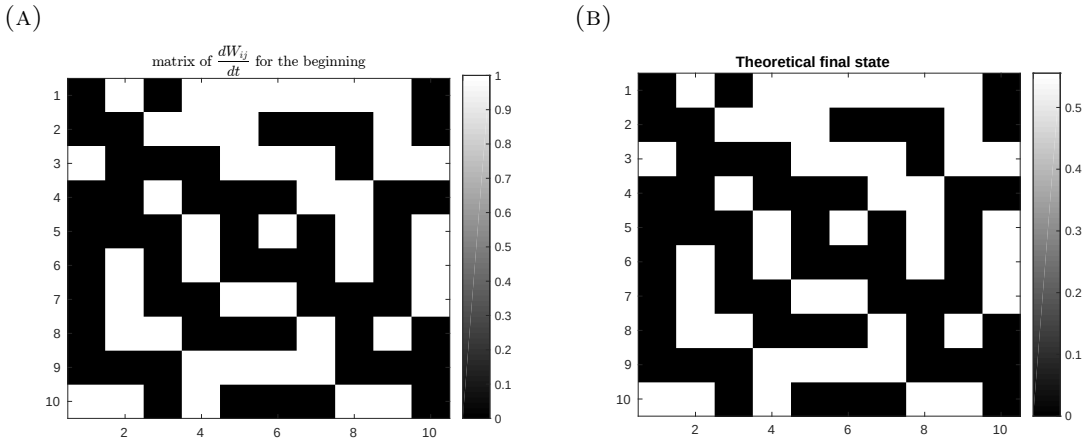

Figure 4.21: **The matrices of $\frac{d\mathbf{W}_{ji}}{dt}$ after transformation, and the theoretical steady states of the weight matrices for all the 5 networks. (A)** The matrices of $\frac{d\mathbf{W}_{ji}}{dt}$ after transformation for all the 5 networks. They are identical. **(B)** The theoretical steady states of weight matrices for the 5 networks. They are also identical.

We can see that the above two matrices correspond with each other exactly. This means that, under balanced Hebbian STDP rule, synaptic weight $\mathbf{W}_{ji}$ will be potentiated if its corresponding $\frac{d\mathbf{W}_{ji}}{dt}$ is positive at the beginning of the training, while it will be depressed if the corresponding $\frac{d\mathbf{W}_{ji}}{dt}$ is negative. Thus, we can predict the steady states of the networks under balanced Hebbian STDP rule just by computing the matrix of $\frac{d\mathbf{W}_{ji}}{dt}$ at the beginning of the training.

CHAPTER 5

Discussion and conclusions

In this dissertation, I examined the role of synaptic plasticity and the properties of neuronal responses in shaping the architecture of recurrent networks. First, I investigated synaptic weight dynamics in two-cell networks. Insights gained from these networks allowed me to understand the evolution of the structure of larger recurrent networks.

In Chapter 2, I introduced the the EIF neuron model which was used in the remainder of the thesis. The EIF neuron has several properties that make it a more faithful representation of an actual neuron than the Poisson model used in previous studies. The EIF neuron model exhibits the same baseline firing rate but distinct

firing statistics at different parameter settings, unlike a Poisson neuron. Next, I discussed the synaptic plasticity rule I used to model weight dynamics, the STDP learning rule. Finally, I illustrated how to use linear response theory to approximated the cross-covariances for recurrent networks, a crucial step in the theoretical approximation of synaptic weight evolution under STDP.

In Chapter 3, I used STDP, and the theoretical tools developed in Chapter 2 to both uni-and bi-directionally connected two-cell networks. I used networks with fixed baseline firing rates for neurons in the same network, but different noise level (σ value). With the same STDP learning rule, lower noise and higher common input lead to faster weight evolution. Moreover, the shape of the cross-covariances contributes more to the weight evolution in the case of $f_+\tau_+ = f_-\tau_-$ in Eq.(3.3), while the shape of the STDP governs weight evolution in other cases ($f_+\tau_+ \neq f_-\tau_-$).

In Chapter 4, I generalized the results for Chapter 3 to large networks (from 10-cell to 100-cell recurrent networks). if the same baseline firing rate for all neurons in the network is the same, lower noise leads to faster weight evolution, as it did in networks of two cells. Moreover, I studied the weight dynamics for large networks with groups of neurons with different noise levels ($\mu - \sigma$ settings). With the same baseline firing rate, the weights from neurons with higher noise (σ) to those with lower noise are more likely to strengthen under a balanced Hebbian STDP rule. However, with an Anti-Hebbian STDP rule, the opposite result holds: the weights from neurons with lower noise to those with higher noise are more likely to strengthen. I also considered asymmetric Hebbian STDP rules, in particular the potentiation dominated case. In this case weights are potentiated in network of neurons with

higher noise. Last but not the least, for the symmetric Hebbian STDP rule, the steady state of given network can be predicted from the the values of the derivatives (positive or negative) of the synaptic weights at the beginning of weight evolution.

There are several interesting extensions of this work. For example, I have not examined the effect of common input to the weight evolution of larger networks. As shown in Chapter 2, a similar theoretical approach can be applied to this case. Moreover, in this thesis, I just consider the EIF neuron model and Hebbian STDP learning rules. However, many more detailed and physiologically realistic neuron models and plasticity rule have been described in the literature. For example, the Connor-Stevens neuron model [14] (which is considered to be more realistic than EIF neuron model) and triplet STDP learning rule [26] are interesting examples that could be studied using similar approaches. These neuron models and plasticity rules could lead to different insights about the role of neuronal properties in shaping network structure, but I leave them for future research.

Bibliography

[1] Morrison A, Aertsen A, and Diesmann M. Spike-timing-dependent plasticity in balanced random networks. *Neural Computation*, 19:1437–1467, 2007.

[2] Cara B Allen, Tansu Celikel, and Daniel E Feldman. Long-term depression induced by sensory deprivation during cortical map plasticity in vivo. *Nature neuroscience*, 6(3):291–299, 2003.

[3] Babadi B and Abbott LF. Intrinsic stability of temporally shifted spike-timing dependent plasticity. *PLoS Computational Biology*, 6:e1000961. doi:10.1371/journal.pcbi.1000961., 2010.

[4] Babadi B and Abbott LF. Pairwise analysis can account for network structures arising from spike-timing dependent plasticity. *PLoS Comput Biol*, 9(2):e1002906. doi: 10.1371/journal.pcbi.1002906, 2013.

[5] Doiron B, Lindner B, Longtin A, Maler L, and Bastian J. Oscillatory activity in electrosensory neurons increases with the spatial correlation of the stochastic input stimulus. *Phys Rev Let*, 93, 2004.

[6] Lindner B, Doiron B, and Longtin A. Theory of oscillatory firing induced by spatially correlated noise and delayed inhibitory feedback. *Phys Rev E*, 72, 2005.

[7] Laurent Badel, Sandrine Lefort, Thomas K Berger, Carl CH Petersen, Wulfram Gerstner, and Magnus JE Richardson. Extracting non-linear integrate-and-fire

models from experimental data using dynamic i–v curves. *Biological cybernetics*, 99(4-5):361–370, 2008.

[8] Dorit Baras and Ron Meir. Reinforcement learning, spike-time-dependent plasticity, and the BCM rule. *Neural Computation*, 19(8):2245–2279, 2007.

[9] Olivier Bichler, Damien Querlioz, Simon J Thorpe, Jean-Philippe Bourgoin, and Christian Gamrat. Extraction of temporally correlated features from dynamic vision sensors with spike-timing-dependent plasticity. *Neural Networks*, 32:339–348, 2012.

[10] Allen C and Stevens C F. An evaluation of causes for unreliability of synaptic transmission. *Proc. Natl. Acad. Sci.*, 91:10380–10383, 1994.

[11] Clopath C, Büsing L, Vasilaki E, and Gerstner W. Connectivity reflects coding: a model of voltage-based STDP with homeostasis. *Nature Neuroscience*, 13:344–352, 2010.

[12] Gardiner C. *Stochastic Methods: A Handbook for the Natural and Social Sciences*. Springer, Berlin Heidelberg, 2009.

[13] Claudia Clopath and Wulfram Gerstner. Voltage and spike timing interact in STDP–a unified model. *Spike-timing dependent plasticity*, page 294, 2010.

[14] JA Connor and CF Stevens. Prediction of repetitive firing behaviour from voltage clamp data on an isolated neurone soma. *The Journal of Physiology*, 213(1):31, 1971.

[15] Lorente de Nó R. Transmission of impulses through cranial motor nuclei. *J Neurophysiol*, 2:402–64, 1939.

[16] Hebb DO. *The organization of behavior: a neuropsychological theory*. L. Erlbaum Associates, Mahwah, N.J., 1949.

[17] Izhikevich E, Gally J, and Edelman G. Spike-timing dynamics of neuronal groups. *Cerebral Cortex*, 14:933–944, 2004.

[18] Lubenov E and Siapas A. Decoupling through synchrony in neuronal circuits with propagation delays. *Neuron*, 58:118–131, 2008.

[19] Oja E. Simplified neuron model as a principal component analyzer. *Journal of Mathematical Biology*, 15:267–273, 1982.

[20] Shimon Edelman and Nathan Intrator. Unsupervised statistical learning in vision: computational principles, biological evidence. *Miscellaneous Papers, Available from kybele. psych. cornell. edu*, 23, 2004.

[21] Bienenstock EL, Cooper LN, and Munro PW. Theory for the development of neuron selectivity: orientation specificity and binocular interaction in visual cortex. *The Journal of Neuroscience*, 2:32–48, 1982.

[22] Kandel ER and Tauc L. Mechanism of prolonged heterosynaptic facilitation. *Nature*, 202:145–147, 1964.

[23] Kandel ER and Tauc L. Heterosynaptic facilitation in neurones of the abdominal ganglion of aplysia depilans. *The Journal of Physiology*, 181:1–27, 1965.

[24] Lugaro Ernesto. *Modern Problems in Psychiatry*. The University Press, Manchester, 1909.

[25] Nicolas Fourcaud-Trocmé, David Hansel, Carl Van Vreeswijk, and Nicolas Brunel. How spike generation mechanisms determine the neuronal response to fluctuating inputs. *The Journal of neuroscience*, 23(37):11628–11640, 2003.

[26] Julijana Gjorgjieva, Claudia Clopath, Juliette Audet, and Jean-Pascal Pfister. A triplet spike-timing–dependent plasticity model generalizes the bienenstock–cooper–munro rule to higher-order spatiotemporal correlations. *Proceedings of the National Academy of Sciences*, 108(48):19383–19388, 2011.

[27] Bi GQ and Poo MM. Synaptic modifications in cultured hippocampal neurons: dependence on spike timing, synaptic strength, and postsynaptic cell type. *Journal of Neuroscience*, 18:10464–10472, 1998.

[28] Lynch GS, Dunwiddie T, and Gribkoff V. Heterosynaptic depression: a postsynaptic correlate of long-term potentiation. *Nature*, 266:737–739, 1977.

[29] Markram H, Lübke J, Frotscher M, and Sakmann B. Regulation of synaptic efficacy by coincidence of postsynaptic aps and epsps. *Science*, 275:213, 1997.

[30] Markram H, Gerstner W, and Sjöström PJ. A history of spike-timing-dependent plasticity. *Frontiers in Synaptic Neuroscience*, 3:4, 2011.

[31] Abarbanel HDI, Gibb L, Huerta R, and Rabinovich MI. Biophysical model of synaptic plasticity dynamics. *Biological Cybernetics*, 89:214–226, 2003.

[32] Eugene M Izhikevich and Niraj S Desai. Relating stdp to bcm. *Neural computation*, 15(7):1511–1523, 2003.

[33] Kozloski J and Cecchi G. A theory of loop formation and elimination by spike timing-dependent plasticity. *Front Neural Circuits*, 4:7. doi: 10.3389/fncir.2010.00007, 2010.

[34] Trousdale J, Hu Y, Shea-Brown E, and Krešimir Josić. Impact of network structure and cellular response on spike time correlations. *PLoS Computational Biology*, 8:e1002408, 2012.

[35] Renaud Jolivet, Alexander Rauch, Hans-Rudolf Lüscher, and Wulfram Gerstner. Integrate-and-fire models with adaptation are good enough: predicting spike times under random current injection. *Advances in neural information processing systems*, 18:595–602, 2006.

[36] Lashley KS. Basic neural mechanisms in behavior. *Psychol Rev*, 37:1–24, 1930.

[37] Abbott LF and Nelson S. Synaptic plasticity: taming the beast. *Nature Neuroscience*, 3:1178–1183, 2000.

[38] Benjamin Lindner. *Coherence and stochastic resonance in nonlinear dynamical systems*. Logos-Verlag, 2002.

[39] Gilson M, Burkitt A, Grayden D, Thomas D, and van Hemmen J. Emergence of network structure due to spike-timing-dependent plasticity in recurrent neuronal networks. i. input selectivity-strengthening correlated input pathways. *Biological Cybernetics*, 101:81–102, 2009.

[40] Gilson M, Burkitt A, Grayden D, Thomas D, and van Hemmen J. Emergence of network structure due to spike-timing-dependent plasticity in recurrent neuronal networks. ii. input selectivity-symmetry breaking. *Biological Cybernetics*, 101:103–114, 2009.

[41] Gilson M, Burkitt A, Grayden D, Thomas D, and van Hemmen J. Emergence of network structure due to spike-timing-dependent plasticity in recurrent neuronal networks iii: Partially connected neurons driven by spontaneous activity. *Biological Cybernetics*, 101:411–426, 2009.

[42] Gilson M, Burkitt A, Grayden D, Thomas D, and van Hemmen J. Emergence of network structure due to spike-timing-dependent plasticity in recurrent neuronal networks iv: structuring synaptic pathways among recurrent connections. *Biological Cybernetics*, 101:427–444, 2009.

[43] Gilson M, Burkitt A, Grayden D, Thomas D, and van Hemmen J. Emergence of network structure due to spike-timing-dependent plasticity in recurrent neuronal networks v: self-organization schemes and weight dependence. *Biological Cybernetics*, 103:1–22, 2010.

[44] Gilson M, Burkitt A, and van Hemmen J. STDP in recurrent neuronal networks. *Frontiers in Computational Neuroscience*, 4:23. doi: 10.3389/fncom.2010.00023, 2010.

[45] Richardson M. Firing-rate response of linear and nonlinear integrate-and-fire neurons to modulated current-based and conductance-based synaptic drive. *Physical Review E*, 76:021919, 2007.

[46] Richardson M. Spike-train spectra and network response functions for non-linear integrate-and-fire neurons. *Biol Cybern*, 99:381–392, 2008.

[47] Van Rossum M, Bi G, and Turrigiano G. Stable hebbian learning from spike timing-dependent plasticity. *Journal of neuroscience*, 20:8812–21, 2000.

[48] Gabriel Koch Ocker, Ashok Litwin-Kumar, and Brent Doiron. Self-organization of microcircuits in networks of spiking neurons with plastic synapses. *PLoS Comput Biol*, 11(8):e1004458, 2015.

[49] Peter O'Connor, Daniel Neil, Shih-Chii Liu, Tobi Delbruck, and Michael Pfeiffer. Real-time classification and sensor fusion with a spiking deep belief network. *Neuromorphic Engineering Systems and Applications*, page 61, 2015.

[50] Srdjan Ostojic, Nicolas Brunel, and Vincent Hakim. How connectivity, background activity, and synaptic properties shape the cross-correlation between spike trains. *Journal of Neuroscience*, 29(33):10234–10253, 2009.

[51] Gütig R, Aharonov R, Rotter S, and Sompolinsky H. Learning input correlations through nonlinear temporally asymmetric hebbian plasticity. *Journal of Neuroscience*, 23:3697–3714, 2003.

[52] Kempter R, Gerstner W, and Van Hemmen JL. Hebbian learning and spiking neurons. *Physical Review E*, 59:4498, 1999.

[53] Kempter R, Gerstner W, and van Hemmen J. Intrinsic stabilization of output rates by spike-based hebbian learning. *Neural Computation*, 13:2709–2741, 2001.

[54] Linsker R. From basic network principles to neural architecture: emergence of spatial-opponent cells. *Proceedings of the National Academy of Sciences*, 83:7508–7512, 1986.

[55] Alexander Rauch, Giancarlo La Camera, Hans-Rudolf Lüscher, Walter Senn, and Stefano Fusi. Neocortical pyramidal cells respond as integrate-and-fire neurons to in vivo–like input currents. *Journal of neurophysiology*, 90(3):1598–1612, 2003.

[56] Douglas RM and Goddard GV. Long-term potentiation of the perforant path-granule cell synapse in the rat hippocampus. *Brain Research*, 86:205–215, 1975.

[57] Jonathan E Rubin, Richard C Gerkin, Guo-Qiang Bi, and Carson C Chow. Calcium time course as a signal for spike-timing–dependent plasticity. *Journal of neurophysiology*, 93(5):2600–2613, 2005.

[58] Song S, Miller K, and Abbott LF. Competitive hebbian learning through spike-timing-dependent synaptic plasticity. *Nature Neuroscience*, 3:919–26, 2000.

[59] Song S and Abbott LF. Cortical development and remapping through spike timing-dependent plasticity. *Neuron*, 32:339–350, 2001.

[60] Michael N Shadlen and William T Newsome. The variable discharge of cortical neurons: implications for connectivity, computation, and information coding. *Journal of neuroscience*, 18(10):3870–3896, 1998.

[61] Yang SN, Tang YG, and Zucker RS. Selective induction of ltp and ltd by postsynaptic [Ca2+]i elevation. *Journal of Neurophysiology*, 81:781–787, 1999.

[62] Charles F Stevens and A Zador. When is an integrate-and-fire neuron like a poisson neuron? *Advances in neural information processing systems*, pages 103–109, 1996.

[63] Dunwiddie T and Lynch G. Long-term potentiation and depression of synaptic responses in the rat hippocampus: localization and frequency dependency. *The Journal of Physiology*, 276:353–367, 1978.

[64] Lømo T. Frequency potentiation of excitatory synaptic activity in the dentate area of the hippocampal formation. *Acta Physiol Scand*, 68, 1966.

[65] Simon J Thorpe. Spike-based image processing: can we reproduce biological vision in hardware? In *European Conference on Computer Vision*, pages 516–521. Springer, 2012.

[66] Sejnowski TJ. Storing covariance with nonlinearly interacting neurons. *Journal of Mathematical Biology*, 4:303–321, 1977.

[67] Bliss TVP and Lømo T. Long-lasting potentiation of synaptic transmission in the dentate area of the anaesthetized rabbit following stimulation of the perforant path. *The Journal of Physiology*, 232:331–356, 1973.

[68] Jacob V, Brasier DJ, Erchova I, Feldman D, and Shulz DE. Spike timing-dependent synaptic depression in the in vivo barrel cortex of the rat. *The Journal of neuroscience: the official journal of the Society for Neuroscience*, 27:1271–1284, 2007.

[69] Gerstner W, Kempter R, van Hemmen JL, and Wagner H. A neuronal learning rule for sub-millisecond temporal coding. *Nature*, 383:76–78, 1996.

[70] Gerstner W, Ritz R, and van Hemmen JL. Why spikes? hebbian learning and retrieval of time-resolved excitation patterns. *Biological Cybernetics*, 69:503–515, 1993.

[71] Levy WB and Steward O. Temporal contiguity requirements for long-term associative potentiation/depression in the hippocampus. *Neuroscience*, 8:791–797, 1983.

[72] Li I Zhang, Huizhong W Tao, Christine E Holt, William A Harris, and Muming Poo. A critical window for cooperation and competition among developing retinotectal synapses. *Nature*, 395(6697):37–44, 1998.